IOWA STATE UNIVERSITY
Digital Repository

2010

Laboratory and field investigations of recycled portland cement concrete subbase aggregates

Thang Huu Phan
Iowa State University

Follow this and additional works at: https://lib.dr.iastate.edu/etd

Part of the Civil and Environmental Engineering Commons

Recommended Citation

Phan, Thang Huu, "Laboratory and field investigations of recycled portland cement concrete subbase aggregates" (2010). *Graduate Theses and Dissertations*. 11259.
https://lib.dr.iastate.edu/etd/11259

Laboratory and field investigations of recycled portland cement concrete subbase aggregates

by

Thang Huu Phan

A dissertation submitted to the graduate faculty

in partial fulfillment of the requirements for the degree of

DOCTOR OF PHILOSOPHY

Major: Civil Engineering (Geotechnical Engineering)

Program of Study Committee:
David J. White, Major Professor
Vernon R. Schaefer
Charles T. Jahren
Halil Ceylan
R. Christopher Williams
Lester W. Schmerr

Iowa State University

Ames, Iowa

2010

DEDICATION

This dissertation is dedicated to my mother, father, wife, brothers, and sister. I doubt I would have ever completed this project without their unconditional love and support throughout my study. They have always shared with me the difficulties and success, given me strength and courage, and helped me to succeed.

TABLE OF CONTENTS

LIST OF FIGURES

LIST OF TABLES

CHAPTER 1: GENERAL INTRODUCTION

Because of transportation, landfill, and environmental costs, it is expensive to dispose of waste concrete material from reconstructed pavement projects. As the volume of waste and the costs of disposal continue to rise, and because natural limestone aggregate is a finite resource, it is important to consider alternatives to natural aggregate and identify more cost-effective ways of addressing waste material. Incorporating recycled portland cement concrete (RPCC) into new pavement subbase is one alternative that addresses many of these obstacles.

However, past field observations have indicated that roads built with RPCC aggregate subbases may experience reduced permeability (Kasai 2004; White et al. 2004). This research investigated and compared permeability of RPCC and crushed limestone subbases using in situ permeameter tests. Because stiffness is a design input parameter to pavement thickness design, lightweight deflectometer (LWD), dynamic cone penetrometer (DCP), and Clegg hammer impact tests were also conducted to understand the long term potential for changes in stiffness and formation of hydration products, the microstructure of RPCC aggregate was analyzed with scanning electron microscopy (SEM) and X-ray microanalysis.

Previous studies (e.g., Gupta and Kneller 1993; Steffes 1999) reported that tufa precipitate from RPCC aggregate subbases may reduce the long-term pavement. To investigate the area affected by leachate, this study mapped the pH values along a flow channel of an RPCC subbase pavement where tufa precipitate had been identified. Tufa samples were characterized with SEM and X-ray microanalysis. The potential for tufa precipitate was analyzed using thermogravimetric tests on RPCC samples collected from 18 sites in Iowa.

In one part of this research, spatial analysis was conducted to investigate the distribution of subgrade stiffness and moisture content using DCP (ASTM. 2003c), Clegg hammer impact (ASTM. 2002), LWD (Vennapusa and White 2009), and nuclear gauge tests at one site with crushed limestone subbase. Further, because seasonal variations (e.g., freeze/thaw cycles, moisture content, temperature) that influence pavement performance, field instrumentation was deployed to monitor subgrade and subbase conditions over a two-year period.

These problems were investigated to explore how they might be mitigated in the field.

These studies revealed that RPCC subbases are about two times stiffer than crushed limestone subbases, and that RPCC subbases have lower permeability than crushed limestone subbases. In general, RPCC subbases provide adequate support to the rigid pavement.

LITERATURE REVIEW

The structure of a portland cement concrete (PCC) pavement is generally composed of a PCC pavement, a granular aggregate subbase, and the subgrade. The subbase and subgrade layers are the main structures that support the PCC pavement. The subbase receives traffic loads from the PCC pavement and transfers and dissipates these loads to the subgrade layer (AASHTO. 1993a). Stiffness of the subgrade and subbase in term of modulus of subgrade (and subbase) reaction, k-value, is an important material property for pavement design that follows the *Mechanical-Empirical Pavement Design Guide* (MEPDG) (NCHRP. 2004) and other pavement design procedures, such as the *AASHTO Guide for Design of Pavement Structures* (AASHTO. 1993a) and the *Thickness Design for Concrete Highway and Street Pavements* (Packard 1984). Modulus of subgrade (and subbase) reaction and drainage coefficient of subbase are two major material properties employed to design PCC pavement using AASHTO method (AASHTO. 1993a, Huang 2004).

Loss of support conditions (i.e., a reduction in stiffness) in subbase and subgrade layers occurs during thawing periods and/or saturated conditions and is one of the primary contributors to distresses in pavements. Variation in moisture in the subgrade layer can contribute to volume change in the soil that may decrease its k-value, resulting in damage to the PCC pavement. A better understanding of seasonal variation in subgrade properties would benefit practitioners who design pavements and select materials.

In this dissertation, each paper contains a literature review section for specific topics. The literature review in this general introduction provides a supplemental review of the general use and properties of RPCC materials and the effects of seasonal variations on the resilient modulus of subgrade layers.

The Use of RPCC Materials

Highway construction consumes large quantities of aggregate materials for

subbase/base courses and pavement that creates high demands for mining, processing, and hauling the material. Collins and Ciesielski (1994) estimated that approximately 3 million tons of removed concrete pavements are being produced in the United States annually. Newly built and/or reconstructed pavements require large volumes of aggregate material for the subbase layer. Yrjanson (1989) reported that highway and bridge construction in the United States consumed over 2 billion tons per year of crushed stone, sand, and gravel.

Because of transportation, landfill, and environmental fees, it is expensive to dispose waste concrete material from reconstructed pavement projects. As the volume of waste and the costs of disposal continue to rise, it has become important to identify more cost-effective ways of dealing with this waste material. In some areas of the United States, natural sources of crushed limestone may not be available near construction projects, or the quality of the aggregate simply does not meet the project requirements. Increased cost of transportation of crushed limestone aggregates to the projects, increased damages of roadways for hauling the materials, and environmental pollution from hauling vehicles are additional concerns that make recycled portland cement concrete (RPCC) a viable economic solution.

The use of RPCC aggregate materials has become a common practice in Iowa since early 1980s. Marks (1984) reported that a project located in Lyon County in 1976 was the first project that Iowa Department of Transportation (DOT) used RPCC as coarse aggregate in PCC pavement. A second project was constructed in Pottawattamie County in 1977, where RPCC aggregate was used in 100 mm (4 in.) econocrete bases and 150 mm (6 in.) PCC shoulders on one lane of the interstate highway I-680. Marks (1984) summarized seven major benefits of using RPCC aggregate materials as follows:

1. Provide aggregate where high quality aggregate is no longer economically available;
2. Eliminate the need for locations to waste the large amount of pavement rubble;
3. Conserve the present aggregate sources;
4. Reduce the need for disrupting land for quarrying purposes;
5. Save fuel and energy by reducing aggregate transportation;
6. Reduce damage due to haul roads near paving projects;
7. Achieve a monetary savings while constructing high quality roadways.

Although the use of RPCC aggregates provided economical and environmental benefits, RPCC aggregates to construction projects at different levels of application were adopted by 26 states as of 2003. RPCC aggregates were used for pavement subbases by several states, but the aggregates were at the stages of experimental research, testing, and development in other states (Vukov 2003).

Despite these benefits, Steffes (1999) reported that roadways built with RPCC aggregate might result in reduced permeability, clog drainage systems, and produce leachate with high pH that could corrode metal drainage pipes and damage vegetation, and deposited tufa. Most of these conditions potentially reduced durability of pavement bases/subbases and affected long-term pavement performance.

Material Properties of RPCC Aggregate

RPCC aggregates have been used for pavement subbase in many states, but the specifications followed by state DOTs for this type of material were derived from previously developed specifications for crushed limestone aggregates. In fact, RPCC aggregates have different physical, chemical, and mechanical properties because cement is a constituent of the aggregate particles.

Table 1.1. Typical grain size distribution of coarse and fine fractions (Marks 1984)

Coarse fraction		Fine fraction	
Sieve size	Percent passing	Sieve size	Percent passing
1 ½ in.	100.0	3/8 in.	100.0
1 in.	72.0	No. 4	76.0
¾ in.	39.0	No. 8	51.0
½ in.	21.0	No. 16	30.0
3/8 in.	9.3	No. 30	16.0
No. 4	2.9	No. 50	8.0
No. 8	2.0	No. 100	3.5
No. 200	0.7	No. 200	2.0

Marks (1984) reported production process of RPCC aggregates in Iowa using crushing operation. The author used the terms "coarse fraction" and "fine fraction" to refer to two groups of aggregate materials that have typical gradations presented in Table 1.1. The crushing operation produced approximately 65% coarse fraction and 35% fine fraction. Conventional aggregate tests were used to evaluate RPCC aggregates. The abrasion loss of RPCC aggregates reported 59% was slightly higher than the allowed abrasion loss of 50% (ASTM. 2003b). The loss from the freeze/thaw test of RPCC aggregates was 42% (ASTM. 2003a). This value was much higher than 6% freeze/thaw loss of crushed stone provided by the standard specification issued by Iowa DOT (Marks 1984). Table 1.2 compares the properties of RPCC aggregates were compared with crushed limestone aggregates (Yrjanson 1989).

Table 1.2. Engineering properties of crushed limestone and RPCC aggregate materials (Yrjanson 1989)

Property	Crushed limestone aggregates	Recycled concrete aggregate
Specific gravity	2.6–2.6	2.2–2.4
Absorption (%)	0.5–1.6	4.3–5.9
Loss in L.A. abrasion test (%)	20.0–30.0	20.0–45.0

Workability and performance of RPCC aggregates in concrete were reported by Burke et al. (1992). Workability for the mixtures of RPCC aggregates were found to be similar to mixtures using crushed limestone aggregates. RPCC aggregates used as fine aggregate required more cement and water. The frost resistance of the concrete made from RPCC aggregate was not reduced if the RPCC aggregates were recycled from high quality concrete. However, RPCC aggregates were reported to significantly affect the strength and performance of the concrete that used the materials as coarse aggregates. Compressive strength and modulus of elasticity of the concrete decreased by 25% and 30%, respectively. Higher amounts of drying shrinkage and creep were measured for the concrete with RPCC aggregate.

Table 1.3. Laboratory and field properties of crushed limestone and RPCC aggregates used in
road bases in Iowa (modified from White et al. 2004)

Test perform	Property	Crushed limestone	RPCC
Laboratory tests			
Sieve analysis	Unified soil classification system (ASTM. 2000)	GP	GP–GM
	AASHTO (AASHTO. 2002)	A–1–a	A–1–a
Sieve analysis	Percent fines (ASTM 2001a)	8%	8%
Specific gravity	G_s (ASTM. 2001b)	2.75	2.54
Vibrating table	$\gamma_{d\ max}$ (kg/m^3)	1554	1410
	$\gamma_{d\ min}$ (kg/m^3)	1458	1346
Abrasion	Percent loss (ASTM. 2003b)	15.3%	22.5%
CBR	*CBR* at 10 mm (0.4 in.) penetration	52%	22%
In situ tests			
Geogauge	Modulus (MPa)	70.8	47.9
DCP	*DPI* (mm/blow) (ASTM. 2003c)	28	24
	CBR[*]	9% [*]	10% [*]
Clegg impact hammer	*CIV* (ASTM. 2002)	13	13
Air permeameter	Permeability (mm/second)	56	48
Gradation	Percent fines (passing #200 sieve) (ASTM. 2001a)	4 – 9	4 – 11 [**]

Notes: [*] Estimated from DCP; [**] Due to breakage of particles under compaction.

White et al. (2004) evaluated material properties on a few samples in the laboratory
and in situ for natural and RPCC aggregates used in Iowa. The properties included gradation,
specific gravity, minimum and maximum density, abrasion loss, California Bearing Ratio
(*CBR*), dynamic penetration index (*DPI*) via use of DCP, Clegg impact value (*CIV*), and in
situ permeability. Results from Table 1.3 suggests that RPCC aggregates have similar
properties to crushed limestone aggregates but that the RPCC aggregates had higher water

absorption, percentage of fines and lower specific gravity, density, compressive strength, and modulus of elasticity when compared with crushed limestone aggregates.

According to White et al. (2004), the hydraulic conductivity normally decreased with increasing compaction energy (i.e., density) for various types of aggregates (Table 1.3). With increased compaction energy, hydraulic conductivity in RPCC could be reduced up to 16 times. The affect of increased compaction energy on permeability was less for crushed limestone aggregates.

Effects of Moisture Variation on Resilient Modulus

Resilient modulus of pavement foundation layers is a strength/stiffness parameter that reflects the support condition of these layers in the pavement system. Resilient modulus is used directly for the design of flexible pavements. In design of rigid or composite pavements, the resilient modulus is converted to a modulus of subgrade reaction (k-value); ((Seed et al. 1962; AASHTO. 1993). According to the AASHTO Guide for Design of Pavement Structures (1993), resilient modulus (M_r) is defined as "a measure of the elastic property of soil recognizing certain nonlinear characteristics." Resilient modulus is the ratio between repeated deviator stress (σ_d) and recoverable strain (ε_r) in the direction of the major principle stress and is generally considered as an appropriate measure indicating the stiffness of unbound pavement materials (e.g., subgrade soil).

Resilient modulus of a subgrade is dependent on several factors, including soil type, moisture content, temperature, and dry density (or compaction level) (Seed et al. 1962; Jin et al. 1994). Jin et al. (1994) incorporated these seasonal variables into a laboratory testing program for resilient-modulus tests and found that the resilient modulus value increased as the moisture content and temperature decreased and the dry density increased.

Li et al. (1994) established the influence of soil physical state on resilient modulus by means of the compaction curves. Soil physical state could be changed by the effects of environment and of compaction caused by traffic. The authors performed 27 repeated load triaxial tests on 11 fine grained soils and from that data results determined a best fit polynomial equation:

$$R_{m1} = 0.98 - 0.28(w - w_{opt}) + 0.029(w - w_{opt})^2 \tag{1}$$

where $R_{m1} = M_r/M_{r\,(opt)}$ for the case of constant dry density; M_r is resilient modulus at moisture content w (%) and the same dry density as $M_{r\,(opt)}$; $M_{r\,(opt)}$ is resilient modulus at maximum dry density and optimum moisture content w_{opt} (%) for any compaction effort. The correlation coefficient, r^2, was equal to 0.76.

Li et al. (1994) also developed a relationship between resilient modulus and moisture content with the same compaction efforts. Results of 26 repeated load triaxial tests on 10 fine grained soils were collected from literature. The best fit polynomial equation for these data was:

$$R_{m2} = 0.96 - 0.18(w - w_{opt}) + 0.0067(w - w_{opt})^2 \tag{2}$$

where $R_{m2} = M_r/M_{r\,(opt)}$ for the case of constant compaction effort; M_r is resilient modulus at moisture content w (%) and the same compaction effort as $M_{r\,(opt)}$; The regression correlation coefficient, r^2, was equal to 0.83.

According to these relationships, a small change in moisture content can result in significant changes in the resilient modulus. Given a constant dry density, M_r can be three times higher than $M_{r(opt)}$ if w is 5% lower than w_{opt}. M_r is equal to half of $M_{r(opt)}$ when w is 2% higher than w_{opt}. In case of constant compaction energy, M_r is approximately two times higher than $M_{r(opt)}$ if w is 5% lower than w_{opt}, and M_r is equal to half of $M_{r(opt)}$ when w is 3% higher than w_{opt}.

Drumm et al. (1997) studied the saturation effects on the subgrade resilient modulus. A series of resilient modulus tests was conducted to investigate the variation in M_r due to the increases of water content after compaction. The results indicated that an increase of water content resulted in a decrease of the resilient modulus, although the magnitude of the decrease in M_r depended on the soil type. The A-7-5 and A-7-6 soils (AASHTO. 1993b) had the largest M_r at optimum, but also had greater reduction in M_r with post-compaction water content than A-4 and A-6 soils (AASHTO. 1993b).

RESEARCH GOAL AND OBJECTIVES

The major objectives of this dissertation are:

- To investigate the mechanical properties of RPCC aggregate subbase and compare permeability and stiffness for recycled portland cement concrete subbase;

- To characterize the microstructure of RPCC aggregate using scanning electron microscopy (SEM) analysis and analyze self-stabilizing recycled portland cement concrete subbase aggregate using field measurements;

- To study the precipitate potential of rigid pavements using recycled portland cement concrete subbases and analyze microstructure of tufa precipitate using SEM analysis;

- To report the seasonal variation in the subgrade layer using in situ instrumentation and perform spatial analysis of subgrade soils prior to placement of the subbase layer.

The results of this research are expected to benefit geotechnical, pavement, and construction engineering researchers and practitioners working in the field of pavement performance and design. The results may also encourage a common use of RPCC aggregates for pavement subbase for a sustainable method of using natural and recycled resources.

ORGANIZATION OF THE DISSERTATION

This dissertation comprised four technical papers. Each paper appears as a dissertation chapter and includes reference to literature, methods, results and significant findings, conclusions, and recommendations. Chapters 2-4 present three technical papers that are in preparation for submission to geotechnical and pavement engineering journals for publication or have been published. Chapter 5, "Seasonal Variation and Spatial Analysis of Pavement Foundation Layers," was published in the *Compendium of Transportation Research Board* in 2009. Thang H. Phan was first author on each of the four technical papers; co-authors and their contributions are provided after the description of each chapter.

These papers focus on two major areas: (1) characterization and comparison of stiffness and permeability of RPCC subbases and analysis of RPCC aggregates and tufa

precipitate potential , and (2) reporting the seasonal variations in a subgrade and analyzed spatial variations in stiffness and moisture content of the subgrade prior to placement of subbase.

Chapter 2, "Comparison of Permeability and Stiffness for Recycled Portland Cement Concrete Subbases," reports laboratory and field investigation studies of 27 pavement subbases, including 21 RPCC aggregate subbases and 6 crushed limestone aggregate subbases, that support portland cement concrete (PCC) pavement. Stiffness and drainage characterization of the subbase layers were conducted using LWD, DCP, Clegg impact hammer, and Mn/DOT permeameter tests. Field test results are used to estimate *CBR* and modulus of subgrade reaction of the subbase layers. Laboratory tests, including mechanical analysis and specific gravity, are performed to classify aggregate samples collected from all 27 sites. Results of permeability and stiffness of RPCC subbases are compared to those of crushed limestone subbases to determine the performance of the RPCC subbases.

This paper will be submitted to the *Journal of Performance of Constructed Facilities, ASCE*. David J. White, Charles T. Jahren, Halil Ceylan, and Sunghwan Kim were co-authors on this paper. The first three co-authors were the principal investigator and co-principal investigators that oversaw the research project from which this paper was developed. These co-authors directed the overall research activities and provided valuable recommendations to the research team. They also revised and commented on this paper. The fourth co-author provided support during field investigations, revised and commented on this paper.

Chapter 3, "Microstructure Characterization of Recycled Portland Cement Concrete Subbase Aggregate," characterizes the microstructure of the RPCC subbase aggregate and compares the subbase stiffness of four RPCC subbases with the subbase stiffness of five crushed limestone subbases. DCP and Clegg impact hammer tests measured the stiffness of the nine subbases. Phase distribution and chemical composition of the RPCC specimens, which were collected based on age: 1983, 1988, 1994, and 2003 from four different sites, were analyzed using SEM and X-ray analyses.

This paper will be submitted to the *Journal of Materials in Civil Engineering*, *ASCE*. David J. White, Warren E. Straszheim, and Peter Taylor were co-authors on this paper. The co-authors provided valuable recommendations, comments, and revisions to this paper.

Straszheim performed SEM and X-ray microanalysis on the RPCC aggregate samples.

Chapter 4, "Tufa Precipitate Formation from Recycled Portland Cement Concrete Subbases," addresses the precipitate potential of RPCC aggregate subbases. Results of field investigations on tufa precipitate from 18 RPCC subbase sites are reported. The amounts of calcium hydroxide and calcium carbonate in cement paste of RPCC aggregate samples collected from these sites are determined using thermogravimetric analysis (TGA). Results of SEM and X-ray analyses performed on tufa samples collected from subdrains of one site (of 18 RPCC sites) are presented.

This paper will be submitted to the *Journal of Materials in Civil Engineering*, *ASCE*. David J. White, Warren E. Straszheim, and Peter Taylor were co-authors on this paper. The first and the third co-authors provided support to develop testing plans for RPCC and tufa samples in the laboratory. The second co-author (Warren E. Straszheim) performed the SEM tests on the tufa samples. The co-authors also revised and edited this paper.

Chapter 5, "Seasonal Variation and Spatial Analysis of Pavement Foundation Layers," which was published in the *Compendium of Transportation Research Board* in 2009 presents the results of a field study of seasonal variations. Field instrumentation monitored the seasonal variations in temperature, moisture content, frost depth, and groundwater levels in subgrade soils. Spatial variation analysis of the subgrade soils was conducted prior to the placement of the subbase. The spatial variation results were obtained from DCP, nuclear gauge, and Clegg impact hammer tests at 64 test locations.

Matthew D. Cushman, David J. White, and Charles T. Jahren were co-authors on this paper. The first and second co-authors (Matthew D. Cushman, David J. White) were directly involved with installation of field instrumentation in the subgrade and subbase layers, and performing field tests at 64 test points on the subgrade surface prior to subbase construction. The second author was also involved with collecting of the seasonal variation data from the in situ data logger, performing sieve analysis and specific gravity tests on the subgrade soil samples in the laboratory, analysis, and writing selective parts of the paper. The co-authors provided valuable assistance with editing.

Chapter 6 summarizes the general conclusions from the entire research project and makes recommendations.

CHAPTER 2: COMPARISON OF PERMEABILITY AND STIFFNESS FOR RECYCLED PORTLAND CEMENT CONCRETE SUBBASES

Modified from a paper to be submitted to the *Journal of Performance of Constructed Facilities, ASCE*

Thang H. Phan[1], David J. White[2], Charles T. Jahren[3], Halil Ceylan[4], and Sunghwan Kim[5]

ABSTRACT

This paper compares the permeability and stiffness values of recycled portland cement concrete (RPCC) subbases to crushed limestone subbases that support portland cement concrete (PCC) pavements. Field investigations were conducted at twenty-one test sites with RPCC subbases and at six control sites with crushed limestone subbases in Iowa. This study used field results from lightweight deflectometer (LWD), Clegg impact hammer, dynamic cone penetrometer (DCP), Minnesota Department of Transportation (Mn/DOT) in situ permeameter tests to calculate modulus of subgrade reaction, California bearing ratio, and hydraulic conductivity design parameter values. Samples from the test sites were collected for gradation analysis. Results show that RPCC subbases are generally stiffer with lower permeability compared to the crushed limestone subbase test sections.

INTRODUCTION

Newly built and/or reconstructed pavements require large volumes of aggregate for the subbase layer. The subbase is generally stiffer, more drainable, and more uniform compared to the underlying subgrade layer. The practice of using crushed limestone aggregate creates a high demand for mining, processing, and material hauling. For reconstruction projects, it is expensive to haul away waste concrete material due to

---

[1] Graduate Research Assistant (corresponding author), Iowa State University of Science and Technology, 2711 South Loop Drive, Suite 4700, Ames, IA 50010-8664; thphan@iastate.edu

[2] Associate Professor, Iowa State University of Science and Technology, 422 Town Engineering, Ames, IA 50011-3232; djwhite@iastate.edu

[3] Associate Professor, Iowa State University of Science and Technology, 428 Town Engineering, Ames, IA 50011-3232; cjahren@iastate.edu

[4] Associate Professor, Iowa State University of Science and Technology, 406 Town Engineering, Ames, IA 50011-3232; hceylan@iastate.edu

[5] Postdoctoral Associate, Iowa State University of Science and Technology, 192 Town Engineering, Ames, IA 50011-3232; sunghwan@iastate.edu

transportation and landfill expenses. The desire for more economical and sustainable construction projects has led to the increased consideration and use of recycled materials as an alternative. In Iowa, using recycled portland cement concrete (RPCC) is common practice for subbase construction. However, field observations indicate that roadways built with RPCC aggregate may experience reduced permeability, clogged drainage systems, and produce a leachate with high pH that can corrode metal drainage pipes and damage vegetation (Steffes 1999). These conditions could negatively affect long-term performance of the pavement system.

Others have investigated properties of RPCC aggregates and have indicated that they can experience breakage of particles, which increases the fines content (Chini et al. 2001; Maher et al. 1997; Miyagawa et al. 1991; Taha et al. 1999; Kuo et al. 2001; White et al. 2004). Increasing the fines content can reduce freeze-thaw resistance and the permeability of pavement subbases (Kasai 2004; White et al. 2004), which potentially results in pavement deterioration (Christopher and McGuffey 1997; FHWA. 1992; Huang 2004). When temperatures are below freezing, water condenses and forms ice lenses at the interface between the pavement and subbase. These ice lenses melt during the thaw periods and can contribute to increases in pore water pressure. In the RPCC pavement subbases with high percentages of fines and low permeability, the pore water pressures can develop under the pavement and potentially reduce shear strength of base and subgrade layers. Under high traffic volumes and loads, pumping of the rigid pavement can be created with the low permeability and saturated conditions of subbase, resulting in erosion of fine materials from the subbases and faulting, cracking, and deterioration of pavement (Eigenbrod 1992; FHWA. 1992). Little information from these past studies directly links some of the concerns associated with in situ RPCC properties and pavement performance. In Iowa, the same specification is used for crushed limestone and recycled concrete aggregates, even though these aggregates have different physical, chemical, and mechanical properties.

Based on the lack of performance data linked to RPCC properties, a field study was conducted to evaluate field performance of pavements supported by RPCC subbases, in comparison to crushed limestone aggregate subbases. This paper summarizes the engineering properties of RPCC and crushed limestone aggregate subbases as compared to assumed

designed parameter values, such as, modulus of subgrade reaction (*k*), California bearing ratio (*CBR*), and hydraulic conductivity values.

TEST METHODS

Preparation for Field Tests

At each test site, five core holes, including four cores with the diameter of 100 mm (4 in.) and one core with the diameter of 250 mm (10 in.), were drilled for each test site (Figure 2.1). The core holes were drilled between the wheel paths in the center area of the concrete slabs in the travel lane to avoid damage from future traffic. When the field tests and sampling process were completed, the voids created in the subbase by the sampling process were refilled with sand and compacted, while the core holes in the PCC pavement were patched with high strength concrete. In situ field tests were conducted on the subbase and subgrade layers through core holes. LWD and Clegg impact hammer tests were conducted on the surfaces of subbase layers in the 250 mm (10 in.) core hole (Figure 2.1(b); Figure 2.1(c)). DCP tests were conducted in the other three 100 mm (4 in.) holes (Figure 2.1(d)). One 100 mm (4 in.) hole was used to conduct a permeability test using the Mn/DOT permeameter (Figure 2.1(e)).

Subbase aggregate samples for laboratory testing were collected by scooping (or by coring at one test site) from 250 mm (10 in.) and 100 mm (4 in.) holes after the field tests were completed.

Light Weight Deflectometer (LWD)

A Keros LWD (Dynatest 2004; Vennapusa and White 2009) was used to determine the in situ modulus of subgrade reaction and modulus of elasticity. The loading plate diameter was 200 mm (7.8 in.) and the drop height was set at a constant height of 700 mm (27.6 in.). Based on the force applied to the plate, its contact area and deflection, LWD elastic modulus (E_{LWD}) was calculated using elastic half-space theory. The application of a concentrated vertical load to a horizontal surface of the subbase layer produces vertical stresses in the layer. Pressure distribution of the stresses is represented by a bell- or dome-shaped space (Terzaghi and Peck 1967), depending on the plate type (rigid or flexible) and

material type. Modulus of elasticity is calculated using the following equation:

$$E = \frac{f(1-\upsilon^2)\sigma\, a}{\delta} \qquad (1)$$

where:

E = modulus of elasticity (kPa),

δ = deflection (mm),

υ = Poisson's ratio,

σ = applied stress at surface (kPa),

a = radius of the plate (mm), and

f = shape factor depending on stress distribution.

The shape factor f depends on type of plate (rigid or flexible) and soil type. The Keros LWD device used for the project was assumed to be rigid. Shape factors used in this study for subgrade soils, which are elastic materials, and subbase aggregate materials are $\pi/2$ and 8/3, respectively (Vennapusa and White 2009). Poisson's ratio of 0.4 was applied for the calculations. In this study, the LWD tests were conducted on the subbase surfaces, except for site numbers 7 and 15.

Dynamic Cone Penetrometer (DCP)

DCP tests were conducted in accordance with the "Standard test method for use of the dynamic cone penetrometer in shallow pavement applications" (ASTM. 2003). *CBR* values were estimated using dynamic penetration index (*DPI*) (mm/blow) by equation (2). This equation, which was recommended by the U.S. Army Corps of Engineers (Webster et al. 1994), is used for all soils except for CL soils with *CBR* below 10 and CH soils.

$$CBR = \frac{292}{DPI^{1.12}} \qquad (2)$$

Clegg Impact Hammer

Clegg impact hammer tests were conducted in accordance with the "Standard test

method for determination of the impact value (*IV*) of a soil" (ASTM. 2002). The Clegg impact hammer uses a drop weight and an accelerometer to indirectly determine the stiffness at the surface of a tested layer. This is a simple and rapid in situ test that can be conducted on base/subbase and subgrade materials. Clegg impact value (*CIV*) is measured as the rebound of the fourth blow of a standard 4.5 kg (9.9 lb) hammer. In this research, the Clegg impact hammer tests were usually conducted after the LWD testing had completed.

Various correlations have been reported for converting *CIV* to *CBR* based on empirical relationships. Clegg (1986) proposed the following relationship:

$$CBR = (0.24 \, CIV + 1)^2 \tag{3}$$

This relationship is generally suitable for evaluating soils. However, for coarse aggregates like crushed limestone or sand with non-plastic fines, the *CBR* values calculated by equation (3) can be high compared to actual values. Al-Amoudi et al. (2002) proposed an alternative correlation between *CIV* and *CBR* for gravel with non-plastic fines (GM or A-1-b) as follows:

$$CBR = 0.861(CIV)^{1.136} \tag{4}$$

Al-Amoudi et al. (2002) also proposed an alternative correlation between *CIV* and *CBR* for sand with non-plastic fines (SM or A-1-b) as

$$CBR = 1.3577(CIV)^{1.011} \tag{5}$$

In this study, equations 4 and 5 were used to calculate *CBR* values for subbase materials, depending on material classifications. Equation 4 was used for the aggregates classified as GP-GM, GW-GM, GP, and GW (A-1-a). Equation 5 was used for the aggregates classified as SP-SM and SW-SM (A-1-a).

Mn/DOT Permeability Test

In situ permeability measurements of the crushed limestone and RPCC subbases were carried out using a Minnesota Department of Transportation (Mn/DOT) permeameter. This apparatus allows water to infiltrate into a subsurface material under a constant head. The infiltration rate with time is converged to a steady value (Clyne et al. 2001).

A 100 mm (4 in.) hole was cored through the PCC pavement to the surface of subbase layer for each Mn/DOT permeameter test (Figure 2.1(e)). A hand auger was then used to excavate a hole in the subbase material to its mid-depth or at least 150 mm (6 in.). The hole was filled with water and then monitored for a period of time to allow saturation of the subbase material. After the saturation period, the remaining water in that hole was removed using cloth rags. The permeameter was then placed in the well hole and kept upright. The air tube of the permeameter was lifted allowing water to flow into the granular subbase layer. The water flowed out of the permeameter under a constant head. The flow rate was measured at regular time intervals until a steady condition was reached. This steady flow rate was then used to calculate the hydraulic conductivity (Clyne et al. 2001).

In situ permeability tests were conducted with two successive head measurements of 50 mm (2 in.) and 100 mm (4 in.). Saturated hydraulic conductivity was calculated by the following equation:

$$k_{fs} = \frac{CQ}{2\pi H^2 [1 + \frac{C}{2}\left(\frac{a}{H}\right)^2}$$ (6)

where: C is the shape factor and is defined as:

$$C = 0.0046\left[\frac{H}{a}\right]^2 + 0.0318\left[\frac{H}{a}\right] - 0.0087$$ (7)

where:

a = radius of well that is roughly 50 mm,

H = head measurement (50 mm or 100 mm), and

Q = flow rate.

A series of large scale permeameter and Mn/DOT permeameter tests was conducted in the laboratory to verify the results obtained from the field investigation. Well-graded limestone subbase aggregates and sand were used to conduct the permeameter tests. The materials were classified as GP, SW and SP, respectively (ASTM. 2006a; ASTM 2006b), or A-1-a, A-1-a, and A-1-b (ASTM. 2004; AASHTO 1993b; AASHTO. 2002) (Table 2.1; Table 2.2). A test was also conducted on the Mn/DOT permeameter to verify its flow rate.

The result revealed that the maximum flow rate of the Mn/DOT permeameter was 7.3 m/day (24 ft/day).

The large-scale permeameter apparatus that was used as a reference test was manufactured to measure the hydraulic conductivity of coarse grained size aggregate materials, such as sands or subbase aggregates. The mold has an inner diameter of 292 mm (11.5 in.) and a height of 298 mm (11.8 in.). The materials were compacted into the permeameter mold by five lifts. A standpipe collar was placed over the mold to contain water for the test. A manometer was permanently attached to the collar to monitor the water level in the collar. Constant head and falling head permeameter tests were conducted with various materials. The results of the permeability tests and corresponding dry density were presented in Table 2.2.

The results showed that hydraulic conductivity of the well graded aggregate sample (material no. 2) obtained from the Mn/DOT permeameter test and the large scale permeameter test were very similar, regarding a similarity in dry density of the samples. The hydraulic conductivity of the poorly graded sand sample (material no. 3) obtained from the large-scale permeameter test was approximately ten times higher than that obtained from the Mn/DOT permeameter test, though the dry density of the sand samples were approximately the same. The results of the verifying tests suggested that the hydraulic conductivities of the subbase materials obtained from field investigation were within about one order of magnitude of the laboratory hydraulic conductivity measurements, and at minimum would provide a relative comparison between sites.

MATERIALS

Samples collected from each site were used to conduct gradation tests and were classified in accordance to the Unified Soil Classification System (ASTM. 2006a) and the AASHTO Soil Classification System (AASHTO 1993b; AASHTO. 2002). Crushed limestone aggregate materials were classified as poorly graded gravel with non-plastic fines (GP-GM or A-1-a) with the apparent specific gravity ranging from 2.65 to 2.71 (ASTM. 2001). RPCC aggregate materials, which had the apparent specific gravity ranging from 2.57 to 2.66, were classified as either poorly or well-graded sand to gravel (GP, GM,

GP-GM, GW-GM, and SP-SM or A-1-a).

Grain size distribution curves of the aggregate materials are shown in Figure 2.2 (ASTM. 2006b). The gradations of materials from the control (crushed limestone aggregate) sites (Figure 2.2(a)) were generally within the range specified by Iowa DOT's gradation table (Article 4109.02, GS-01016) (Iowa DOT. 2009). The aggregates retained on the ½ in. (12.5 mm) sieve were within the specification range. Sites 1 and 6 had higher percentages of aggregates passing the #8 (2.36 mm) sieve than the percentage allowed by the Iowa DOT specification. In addition, the percentage of fine grained particles that passed the #200 (0.075 mm) sieve from control sites 1, 3, 5, and 6 was higher than the 6% allowed by the specification. However, the grain size distribution curves of the crushed limestone aggregates from the control sites were similar and within the gradation range specified by Iowa DOT (2009).

The gradations of the RPCC aggregates collected from twenty-one test sites were highly variable (Figure 2.2(b), (c), and (d)). Aggregates from all sites, except site numbers 7, 14, 15, and 24, were all or partly finer than the gradation provided by Iowa DOT (2009) for subbase aggregate using RPCC. Aggregates from many of those sites had very high percents of grains that were finer than sieve ½ in. (12.5 mm) and sieve number 200 (0.075 mm).

FIELD TESTS

Strength of Subbase Layers

Results from the LWD elastic modulus of the subbase layers show that the LWD elastic modulus of the crushed limestone aggregate subbase layers was low compared to those obtained from the RPCC layers and varied from 43 MPa to 547 MPa with a coefficient of variation of 91% and standard deviation of 210. On the other hand, the LWD moduli of elasticity of the RPCC aggregate subbase layers were very high and varied from 90 MPa to 2,126 MPa with the coefficient of variation of 95% and standard deviation of 594 MPa. These values of the LWD modulus of elasticity suggested that RPCC subbase layers were much stiffer than crushed limestone aggregate subbase layers.

CIV and *DPI* values are also presented to give indications of the stiffness of the subbase layers. The RPCC subbase layers with higher LWD modulus of elasticity normally

had high *CIV* and low *DPI* values correspondingly (Table 2.3). Several results of the Clegg impact hammer tests were outside of measurement range on the high end, indicating that the subbase layers were very stiff. The *DPI* values reported in Table 2.3 were weighted average values with depth for the whole thickness of the subbase layer. These *DPI* values were used to estimate *CBR* values.

Results of the Clegg impact hammer and DCP testing were used to estimate *CBR* values for the subbase layers. The *CBR* values were calculated from *CIV* values using either equation 4 for the aggregate materials classified as GP-GM, GW-GM, GP, and GW (A-1-a) or equation 5 for the aggregate materials classified as SW-SM and SP-SM (A-1-a) (Al-Amoudi et al. 2002). The *CBR* values were converted from *DPI* values using equation 2. Figure 2.4 shows that *CBR* values of the RPCC subbase layers were normally higher than those obtained from the crushed limestone subbase layers. In particular, the *CBR* values of several RPCC subbase layers were over 100, which indicate that the layers were very stiff. In fact, some of these RPCC subbase layers were so stiff that the subbase aggregate materials had to be collected by using a coring bit (Figure 2.1(f)).

In the rigid pavement design, the PCC slab thickness is selected based on the support provided by the subgrade and the subbase layers (Packard 1984; AASHTO. 1993a; Huang 2004;). Subgrade and subbase support is defined in terms of modulus of subgrade reaction (k_s). The value of k_s is directly proportional to roadbed soil resilient modulus. The modulus of subgrade reaction is estimated based on the results of a plate loading test on a circular plate of 762 mm (30 in.) diameter (Huang 2004).

Since the plate load test is time consuming and expensive, k_s is usually estimated using correlations between the California Bearing Ratio or R-value and other tests that are more easily performed (Huang 2004). In this study, *CBR* values correlated from Clegg impact hammer or DCP testing were used to estimate elastic moduli, M_R, of the subbase layers using equation 8 (Chen et al. 2001). Modulus of subgrade reaction was then estimated using equation 9 (AASHTO. 1993a).

$$M_R = 2{,}550 \times CBR^{0.64} \ \text{(psi)} \tag{8}$$

$$k_s = \frac{M_R}{19.4} \quad \text{(psi/in.)} \tag{9}$$

Modulus of subgrade reaction from a LWD testing, k_{LWD}, can be calculated based on the measurement of applied stress under the LWD loading plate and its deflection using equation 10 (Huang 2004; Vennapusa and White 2009). The diameter of the loading plate of the LWD equipment used for this study is 200 mm (7.9 in.).

$$k_{LWD} = \frac{\sigma}{\delta} \quad (kPa/m) \tag{10}$$

where:

σ = applied stress under the LWD loading plate (kPa),

δ = measured settlement (m).

A comprehensive study by Terzaghi (1955) of the parameters affecting the modulus of subgrade reaction indicated that the value of the modulus decreases with the increases of the width of the foundation. Therefore, the effect of k_s of using various sizes of loading plates must be estimated. Terzaghi proposed equation 11 and 12 to estimate k_s for various footing sizes from plate load tests. The plate load tests can be carried out by means of square plates measuring 0.3 m * 0.3 m (1 ft * 1 ft). According to these equations, modulus of subgrade reaction determined from a 200 mm (7.9 in.) plate is approximately 3.22 times (for sandy soils) to 3.82 times (for clay) greater than that from a 762 mm (30 in.) plate.

$$k = k_{0.3}\left(\frac{B+0.3}{2B}\right)^2 \quad \text{[for foundations on sandy soils]} \tag{11}$$

$$k = k_{0.3}\left(\frac{0.3}{2B}\right) \quad \text{[for foundations on clays]} \tag{12}$$

where:

B = width of footing (m),

k = modulus of subgrade reaction (kPa/m) of foundation measuring B (m) * B (m),

$k_{0.3}$ = modulus of subgrade reaction of square plates measuring 0.3m * 0.3m (kPa/m).

Subgrade modulus of reaction, k_s, of the subbase layers were estimated from LWD, Clegg impact hammer, and DCP testing results (Figure 2.5). The results showed that k_s of the crushed limestone aggregate subbase layers were generally lower than those of the RPCC

subbase layers. The values of k_s from these three types of testing devices were normally consistent with the stiffness of those subbase layers. For stiff RPCC subbase layers, when the LWD and DCP testing results provided very high k_s values, the Clegg impact hammer displayed results that were outside of the measurement range.

The results showed that *k*-values obtained from LWD, or Clegg impact hammer, or DCP for a certain subbase layer were not similar. In fact, results of the LWD testing were strongly affected by the contact area between the plate and the subbase surface. In addition, the LWD testing might reflect the stiffness of a limited area near the subbase surface due to the small area of the LWD plate. Similar situations might occur with the Clegg impact hammer. However, k_s of a subbase layer inferred from DCP test results from weighted average *DPI* value over the depth of the entire subbase layer. Thus, k_s obtained from DCP tests might best reflect the stiffness of the layer of interest.

The modulus of subgrade reaction for the RPCC subbase layers in this study were higher in comparison with those values provided in the engineering bulletin *Thickness Design for Concrete Highway and Street Pavements* (Packard 1984). In this bulletin, the maximum *k*-value for the treated subbase is 225 MPa/m (830 psi/in.). This may explain why the rigid pavement surface of the RPCC subbase sections were comparable to that of crushed limestone aggregate subbase sections in terms of the Pavement Condition Index (*PCI*) and the International Roughness Index (*IRI*); the RPCC subbase pavement sections were performing adequately (White et al. 2008).

Hydraulic Conductivity of the Subbase Layers

Table 2.4 presents the hydraulic conductivity of the crushed limestone and RPCC subbase layers obtained from field investigation using the Mn/DOT permeameter. The hydraulic conductivity of crushed limestone aggregate layers were low and very variable that ranged from $4*10^{-3}$ to $5,819*10^{-3}$ m/day ($15*10^{-3}$ to $19,090*10^{-3}$ ft/day). The hydraulic conductivity of the RPCC subbase layers was also low and variable. The maximum and minimum hydraulic conductivity values of the RPCC subbase layers were $1,567*10^{-3}$ m/day and $5*10^{-3}$ m/day ($5,140*10^{-3}$ ft/day and $17*10^{-3}$ ft/day), respectively. The average hydraulic conductivity of RPCC subbases for both 50 mm and 100 mm fixed heads of water was

$295*10^{-3}$ m/day ($969*10^{-3}$ ft/day) with a standard deviation of $390*10^{-3}$ m/day ($11,280*10^{-3}$ ft/day) and a coefficient of variation of 132%.

These values of hydraulic conductivity were far less than that of the free-draining subbases that range from 15 m/day to 46 m/day (50 to 150 ft/day) or of the permeable subbases of 107 m/day (350 ft/day) (Rodden 2008). In order to effectively remove infiltrated water, a minimum value of 300 m/day (1,000 ft/day) is generally recommended for most permeable bases (Christopher 1997; FHWA. 1992).

As described by the *Guide for design of Pavement Structures* (AASHTO. 1993a), low permeability of the subbase layers may compromise the performance of pavements. Early distress of the pavement structure may be the result of excess water combined with increased traffic volumes and loads. When water enters the pavement structure through cracks, joints, or pavement infiltration, it can reduce strength of the unbounded subbase and subgrade layers. Under high traffic volumes and loads, pumping of the rigid pavement is created with a saturated condition, resulting in subsequent faulting, cracking, and general shoulder deterioration. However, the results of investigation show that the rigid pavement sections perform adequately even with the impermeable RPCC subbase layers (White et al. 2008). One possible explanation is that the well compacted RPCC aggregate subbase sections had very high stiffness that could provide sufficient support to the pavement layers and that this advantage compensated for the disadvantage of low permeability.

CONCLUSIONS

Material properties, specific gravity, and field testing were conducted on the RPCC and crushed limestone aggregate subbase layers at 27 test sites. RPCC aggregate materials were classified as either poorly or well-graded sand to gravel. The specific gravity of the RPCC aggregate materials were from 2.57 to 2.66. Results from field investigation using LWD, Clegg impact hammer, and DCP testing indicated that RPCC subbase layers were generally stiffer than those of crushed limestone subbase layers. The average values of modulus of elasticity and *CBR* values estimated from Clegg impact hammer and DCP tests of RPCC subbases were $1,108*10^3$ kPa (1,576 psi), 73, and 89, respectively, compared to those of the crushed limestone subbase layers of $449*10^3$ kPa (639 psi), 43, and 45, respectively.

In situ tests using LWD, Clegg impact hammer, and DCP on RPCC and crushed limestone subbases provided different values of modulus of subgrade reaction. The average k-values of the RPCC subbases correlated from these testing devices were $1,533*10^3$ kPa/m, $7,366*10^3$ kPa/m, and $8,206*10^3$ kPa/m (5,109 psi/in., 16,799 psi/in., and 30,231 psi/in.), respectively. These values were higher than the average k-values of the crushed limestone subbases of $621*10^3$ kPa/m, $5,326*10^3$ kPa/m, and $5,386*10^3$ kPa/m (2,287 psi/in., 16,350 psi/in., and 19,842 psi/in.), respectively, and were much higher than the maximum value of $225*10^3$ kPa/m (830 psi/in.) that has been applied in pavement design.

In situ permeability testing showed that RPCC subbase layers were much lower than the recommended range of permeability, which varies from 91 m/day to 300 m/day (300 ft/day to 1,000 ft/day), for most permeable subbases. In summary, the findings from this research showed that although the RPCC subbases had generally low permeability, they were much stiffer than values that are normally used for pavement design criteria. Based on road performance observations, apparently RPCC subbases provide adequate support for rigid pavements.

ACKNOWLEDGEMENTS

25

REFERENCES

AASHTO. (1993a). AASHTO guide for design of pavement structures, American Association of State Highway and Transportation Officials, Washington, D.C.

AASHTO. (1993b). Standard specification for aggregate and soil-aggregate subbase, base and surface courses M 147-70, Part I Specifications, 16th Ed., American Association of State Highway and Transportation Officials, Washington, D.C.

AASHTO. (2002). Standard specification for reclaimed concrete aggregate for unbound soil aggregate base course M 319, American Association of State Highway and Transportation Officials, Washington, D.C.

ASTM. (2001). "Standard test method for density, relative density (specific gravity), and absorption of coarse aggregate." Annual book of ASTM standards, ASTM C127, West Conshohocken, PA.

ASTM. (2002). "Standard test method for determination of the impact value (IV) of a soil." Annual book of ASTM standards, ASTM D5874, West Conshohocken, PA.

ASTM. (2003). "Standard test method for use of the dynamic cone penetrometer in shallow pavement applications." Annual book of ASTM standards, ASTM D6951, West Conshohocken, PA.

ASTM. (2004). "Standard practice for classification of soils and soil-aggregates mixtures for highway construction purposes." Annual book of ASTM standards, ASTM D3282, West Conshohocken, PA.

ASTM. (2006a). "Standard practice for classification of soils for engineering purposes (unified soil classification system)." Annual book of ASTM standards, ASTM D2487, West Conshohocken, PA.

ASTM. (2006b). "Standard test method for sieve analysis of fine and coarse aggregates." Annual book of ASTM standards, ASTM C136, West Conshohocken, PA.

Al-Amoudi, S. B. O., Asi, M. I., Wahhab, A-A. I. H., and Khan, A. Z. (2002). "Clegg Hammer—California-Bearing Ratio Correlations." *J. Mater. Civ. Eng.*, 14(6), 512-523.

Clegg, B. (1986). "Correlation with California Bearing Ratio." *News Letter 2*, <http://www.clegg.com.au/information_list12.asp> (Apr. 30, 2008).

Clyne, T. R., Voller, V. R., and Birgisson, B. (2001). "Evaluation of a Field Permeameter to Measure Saturated Hydraulic Conductivity of Base/Subgrade Materials." Final Report No. MN/RC – 2001-19, Minnesota Department of Transportation (Mn DOT), St. Paul, MN.

Chen, H. D., Wang, N. J., and Bilyeu, J. (2001). "Application of dynamic cone penetrometer in evaluation of base and subgrade layers." *J. Trans. Research Board*, No. 1764, Washington, D.C., 1-10.

Chini, A. R., Kuo, S. S., Armaghani, J. M., and Duxbury, J. P. (2001). "Test of recycled concrete aggregate in accelerated test track." *J. Trans. Eng.*, 127(6), 486-492.

Christopher, B. R. and McGuffey, V. C. (1997). "Pavement subsurface drainage systems." *NCHRP Synthesis of Highway Practice 239*. Transportation Research Board of the National Academies, Washington D.C.

Dynatest (2004). "Keros portable FWD – instruction manual for use and maintenance.", Issue No. 010704, Denmark.

Eigenbrod, K. D. and Knutsson, S. (1992). "Measurement of pore water pressures at the interfaces of asphalt cement concrete pavement and soil." *Proc. 45th Canadian Geotec. Conf.*, Toronto, Ontario, Canada, 44.1-44.10.

Federal Highway Administration (1992). "Drainable pavement systems." FHWA-SA-92-008, Washington, D.C.

Iowa Department of Transportation (2009). "General supplementation of specifications for highway and bridge construction - GS-01016." <http://www.iowadot.gov/specifications/new_docs/Complete%20GS-01016.pdf> (Jul. 10, 2010).

Huang H. Yang (2004). "Pavement analysis and design." 2nd Ed., Pearson Prentice Hall, Upper Saddle River, NJ.

Kasai, Y. (2004). "Recent trends in recycling of concrete waste and use of recycled aggregate in Japan." in *Recycling Concrete and Other Materials for Sustainable Development*, Editors Lui, T. C. and Meyer, C. ACI SP-219, 11-34.

Kuo, S-S, Chini. A., Mahgoub, H., Ortega, J., and Monteiro, A. (2001). "Use of recycled concrete made with Florida limestone aggregate for a base course in flexible pavement." Final Report, Florida Department of Transportation, Tallahassee, FL.

Maher, M. H., Gucunski, N., and Papp Jr., W. J. (1997). "Recycled asphalt pavement as a base and sub-base materials," in *Testing Soil Mixed with Waste or Recycled Materials, ASTM STP 1275*, Mark A. Wasemiller, Keith B. Hoddinott, Eds., American Society for Testing and Materials.

Miyagawa, F. K. (1991). "Permeability of granular subbase materials." Interrim Report for Project MLR-90-4. Iowa Department of Transportation, Ames, Iowa.

Packard, R. G. (1984). "Thickness design for concrete highway and street pavements." Paving Transportation Department, Portland Cement Association.

Rodden, R. (2008). "Presentation at ACPA education and training." *2008 Webinar Series*, American Concrete Pavement Association.

Steffes, R. (1999). "Laboratory Study of the Leachate from Crushed Portland Cement Concrete Base Material." Final Report, Project MLR-96-4, Iowa Department of Transportation, Ames, IA.

Taha, R., Ali, G., Basma, A., and Al-Turk, O. (1999). "Evaluation of reclaimed asphalt aggregate in road bases and subbases." *J. Trans. Research Board*, No. 1652, Washington, D.C., 264-269.

Terzaghi, K. (1955). "Evaluation of coefficient of subgrade reaction." *Geotechnique*, 5(4), 297-326.

Terzaghi, K. and Peck, R. B. (1967). "Soil mechanics in engineering practice." 2nd Ed., John Wiley & Sons, Inc., NY.

Vennapusa, P. K. R. and White, D. J. (2009). "Comparison of light weight deflectometer measurement for pavement foundation materials." *Geotech. Testing J.*, 32(3), 239-251.

Webster, S. L., Brown, R. W., and Porter, J. R. (1994). "Force projection site evaluation using the electric cone penetrometer (ECP) and the dynamic cone penetrometer (DCP)." Technical Report No. GL-94-17, Air Force Civil Engineering Support Agency, U.S. Air Force, Tyndall Air Force Base, FL.

White, D. J., Jahren, C. T., Cackler, E. T., and Vennapusa, P. (2004). "Determination of the optimum base characteristics for pavements." Final Report, Iowa DOT Project TR-482, CTRE Project 02-119, Iowa Department of Transportation, Ames, IA.

White, D. J., Ceylan, H., Jahren, C. T., Phan, T. H., Kim, S., Gopalakrisnan, K., and Suleiman, M. T. (2008). "Performance evaluation of concrete pavement granular subbase – pavement surface condition evaluation." Final Report, Iowa DOT Project TR-554, CTRE Project 06-250, Iowa Department of Transportation, Ames, IA.

Table 2.1. Properties of aggregate samples used for Mn/DOT and large scale permeameter
tests

Material no.	Material type	AASHTO classification (AASHTO. 1993b)	USCS classification and description (ASTM. 2006a)	c_u	c_c
1	Crushed limestone	A–1–a	GP – poorly graded gravel	1.58	1.01
2	Crushed limestone	A–1–a	SW – well graded sand	77.33	2.78
3	Sand	A–1–a	SP – poorly graded sand	2.36	1.24

Notes: c_u = coefficient of uniformity; c_c = coefficient of curvature.

Table 2.2. Hydraulic conductivities and dry densities of aggregate samples used for
large-scale and Mn/DOT permeameter tests

Material no.	Large scale permeameter				Mn/DOT permeameter					
	k [a]		ρ_d [b]		k_1 [c]		k_2 [d]		ρ_d	
	m/day	ft/day	kg/m^3	lb/ft^3	m/day	ft/day	m/day	ft/day	kg/m^3	lb/ft^3
1	2393	7852	1773	111	–[e]	–	–	–	1679	105
2	0.30	1.13	1921	120	0.3	0.9	0.2	0.75	1976	123
3	23.0	75.4	1890	118	3.5	11.6	2.3	7.43	1829	114

Notes: [a] hydraulic conductivity; [b] hydraulic conductivity with fixed head of 50 mm; [c] hydraulic conductivity with fixed head of 100 mm; [d] dry density; [e] Mn/DOT permeameter was not able to conduct to this material because the material had very high permeability.

Table 2.3. Summary of LWD modulus of elasticity, *CIV*s, and the average *DPI* values

| Site no. | Material | Construction year | Classification | | Stress | Deflection | E_{LWD} (MPa) | CIV | DPI_{avg} [a] |
			USCS	AASHTO	σ, kPa	$\delta\,(10^{-6}\,\text{m})$			
1	C-L[b]	1990	GP–GM	A–1–a	249	183	305	30	9.0
2	C-L	2005	GP–GM	A–1–a	216	659	74	22	12.0
3	C-L	2005	GP–GM	A–1–a	239	168	318	38	4.7
4	C-L	1968	GP–GM	A–1–a	261	185	316	27	7.6
5	C-L	1993	GP–GM	A–1–a	261	63	928	39	4.0
6	C-L	1994	GP–GM	A–1–a	255	76	751	– [d]	3.0
7	RPCC	2003	GP–GM	A–1–a	N/A[c]	N/A	N/A	17	5.3
8	RPCC	2006	GW–GM	A–1–a	261	383	153	37	10.1
9	RPCC	1999	GP–GM	A–1–a	267	247	242	36	5.6
10	RPCC	2003	GP	A–1–a	261	252	232	48	6.5
11	RPCC	1996	GW–GM	A–1–a	267	56	1070	–	2.0
12	RPCC	1994	GW–GM	A–1–a	274	101	607	74	3.0
13	RPCC	1983	SW–SM	A–1–a	261	185	316	52	4.0
14	RPCC	1999	GP	A–1–a	267	66	907	38	3.0
15	RPCC	2003	GW	A–1–a	N/A	N/A	N/A	N/A	7.0
16	RPCC	1988	GP–GM	A–1–a	258	16	3610	–	1.5
17	RPCC	1987	SP–SM	A–1–a	261	29	2016	77	1.0
18	RPCC	2003	GW–GM	A–1–a	264	53	1117	49	6.0
19	RPCC	1991	GW–GM	A–1–a	245	109	504	39	2.5
20	RPCC	1992	GP–GM	A–1–a	261	29	2016	–	2.5
21	RPCC	1992	GP–GM	A–1–a	264	18	3288	–	2.5
22	RPCC	1992	GW–GM	A–1–a	258	114	507	59	3.0
23	RPCC	1992	GP–GM	A–1–a	264	135	438	33	3.0
24	RPCC	1994	GP–GM	A–1–a	251	28	2012	–	3.0
25	RPCC	1992	GP–GM	A–1–a	255	65	878	–	4.0
26	RPCC	1992	GW–GM	A–1–a	261	88	664	–	3.0
27	RPCC	1991	GW	A–1–a	258	123	470	83	3.0

Notes: [a] average value over the subbase thickness, which ranges from 200 mm to 280 mm (8–11 in.); [b] crushed limestone; [c] not available; [d] out of measurement range due to hard material surface.

Table 2.4. Hydraulic conductivity of subbases using Mn/DOT permeameter

Site no.	Subbase material	k_1 [a]		k_2 [b]	
		(10^{-3} m/day)	(10^{-3} ft/day)	(10^{-3} m/day)	(10^{-3} ft/day)
3	Crushed limestone	2469	8101	5819	19090
4	Crushed limestone	4	15	5	15
6	Crushed limestone	22	74	22	73
8	RPCC	15	50	16	51
9	RPCC	404	1326	369	1211
10	RPCC	673	2209	582	1909
11	RPCC	79	258	71	233
12	RPCC	97	319	–	–
13	RPCC	135	442	104	343
15	RPCC	943	3093	1455	4772
16	RPCC	5	17	5	17
17	RPCC	13	42	12	39
18	RPCC	460	1510	119	392
19	RPCC	56	184	60	196
20	RPCC	9	31	41	135
21	RPCC	505	1657	567	1860
22	RPCC	112	368	93	306
23	RPCC	168	552	164	538
24	RPCC	51	166	60	196
25	RPCC	359	1178	485	1591
26	RPCC	1010	3314	1567	5140
27	RPCC	140	460	224	734

Notes: [a] hydraulic conductivity obtained from tests using a fixed head of 50 mm (2 in.); [b] hydraulic conductivity obtained from tests using a fixed head of 100 mm (4 in.)

Figure 2.1. Field tests: a) 250 mm core hole; b) LWD; c) Clegg impact hammer; d) DCP;
e) in situ Mn/DOT permeameter; f) a sample collected by coring by from a 250 mm core hole
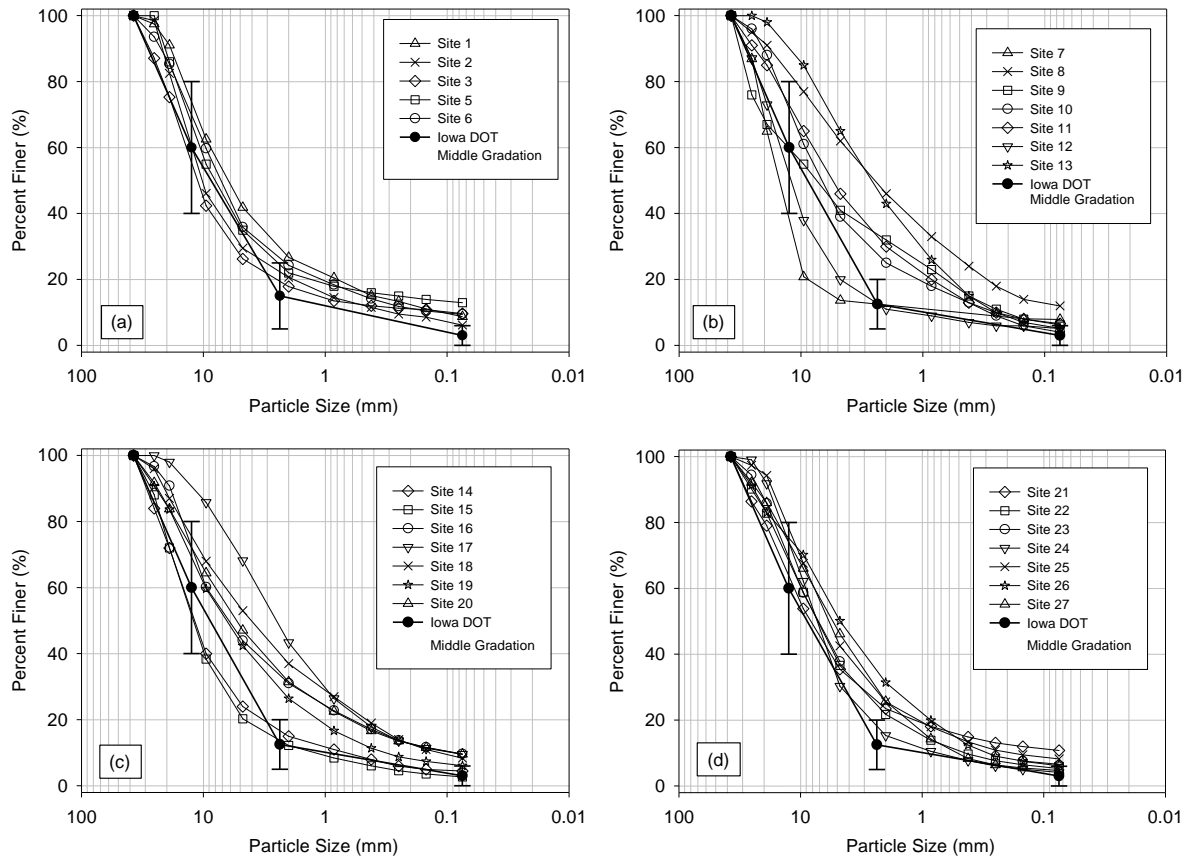
Figure 2.2. Grain size distributions of (a) crushed limestone control sites and (b, c, and d) RPCC aggregate test sites compared to the middle range of the Iowa DOT gradation
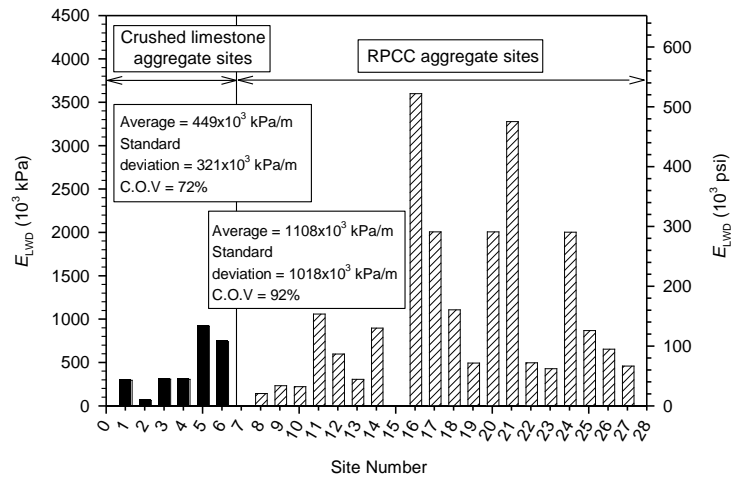
Figure 2.3. LWD modulus of elasticity of crushed limestone and RPCC subbase layers
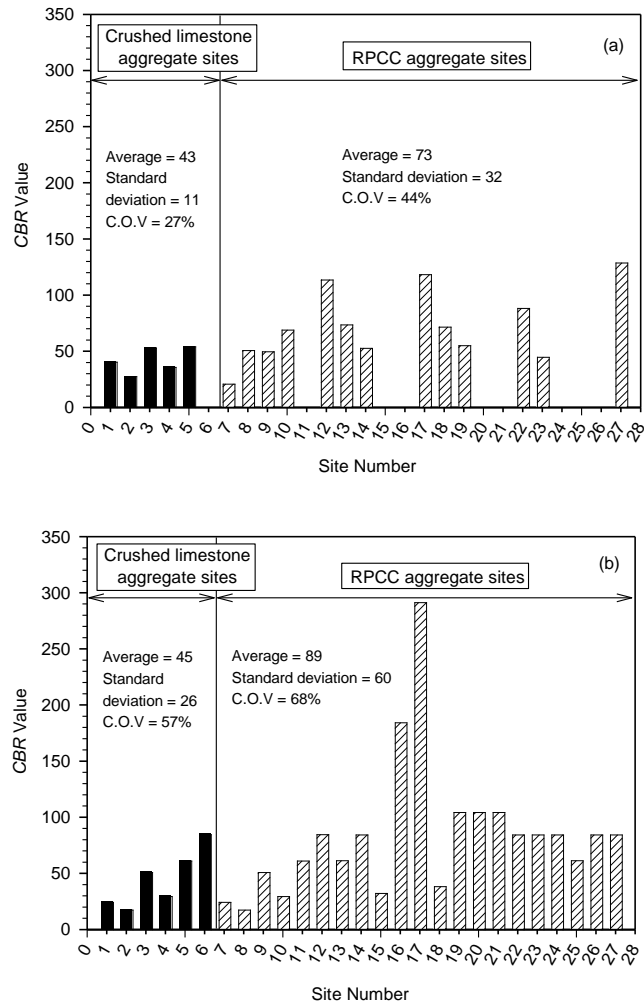
Figure 2.4. CBR values of subbase layers estimated from the weighted average values of:
a) *CIV*s; and b) *DPI* values
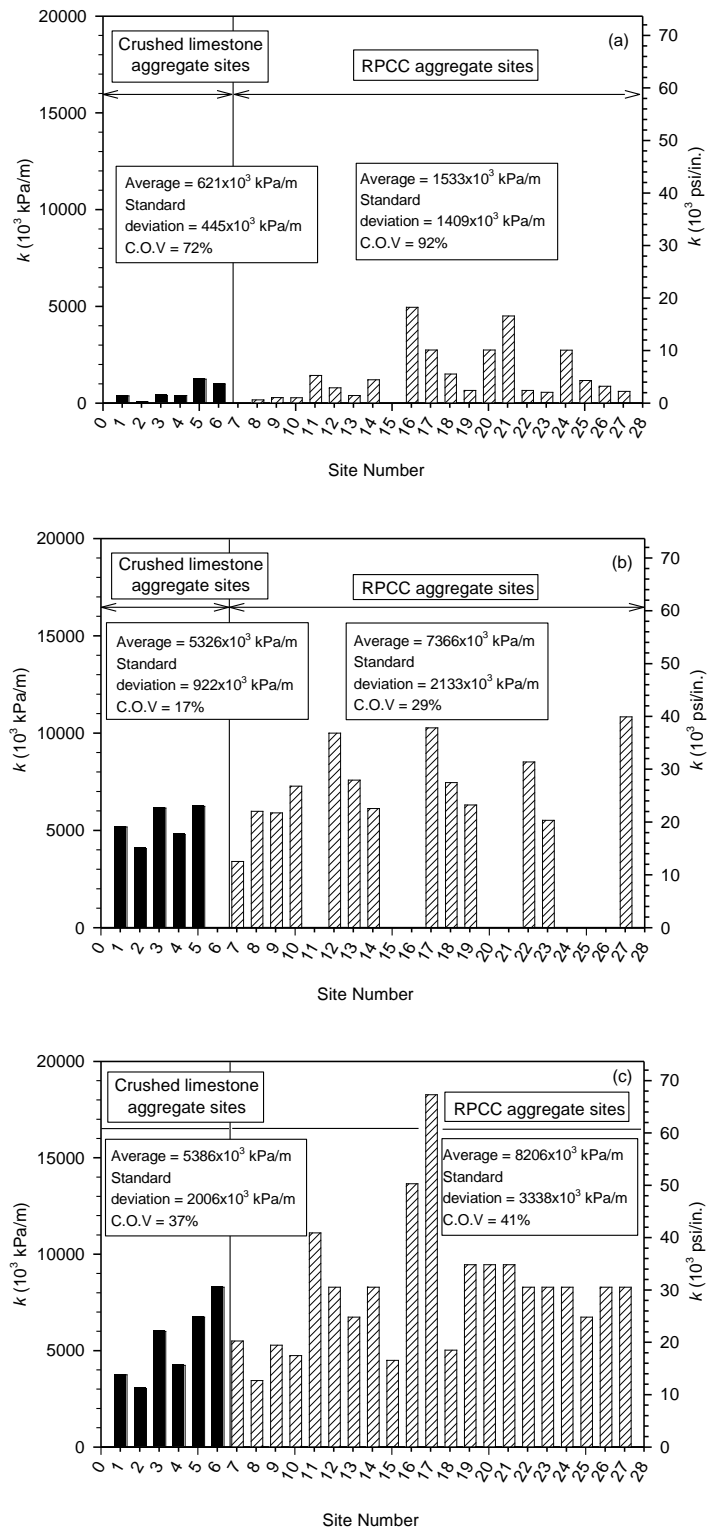
Figure 2.5. Modulus of subgrade reaction of subbase layers estimated from: a) LWD;
b) Clegg impact hammer; and c) DCP tests

CHAPTER 3: MICROSTRUCTURE CHARACTERIZATION OF RECYCLED PORTLAND CEMENT CONCRETE SUBBASE AGGREGATE

Modified from a paper to be submitted to the *Journal of Materials in Civil Engineering, ASCE*

Thang H. Phan[1], David J. White[2], Warren E. Straszheim[3], and Peter Taylor[4]

ABSTRACT

Field investigations were conducted at four sites with recycled portland cement concrete (RPCC) aggregate subbases and five sites with crushed limestone subbases in Iowa and subbase aggregate samples were collected for laboratory tests. The crushed limestone sites provided references for comparison. Dynamic cone penetrometer (DCP) and Clegg impact hammer tests were performed through core holes in the pavement were used to characterize the stiffness/strength of these subbases. Results of field measurements indicated that the RPCC subbases were about 200% stiffer than the crushed limestone aggregate subbases, yet had similar particle size gradations. The higher stiffness values are attributed to formation of cementitious reaction products after subbase placement. Scanning electron microscopy (SEM) and X-ray microanalyses of RPCC aggregate samples showed the amounts of unhydrated cement in RPCC correlated with the stiffness values of the corresponding RPCC subbases and supported these findings.

INTRODUCTION

When road reconstruction includes removing the pavement foundation materials, it can be expensive to remove and dispose of the original concrete pavement materials, and it can be expensive to mine, process, and haul natural aggregate for new subbase layers. Since the early 1980s, the need for more economical and sustainable construction projects has led

---

[1] Graduate Research Assistant (corresponding author), Iowa State University of Science and Technology, 2711 South Loop Drive, Suite 4700, Ames, IA 50010-8664; thphan@iastate.edu

[2] Associate Professor, Iowa State University of Science and Technology, 422 Town Engineering, Ames, IA 50011-3232; djwhite@iastate.edu

[3] Associate Scientist, Iowa State University of Science and Technology, 46 Town Engineering, Ames, IA 50011-3230; wesaia@iastate.edu

[4] Associate Director, National Concrete Pavement Technology Center, 2711 South Loop Drive, Suite 4700, Ames, IA 50010-8664; ptaylor@iastate.edu

to the increased use of recycled portland cement concrete (RPCC) as an alternative to natural aggregate (e.g., dolomite or limestone). For example, using RPCC aggregate for subbase layer construction has become a common practice in Iowa (White et al. 2008).

Portland cement concrete (PCC) pavement generally contains cement grains that are not fully hydrated in the paving process. When old PCC pavement is crushed and used as RPCC subbase aggregate, these unhydrated cement grains are exposed to water from precipitation or groundwater that stimulates the formation of new cementitious reaction products in the subbase (Bruinsma et al. 1997). Compaction during road construction and from traffic loads also break up RPCC aggregate and provide more opportunities for hydration of unhydrated cement grains. In terms of long-term pavement performance, a recent study in Iowa shows that RPCC subbase can provide a durable pavement foundation for rigid pavements as demonstrated by long-term pavement performance measurements (White et al. 2008).

The study described in this paper investigated the question of whether unhydrated cement grains contribute to increases in RPCC subbase stiffness. Four sites in Iowa with RPCC subbase aggregate were studied. Field and laboratory measurements were used to investigate the field performance of and to identify mechanism at the micro level that contributes to high stiffness in the RPCC subbases. Comparison measurements were conducted at five sites with crushed limestone subbases. In situ stiffness of the subbases was calculated from test results of dynamic cone penetrometer (DCP) (ASTM. 2003) and Clegg impact hammer (ASTM. 2002) conducted through core-holes in the pavement. Subbase aggregates collected from these sites were used to conduct gradation and specific gravity tests in the laboratory.

Although adequate pavement performance was observed at all of the field sites, additional research was needed to better understand the stabilization mechanism of the RPCC subbase. Samples of RPCC aggregate from four sites (I-35-1983, I-80-1988, I-80-1994, and I-35-2003) were carefully collected and transported for analysis in the laboratory where scanning electron microscopy (SEM) imaging and X-ray microanalysis techniques were used to analyze the phase distributions and chemical compositions of the RPCC samples. These RPCC test sites were selected based on subbase construction dates: 1983, 1988, 1994, and

2003. The RPCC aggregates used for these sites were recycled from PCC pavements that were constructed between 1967 and 1969. Table 3.1 provides the project locations and original pavement construction dates from which the RPCC was derived.

BACKGROUND

Microstructure of Cement Paste

To characterize features of RPCC using SEM and X-ray microanalysis, it is important to understand the microstructure of cement paste. Unhydrated cement grains are found in all or nearly all cement pastes. Most individual cement grains contain fragments of several different kinds of crystals in the clinker. These crystals included C_3S (tricalcium silicate), C_2S (dicalcium silicate), C_3A (tricalcium aluminate), C_4AF (tretracalcium aluminoferrite), $CS'H_2$ (calcium sulfate di-hydrate or gypsum), and several minor components. Clinker is normally ground to sizes between 2 μm to 80 μm, with the mean diameter of about 10-12 μm (Taylor 1997; Diamond 1976; Jennings and Pratt 1979). Stutzman (2004) used SEM and X-ray microanalysis to provide a quantitative assessment of the phases in portland cement.

The microstructure of cementitious systems is formed by the hydration of cement grains in the presence of water. Hydration of portland cement is mainly dominated by the reactions of C_3S (tri-calcium silicate) and C_2S (di-calcium silicate), producing C-S-H (calcium silicate hydrate) and calcium hydroxide (CH). These hydration products gradually increase, filling the spaces and forming a solid mass. C-S-H is a principal hydration product and is a poorly crystalline material that forms extremely small particles of less than 1 μm in any dimension. In contrast, calcium hydroxide is a crystalline material with fixed composition (Diamond 1976; Taylor 1979; Jennings and Pratt 1979).

C-S-H is produced by hydration of C_3S and C_2S in cement and is the most important hydration component that accounts for half of the volume of a hydrated paste. Two forms of C-S-H that are indentified in the microstructure of cement paste are *outer product* C-S-H and *inner product* C-S-H. The outer product C-S-H is formed during early hydration in the originally water-filled space and has a higher micro-porosity. It is probably admixed with monosulfoaluminate at the nanometer level and contains a high level of impurities. The inner product refers to the dense C-S-H coating around the hydrating cement grains that develop

within the boundaries of cement grains. The coatings form a diffusion barrier during final stages of hydration and become thicker with time by developing inwards. These hydration shells have smooth textures and are mostly uniform gray color (Diamond and Bonen 1995; Taylor 1997).

Diamond (1976) reported that for a fully hydrated cement paste, C-S-H makes up the largest proportion (by weight) of about 70% of cement hydration products. CH accounts for a lesser proportion of about 20%. Ettringite and monosulfatealuminate products are present in relatively minor amounts that account for about 7% together. Unhydrated cement and other constituents account for about 3% by weight.

Diamond (1986) reported that the total of cement hydration products increases with degree of hydration, as the unhydrated cement grains and the relative volume of pore space decrease. Taylor (1984) calculated the weight and volume proportions of each of the products in several specific portland and portland-fly ash pastes. For example, Taylor (1984) reported that a three-month old portland cement paste (cement/water = 0.5) in saturated state composed of 40% C-S-H gel, 16% calcium monosulfatealuminate, 12% CH, 8% of unhydrated cement, and 24% pore space by volume. When the concrete was recycled and used as RPCC aggregate for pavement subbase, an amount of unhydrated cement could be exposed to water in the subbase and improve the stiffness of the subbase through hydration process.

SEM and X-ray Microanalysis

SEM imaging and X-ray microanalysis techniques have been widely used to study the microstructure of concrete. Despite limitations of SEM analysis, such as two-dimensional surface analysis and only a small portion of the surface exposed in a given sample, backscatter-mode SEM (BSE) is the only imaging method that provides a clear assessment of the microstructure of cement paste (Diamond 2004). BSE has been widely used to investigate the microstructure of cement paste and concrete since the early 1980s (Scrivener and Pratt 1984; Diamond 2004).

Contrast in SEM images is generated when the composition of different phases of cement paste is related to the average atomic number of the compositions of the phases.

Differences in the brightness of the BSE signals reveal differences in chemical composition in the cement paste. Unhydrated cement grains, which have the highest electron backscatter coefficients (higher than hydrated products), appear brightest in backscatter images followed by calcium hydroxide, calcium silicate hydrate, and natural aggregate. Voids in the cement paste appear dark in SEM images. The size of unhydrated cement typically varies from 5 μm to 40 μm. (Kjellsen et al. 1990, 1991; Diamond 2004; Scrivener 2004).

X-rays are produced when a sample is struck by high-energy electrons. The X-rays can be analyzed by energy-dispersive or wavelength-dispersive spectrometers to report chemical composition of the scanned area. X-rays are used to identify the elements and their spatial distribution. For cementitious materials, X-rays are generated from an interaction volume of about 1-2 μm, which is comparable to the size of many hydrate phases, allowing the differentiation of the phases (Scrivener 2004).

TEST METHODS

This study included laboratory and field investigation tests of portland cement concrete (PCC) pavement subbases. Stiffness/strength characterization of these subbase layers was conducted using dynamic cone penetrometer (DCP) and Clegg impact hammer. The investigations were aimed at studying the performance of the pavement layers and comparing the stiffness of the RPCC subbases to those of the limestone aggregate subbases. The stiffness values of the RPCC subbases were also compared to amounts of unhydrated cement in the RPCC aggregates observed using SEM images.

Field Test

Field investigations were conducted at nine interstate and state highway sites in Iowa. Four sites had RPCC aggregate subbases, and five sites had crushed limestone aggregate subbases. At each site, five core holes, including one 250 mm (10 in.) core hole and four 100 mm (4 in.) core holes, were drilled through the PCC pavement layer to the subbase surface. Test holes were cored at the middle of the concrete slabs in the travel lane. DCP (ASTM. 2003) and Clegg impact hammer (ASTM. 2002) tests were conducted on the subbase layers through core holes.

Subbase stiffness was characterized by the weighted average values of dynamic penetration index (DPI_{avg}) and surface Clegg impact value (CIV). The DPI_{avg} of a subbase layer was obtained by averaging DPI values with depths for the whole thickness of the layer. DPI values were measured in mm per blow. Lower DPI_{avg} values indicated higher stiffness.

Clegg impact hammer tests use a drop weight and an accelerometer to indirectly determine the stiffness at the surface. CIV is measured as the rebound of the fourth blow of a standard 4.5 kg (9.9 lb) hammer. Higher CIVs reflect higher stiffness of the subbase layers. In this study, if a CIV measurement was outside of the device measurement range, a CIV value of 100^+ was recorded.

Laboratory Test

After field tests were conducted, samples of the subbase aggregate at all sites except the I-80-1988 site (site 7) were collected with a scoop. RPCC samples were obtained by coring at the I-80-1988 site (site 7) where the RPCC subbase was extremely stiff. All samples were carefully contained in sealed bags, buckets, or plastic bags; properly labeled; and transported to the laboratory for testing. The aggregate samples were performed mechanical analysis in the laboratory (AASHTO. 1993; AASHTO. 2002; ASTM. 2001; ASTM. 2004; ASTM. 2006a; ASTM. 2006b).

SEM and X-ray microanalysis was performed on the RPCC samples collected from the RPCC sites. The sample surface was brushed, air-pressure cleaned to remove fine aggregates. Epoxy was used to fill voids and stabilize the microstructure. Epoxy also created a contrast between pores and other chemical components. The sample was ground to expose a fresh surface that was polished using successively finer grades of silicon carbide paper and diamond paste to show the material's microstructure.

During the SEM and X-ray microanalysis, care was taken to collect images that provided the most representative microstructures of the RPCC samples. Images were selected to show the microstructure of the cement paste, cracks, air voids, and unhydrated cement grains. For each sample, two images were collected at 30x magnification. One image was collected near the center area of the sample and the other was taken at the edge of the sample. The low magnification images provided a preliminary analysis of the sample to evaluate how

the individual features fit together in the total structure. Details of microstructure features were observed in images collected at higher magnifications (100x, 300x, and 1000x).

RESULTS OF MECHANICAL ANALYSIS AND SUBBASE STIFFNESS

Field tests returned results of engineering properties and measures of stiffness of crushed limestone and RPCC aggregate subbases at all 28 sites in the study.

Engineering Properties

The RPCC aggregates collected from the core holes used for the field tests were classified as SW-SM, GP-GM, GW-GM, and GP (either poor-graded or well-graded sand to gravel); (ASTM. 2006a), or as A-1-a (AASHTO. 2002). Table 3.2 summarizes the engineering properties of the aggregate samples.

The RPCC aggregates oven-dry (OD) specific gravity varied from 2.14 to 2.21, and the saturated-surface-dry (SSD) specific gravity varied from 2.33 to 2.36. The absorption of RPCC aggregates varied from 6.4% to 8.9% (Table 3.2). The gradation of RPCC aggregate of site 8 was within the specification of Iowa DOT (2009) for RPCC subbase aggregate, while the RPCC aggregates of site nos. 6, 7, and 9 were finer than the average gradation for RPCC subbase aggregate provided by the specification (Figure 3.1).

Five crushed limestone subbases were constructed in 1990, 1993, and 2005. Crushed limestone aggregates were classified as poorly graded gravels with some silty gravel (GP-GM) (ASTM. 2006a), or as A-1-a (AASHTO. 1993). The OD specific gravity of the crushed limestone aggregates varied from 2.53 to 2.64, and the SSD specific gravity varied from 2.59 to 2.66. These values were about 20% higher than RPCC aggregate. The absorption of crushed limestone aggregates were from 0.8% to 2.4% (Table 3.2). Three of five gradations of crushed limestone aggregates were outside of the specification of Iowa DOT (2009) for subbase aggregate (Figure 3.1).

Stiffness/Strength of Subbases

In this study, *CIV* and *DPI*$_{avg}$ values were used to characterize the in situ stiffness/strength of crushed limestone and RPCC subbases (Figure 3.2). Although the Clegg

impact hammer test was conducted on the subbase surface while the DCP measured the subbase strength with depth, their results consistently reflected the stiffness of the subbases. Stiffer subbases resulted in higher *CIV* and lower *DPI*$_{avg}$ values (Table 3.2). According to the test results, RPCC subbase layer from the I-80-1988 site (site 7) was the stiffest subbase layer compared with those of the other sites. This layer provided the lowest value of *DPI*$_{avg}$, while its *CIV* value was outside the measurement range of the device (i.e., high stiffness).

Comparison of the stiffness of the crushed limestone and RPCC subbases suggest that RPCC subbases were generally stiffer than the crushed limestone subbases. The average *DPI*$_{avg}$ value of the RPCC subbases (3.8) was 50% that of the crushed limestone subbases (7.5). The average *CIV* (69) of the RPCC subbases was 222% of that (31) of the crushed limestone subbases (Figure 3.2). The results of DCP and Clegg impact hammer also showed that variability in the stiffness values of the RPCC subbases was higher than variability in the stiffness values of the crushed limestone subbases. The coefficient of variation of the *CIV*s should be higher than 35% given the fact that the RPCC subbase layer at the I-80-1988 site (site 7) was so stiff that the *CIV* value was outside of the measurement range.

Results of the stiffness comparison suggested that RPCC subbases were generally stiffer than crushed limestone subbases, and the stiffness of RPCC subbases were consistently reflected in *CIV* and *DPI*$_{avg}$ values. These results had led to a question of whether the hydration of some amounts of unhydrated cement in RPCC aggregates when these amounts of cement were exposed to water had improved strength/stiffness to the RPCC subbases. Further, whether the RPCC aggregates containing higher amounts of unhydrated cement provided higher strength/stiffness of the RPCC subbases.

RESULTS OF SEM AND X-RAY MICROANALYSIS OF RPCC AGGREGATE SAMPLES

Unhydrated Portland Cement Grains

SEM images of the four RPCC aggregate samples showed unhydrated cement grains in the recycled concrete in all of the samples (Figure 3.3). The unhydrated cement grains appeared as bright white areas ranging in size from several μm to more than 100 μm. However, limited amounts of unhydrated cement grains found in sample I-35-2003 (site 9)

(Figure 3.3). Unlike the hardened fresh concrete samples where hydration shells surrounding unhydrated cement grains and other hydrated components were observed (Diamond 2004), hydration products of old cement pastes seemed to intermix with each other, resulting in a gray color. No hydration shells were observed from SEM images of these four RPCC samples.

The areas of unhydrated cement grains measured from SEM images of the RPCC samples (300x magnification) were used to determine the amounts of cement existing in the samples. The measurement results showed that the I-80-1988 site (site 7) had the highest area of unhydrated cement grains that accounted for 10.6% of its SEM image area. The maximum grain size of unhydrated cement of this sample was larger than 100 μm (Figure 3.3). This RPCC sample was considered to contain the highest amounts of unhydrated cement compared to three other RPCC samples.

Unhydrated cement areas of samples I-35-1983, I-80-1994, and I-35-2003 (from sites 6, 8, and 9, respectively) accounted for 4.8%, 2.8%, and 2.3% of the total image areas, respectively. The I-35-1983 sample (site 6) with an unhydrated cement grain size of about 50 μm had less unhydrated cement than the I-80-1988 sample. The I-80-1994 sample (site 8) had fewer unhydrated cement grains than either sample I-35-1983 (site 6) or I-80-1988 (site 7).

C-S-H

The SEM images on the cross sectional surfaces of four RPCC samples (Figure 3.3) were collected on the inside areas of the samples where hydrated products were denser and had fewer impurities than those on the outside areas near the edge of the samples. The images showed that the hydrated components were mostly composed of C-S-H, unhydrated cement grains, and ettringite. The SEM image of the sample from site I-35-1983 (site 6) shows that the *inner product* C-S-H intermixed with other hydration products in the groundmass, and the hydrated shells were not observed (Figure 3.3). Irregularly textured areas surrounding cement grains suggested that the areas were originally formed from filled space. These areas appeared darker than the inner hydration shells and contained deposits of other minor hydration products, such as ettringite and monosulfate. Hydrated components

with low level of impurities were found in SEM images of samples I-80-1988, I-80-1994, and I-35-2003 (sites 7, 8, and 9). Single hydration shells were not recognized in these samples, but instead, masses of inner product C-S-H surrounded the unhydrated cement grains.

Calcium Hydroxide

Calcium hydroxide, CH, crystals grow within capillary pore spaces and normally stop developing or developing around hydrating cement grains that the crystals encounter. CH in cement pastes usually appears as irregular masses of various sizes. In SEM images, CH appears as a slightly brighter gray color than C-S-H gel (Mindess et al. 2002; Diamond 2004).

However, CH was not easily observed within the matrix of the RPCC cement pastes, though it could be identified using X-ray elemental maps from SEM images. In sample I-80-1988 (site 7), the area containing CH was identified on the X-ray elemental map for its brightness intensity of O and Ca (Figure 3.5 and Figure 3.6). The presence Si was not detected in this area. These characteristics were applied for CH identification of other samples. Hydration products of sample I-35-1983 (site 6) had high level of impurities and no obvious CH crystals were observed. The hydrated products of samples I-80-1988 and I-80-1994 (sites 6 and 7) had low levels of impurities, appearing in a gray color at a similar level of brightness. Calcium hydroxide appeared in slightly bright gray color and was observed in irregular shapes (Figure 3.3).

Aluminate Containing Phases

The hydration of C_3A leads to the formation of hydration products containing aluminum. At early ages, calcium sulfoaluminate hydrate (6-calcium aluminate trisulfate-32-hydrate), which is commonly called "ettringite", is the product of tricalcium aluminate with sulfate ions that are supplied by the dissolution of gypsum. Ettringite masses in cement paste usually appear in shrinkage pattern of curved cracks that resemble "tiger stripe" morphology. At later ages, if the sulfate is all consumed before the C_3A has completely hydrated, then the ettringite reacts with the available C_3A, forming monosulfate. Under some conditions, ettringite may re-crystallize in pores and voids into large masses. Ettringite is found in old

cement paste in needle-like shapes (Diamond 2004; Scrivener 2004).

Ettringite masses were found in the RPCC aggregates samples from all four sites (Figure 3.3 – Figure 3.5). Individual crystals of the ettringite masses from sample I-35-1983 (site 6) seemed to intermix with C-S-H and were not clearly identified (Figure 3.3). In contrast, although the ettringite crystals in samples I-80-1988, I-80-1994, and I-35-2003 were from old concrete materials, the crystals were obvious in the SEM images (Figure 3.4, Figure 3.5).

Pore Space and Cracks

SEM images typically show visible pore spaces in most cement pastes. The actual content of these pore spaces depends mostly on water/cement ratio and air entrainment. The visible pore spaces observed on the images of four RPCC samples were either filled by epoxy resin or ettringite masses. The epoxy resin that filled the pore spaces in prepared samples causes dark areas on the SEM images. High numbers of visible pore spaces filled with ettringite masses were detected in samples I-80-1988, I-80-1994, and I-35-2003 (sites 7, 8, and 9) (Figure 3.3 – Figure 3.5). These pore spaces were interconnected by cracks. Pore space was not identified in the sample I-35-1983, although an amount of ettringite mass was observed in the sample using the SEM images. Also, not many cracks were observed in the sample I-35-1983 (site 6).

DISCUSSION

RPCC subbases were generally stiffer than crushed limestone subbases. Results of the DCP tests showed that the average DPI_{avg} value of RPCC subbases was about 50% of that of the crushed limestone subbases, while the average CIV of the RPCC subbases was about 222% of the average CIV of the crushed limestone subbases. These results, incorporating with the results of the SEM and X-ray microanalysis of the RPCC aggregates, suggested that hydration of unhydrated cement in RPCC aggregates increased stiffness of the RPCC subbases.

During construction, unhydrated cement grains in the RPCC aggregates exposed to the atmosphere when the aggregates are broken up under compaction loads. Additional

amounts of unhydrated cement expose to the surrounding environment when more cracks appear and develop in the PCC pavement and/or subbase aggregates under repeating traffic loads. These unhydrated cement grains react with pore water in the subbase to produce hydration products that partly improve the stiffness of the RPCC subbase.

The SEM images of four RPCC sites showed that the RPCC sample collected from the stiffest site, site I-80-1988 (site 7), which had the highest *CIV* and the lowest value of *DPI*$_{avg}$, contained the highest amount of unhydrated cement. The limited amount of unhydrated cement measured from the SEM image of sample I-35-2003 suggested that the RPCC subbase from site 9 was the least stiff. This relationship between the amount of unhydrated cement in the RPCC aggregates and subbase stiffness was not obvious when compared to stiffness values and amounts of unhydrated cement of sites I-35-1983 (site 6) and I-80-1994 (site 8). The RPCC subbase of site 8 was stiffer than that of site 6, but less unhydrated cement was measured in the SEM image of the I-80-1988 RPCC (site 8). However, the differences in stiffness values and the amounts of unhydrated cement from these two sites were not significant.

The relationship between the amounts of unhydrated cement in RPCC aggregates and the stiffness of RPCC subbases were examined using field test results and SEM images (Figure 3.2, Figure 3.3). Stiffness of a RPCC subbase was found to be proportional with the amount of unhydrated cement of the RPCC aggregates of that subbase. RPCC subbases using RPCC aggregates with higher amounts of unhydrated cement were stiffer than those using RPCC aggregates with lower amounts of unhydrated cement. Given that the RPCC subbases were constructed using RPCC aggregates of similar gradations and with similar compaction efforts, more cement grains from RPCC aggregates with higher amounts of unhydrated cement were able to expose, and eventually produced more hydration products with the appearance of water. As the result, higher amounts hydration products provided better improvement to the stiffness of the subbases.

CONCLUSION

Field results indicated that RPCC aggregate subbases were stiffer than crushed limestone aggregate subbases. The average *CIV* and *DPI* values of stiffness of the RPCC

subbases were between 200% and 222% of the *CIV* and *DPI* values of crushed limestone aggregate subbases. SEM and X-ray microanalysis in the laboratory analyses revealed that RPCC aggregates contained unhydrated cement. When RPCC aggregates were used for pavement subbases, some mounts of unhydrated cement grains exposed to the surrounding environments and reacted with water. The hydration of these cement grains increased the stiffness/strength of the RPCC subbases. The amounts of unhydrated cement existing in RPCC aggregates also affected the subbase stiffness through hydration products. RPCC aggregates with higher amounts of unhydrated cement provided higher strength/stiffness values to the subbases than RPCC aggregates with lower amounts of unhydrated cement.

ACKNOWLEDGEMENTS

REFERENCES

AASHTO. (1993). Standard specification for aggregate and soil-aggregate subbase, base and surface courses M 147-70, Part I Specifications, 16th Ed., American Association of State Highway and Transportation Officials, Washington, D.C.

AASHTO. (2002). Standard specification for reclaimed concrete aggregate for unbound soil aggregate base course M 319, American Association of State Highway and Transportation Officials, Washington, D.C.

ASTM. (2001). "Standard Test Method for Density, Relative Density (Specific Gravity), and Absorption of Coarse Aggregate." Annual book of ASTM standards, ASTM C127, West Conshohocken, PA.

ASTM. (2002). "Standard Test Method for Determination of the Impact Value (IV) of a Soil." Annual book of ASTM standards, ASTM D5874, West Conshohocken, PA.

ASTM. (2003). "Standard Test Method for Use of the Dynamic Cone Penetrometer in Shallow Pavement Applications." Annual book of ASTM standards, ASTM D6951, West Conshohocken, PA.

ASTM. (2004). "Standard Practice for Classification of Soils and Soil-Aggregates Mixtures for Highway Construction Purposes." Annual book of ASTM standards, ASTM D3282, West Conshohocken, PA.

ASTM. (2006a). "Standard Practice for Classification of Soils for Engineering Purposes (Unified Soil Classification System)." Annual book of ASTM standards, ASTM D2487, West Conshohocken, PA.

ASTM. (2006b). "Standard Test Method for Sieve Analysis of Fine and Coarse Aggregates." Annual book of ASTM standards, ASTM C136, West Conshohocken, PA.

Bruinsma, J. E., Peterson, K. R., and Snyder, M. B. (1997). "Chemical approach to formation of calcite precipitate from recycled concrete aggregate base layers." *Trans. Research Record: J. Trans. Research Board*, No. 1577, 10-17.

Diamond, S. (1976). "Cement paste microstructure – an overview at several levels." in *Hydraulic cement pastes: their structure and properties*, proceedings of a conference at Sheffield, University of Sheffield, Sheffield, England, 2-31.

Diamond, S. (1986). "The microstructures of cement paste in concrete." *8th Int. Congr. Chem. of Cement*, Rio de Janeiro, 1, 123-147.

Diamond S and Bonen D. (1995). "A re-evaluation of hardened cement paste microstructure based on backscatter SEM investigations." In: Microstructure of Cement-Based Systems/Bonding and Interfaces in Cementitious Materials. Diamond S, Mindess S, Glasser FP, Roberts LW, Skalny JP, Wakeley LD, editors, *Materials Research Society Symposium Proceedings*, Pittsburgh: Materials Research Society, 370, 13-22.

Diamond, S. (2004). "The microstructure of cement paste and concrete – a visual primer." *Cement & Concrete Composites*, 26, 919-933.

Iowa Department of Transportation (2009). "General supplementation of specifications for highway and bridge construction - GS-01016." <http://www.iowadot.gov/specifications/new_docs/Complete%20GS-01016.pdf> (Jul. 10, 2010).

Jennings, H. M. and Pratt, P. L. (1979). "On the hydration of portland cement." *Proc. British Ceramic Society*, edited by D. Taylor and P.S. Rogers, 28, 179-193.

Kjellsen, K. O., Detwiler, R. J. and Gjorv, O. E. (1990). "Backscattered electron imaging of cement pastes hydrated at different temperatures." *Cement and Concrete Research*, 20(2), 308-311.

Kjellsen, K. O., Detwiler, R. J. and Gjorv, O. E. (1991). "Development of microstructures in plain cement pastes hydrated at different temperatures." *Cement and Concrete Research*, 21(1), 179-189.

Mindess, S., Young, J. F., and Darwin, D. (2002). "Concrete." 2nd Ed., Prentice Hall, Upper Saddle River, NJ.

Scrivener, K. L. and Pratt, P. (1984). "Backscattered electron images of polished cement sections in the scanning electron microscope." In Bayless J., editor. *Proc. 6th Int. Conf. Cement Microscopy*, Albuquerque. Duncanville, TX: ICMA; 145-155.

Scrivener, K. L. (2004). "Backscattered electron imaging of cementitious microstructures: understanding and quantification." *Cement & Concrete Composites*, 26, 935-945.

Stutzman, P. (2004). "Scanning electron microscopy imaging of hydraulic cement." *Cement & Concrete Composites*, 26, 957-966.

Taylor, H. F. W. (1979). "Mineralogy, microstructure and mechanical properties of cements." *Proc. British Ceramic Society*, 35, 65-82.

Taylor, H. F. W. (1984). "Studies on the chemistry and microstructure of cement pastes." *Proc British Ceramic Society*, edited by D. Taylor and P.S. Rogers, 28, 147-163.

Taylor, H.F.W. (1997). "Cement chemistry." 2nd Ed., London: Thomas Telford.

White, D. J., Ceylan, H., Jahren, C. T., Phan, T. H., Kim, S., Gopalakrisnan, K., and Suleiman, M. T. (2008). "Performance evaluation of concrete pavement granular subbase – pavement surface condition evaluation." Final Report, Iowa DOT Project TR-554, CTRE Project 06-250, Iowa Department of Transportation, Ames, IA.

Table 3.1. Properties of crushed limestone and RPCC aggregates

Site number	Site name	Subbase material	Batching year[a]	Construction year[b]
1	US-20E		–	1990
2	US-20W		–	2005
3	US-30E	Crushed limestone	–	2005
4	I-235S		–	2005
5	IA-92E		–	1993
6	I-35-1983		1967	1983
7	I-80-1988	RPCC	1969	1988
8	I-80-1994		1968	1994
9	I-35-2003		1969	2003

Notes: [a] Year the original PCC pavement was constructed (Iowa DOT Milepost book 2005);
[b] Year the original PCC pavement was recycled and was used for the subbase in new construction.

Table 3.2. Mechanical properties of aggregates and field measurement values of the subbases

Site no.	Classification		OD[a]	SSD[b]	Absorption[c] (%)	CIV	DPI_{avg}[e] (mm/blow)
	ASTM. 2006a	AASHTO. 1993; AASHTO. 2002					
1	GP–GM	A–1–a	2.64	2.66	0.8	30	9.0
2	GP–GM	A–1–a	2.59	2.62	1.2	22	12.0
3	GP–GM	A–1–a	2.55	2.61	2.4	38	4.7
4	GP–GM	A–1–a	2.58	2.63	1.9	27	7.6
5	GP–GM	A–1–a	2.53	2.59	2.4	39	4.0
6	SW–SM	A–1–a	2.18	2.36	8.2	52	4.0
7	GP–GM	A–1–a	2.14	2.33	8.9	100[d]	1.5
8	GW–GM	A–1–a	2.20	2.36	7.2	74	3.0
9	GP	A–1–a	2.21	2.35	6.4	48	6.5

Notes: [a] Oven-dry specific gravity; [b] Saturated-surface-dry specific gravity; [c] Dry to saturated-surface-dry; [d] The actual *CIV* value was outside of measurement range due to hard material surface; [e] The weighted average value over the subbase thickness, which varies from 200 mm to 280 mm.
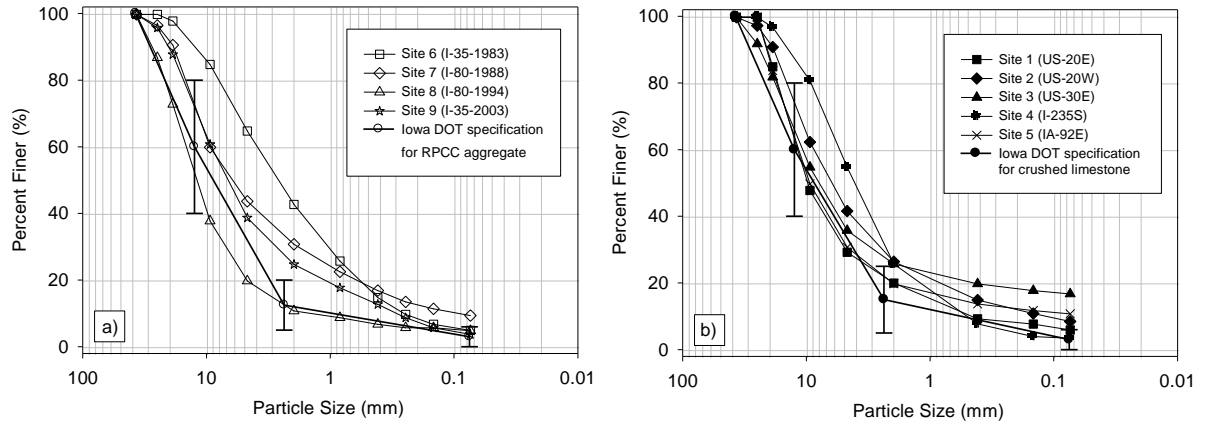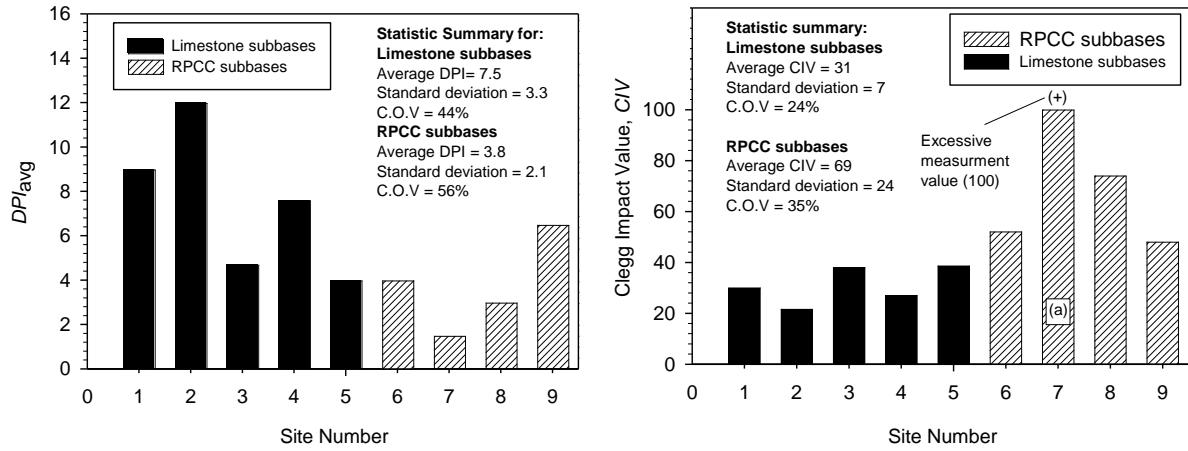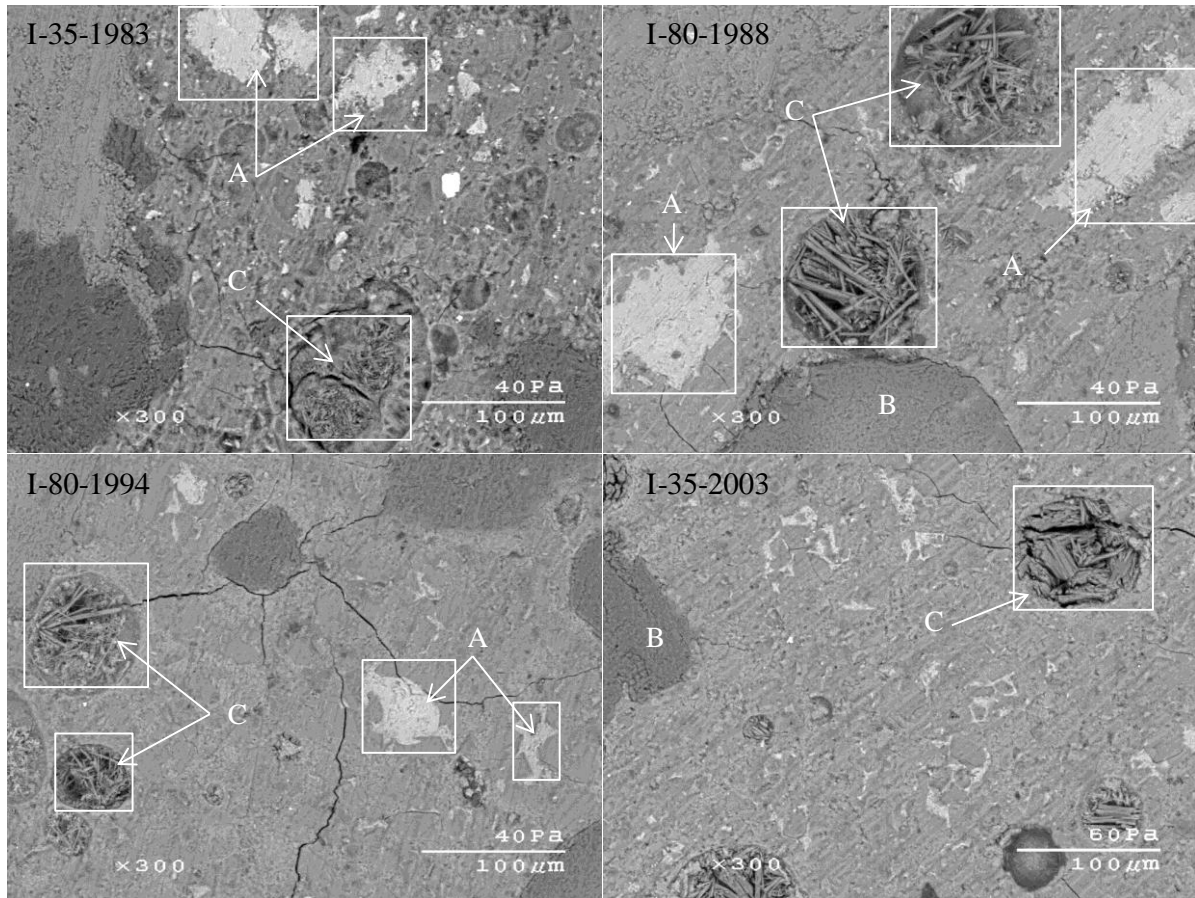
Figure 3.1. Sieve analysis of: a) RPCC aggregates; b) crushed limestone aggregates
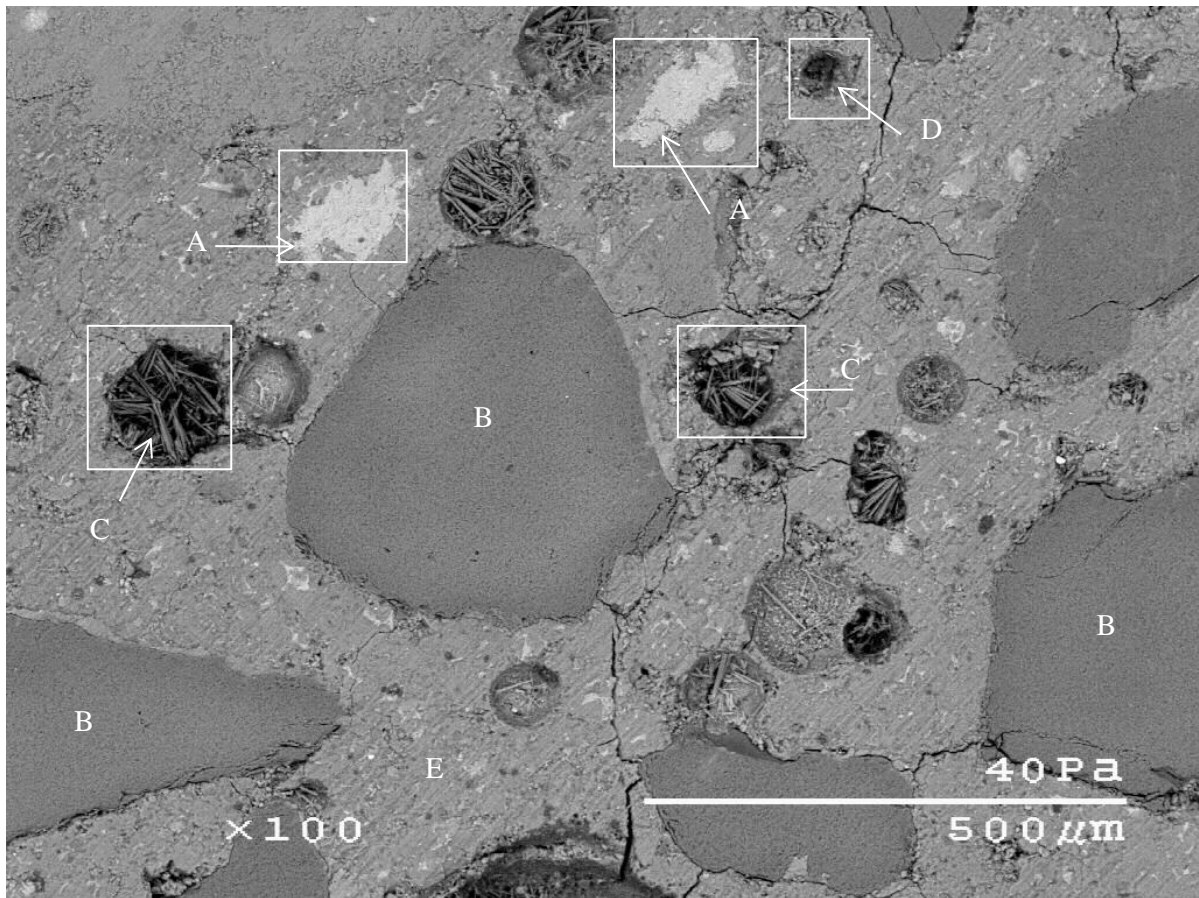
Note: (a) − the actual *CIV* value was outside of measurement range because of stiff surface

Figure 3.2. Comparison of *DPI*_{avg} values and *CIV*s of crushed limestone and RPCC aggregate subbases

Notes: A–unhydrated cement grains; B–aggregate; C–ettringite.

Figure 3.3. SEM images of I-35-1983, I-80-1988, I-80-1994, and I-35-2003 samples
(300x magnification)

58

Notes: A–unhydrated cement grains; B–aggregate; C–ettringite; D–void space; and E–intermixed C-S-H and other products.

Figure 3.4. SEM image of sample I-80-1988 (site 7) (100x magnification)
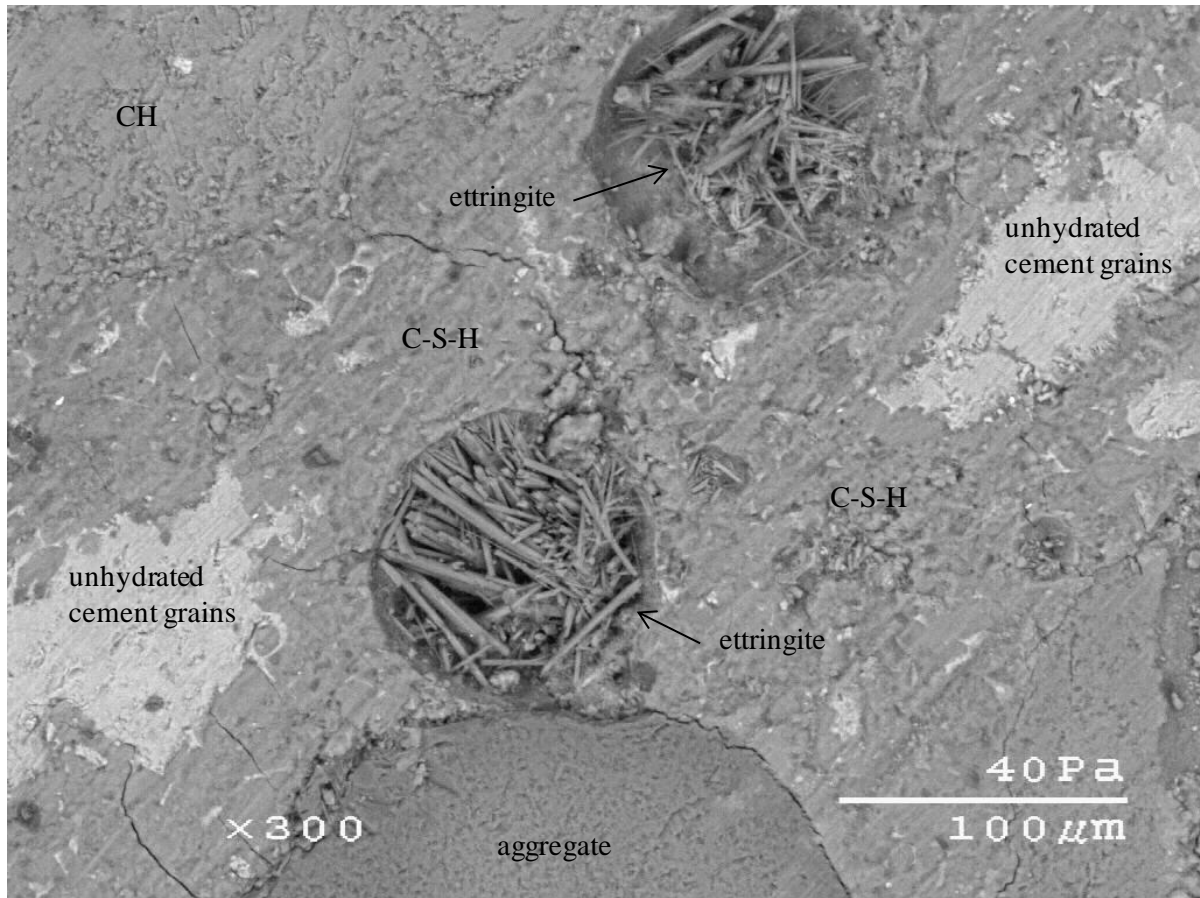
59

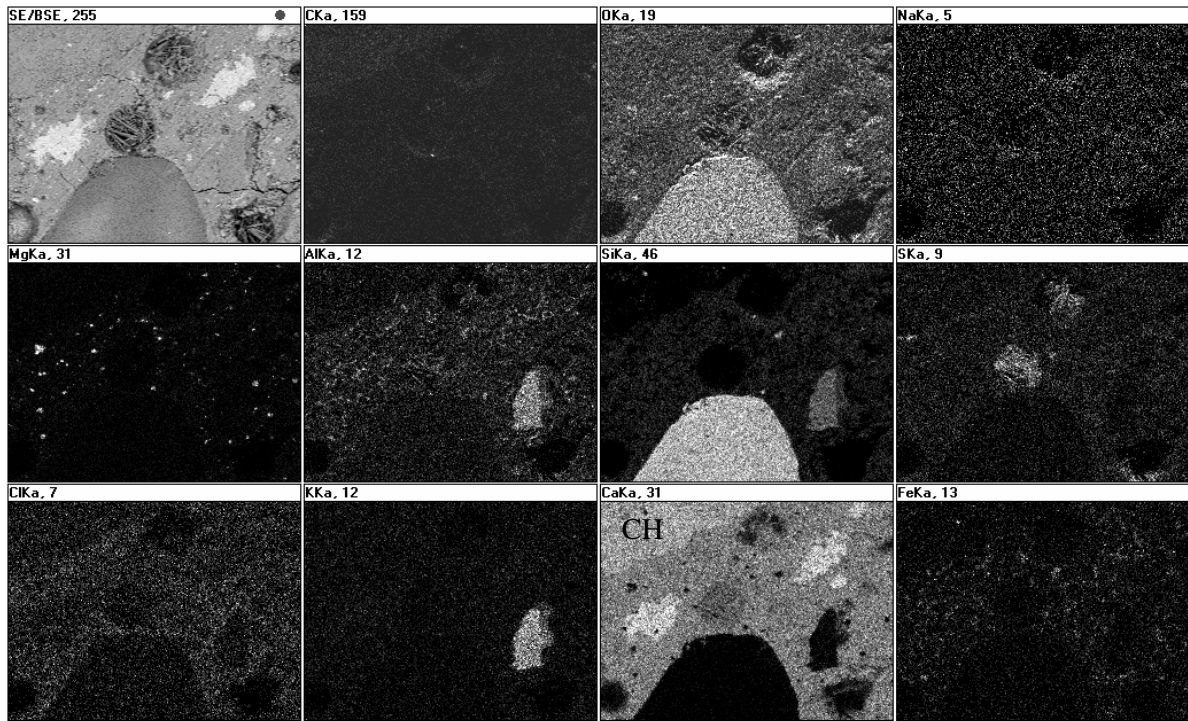Figure 3.5. Hydration products of sample I-80-1988 (300x magnification)

Figure 3.6. X-ray elemental map of sample I-80-1988 (200x magnification)

CHAPTER 4: TUFA PRECIPITATE FORMATION FROM RECYCLED PORTLAND CEMENT CONCRETE SUBBASES

Modified from a paper to be submitted to the *Journal of Materials in Civil Engineering, ASCE*

Thang H. Phan[1], David J. White[2], Warren E. Straszheim[3], and Peter Taylor[4]

ABSTRACT

Recycled portland cement concrete (RPCC) aggregate material has been widely used for pavement subbases in Iowa. Previous studies suggest that calcium hydroxide in the RPCC subbases is responsible for the deposition of calcium carbonate in highway subdrains. In this study, field investigations were performed at 18 rigid pavement sites supported by RPCC subbases. Extensive tufa formation was observed at the subdrain outlets and flow channels at two RPCC sites. Soil and water samples were collected from a flow channel of one site for pH testing in the laboratory. Spatial analysis was performed to analyze the distribution of pH values of soil in the flow channel. RPCC aggregate samples were tested using thermogravimetric analysis (TGA). Tufa samples were collected from one RPCC site for scanning electron and microscopy (SEM) and X-ray microanalysis. Results showed that pH values of water samples varied from 11.7 to 12.5 and that pH values of soil samples varied from 6.7 to 9.8. TGA test results showed that the amounts of calcium hydroxide in RPCC cement paste varied from 10.9% to 21.7% (by weight). Ca^{2+} ions from calcium hydroxide in RPCC cement paste were the main donor for calcite precipitate of RPCC subbases. Tufa was composed of a dense part and a flaky part with different morphologies and elemental composition. The dense part was composed mostly of calcite, while the flaky part was composed mostly of C-S-H, a cement hydration product.

---

[1] Graduate Research Assistant (corresponding author), Iowa State University of Science and Technology, 2711 South Loop Drive, Suite 4700, Ames, IA 50010-8664; thphan@iastate.edu

[2] Associate Professor, Iowa State University of Science and Technology, 422 Town Engineering, Ames, IA 50011-3232; djwhite@iastate.edu

[3] Associate Scientist, Iowa State University of Science and Technology, 46 Town Engineering, Ames, IA 50011-3230; wesaia@iastate.edu

[4] Associate Director, National Concrete Pavement Technology Center, 2711 South Loop Drive, Suite 4700, Ames, IA 50010-8664; ptaylor@iastate.edu

INTRODUCTION

In Iowa where recycled portland cement concrete (RPCC) pavement subbase has been used for about 30 years, field personnel have observed the presence of tufa blocking subdrains. Tufa has reduced the permeability of subbases, damaged of vegetation, and may cause pavement shoulders to erode (Steffes 1999; White et al. 2008).

In 1993, a survey about the use of slag and/or RPCC as subbase aggregates and related tufa problems was sent to all 50 state departments of transportation (DOT). Forty-three state DOTs responded, and of those, 23 states reported the use of RPCC aggregate for pavement subbase material. Of these 23 state DOTs, 8 state DOTs, including the Iowa DOT, reported tufa problems (Gupta and Kneller 1993). The survey indicated that not all RPCC subbase aggregates produced tufa, however. Although precipitate potential was previously studied, it was still not clear why tufa precipitates did not form at all sites using RPCC subbase.

In this study, field investigations were performed on 18 rigid pavement sites using RPCC aggregate subbase in Iowa. Samples were collected from the RPCC subbases through core holes at the center areas of the pavements for thermogravimetric analysis (TGA) to access tufa potential. Subdrain outlets and flow channels along the pavements at each site were examined to assess the extent of any tufa problem. Tufa samples were collected from a subdrain outlet of one site that had tufa precipitate and were analyzed using scanning electron microscopy (SEM) and X-ray techniques. Spatial analysis of pH distribution in a flow channel along an RPCC subbase was conducted.

LITERATURE REVIEW

Previous studies (Narita et al. 1980; Gupta and Kneller 1993; Gupta and Dollimore 2002) on potentials of producing tufa of pavement subbases using RPCC and/or slags aggregates considered free lime [CaO] as a chemical component to produce tufa. However, the term free lime was not consistently defined among these studies. For instance, Gupta and Kneller (1993) considered the total original free lime of a sample as the sum of CaO existing in the sample and the calculated percentages of CaO from calcium hydroxide [$Ca(OH)_2$] and calcite [$CaCO_3$]. In contrast, Narita et al. (1980) and Gupta and Dollimore (2002) considered

free lime as only the amount of calcium oxide [CaO] present in the RPCC aggregates. In fact, free lime is a chemically unstable substance and will weather over time through reactions with moisture and carbon dioxide dissolved in water.

In a study of weathering mechanism of Linz-Donawitz slags, Narita et al. (1980) suggested that slags containing more than 1% of CaO were likely to produce tufa. In later studies on the precipitate potential of pavement subbases using RPCC aggregates (Gupta and Kneller 1993; Snyder 1995; Bruinsma et al. 1997; Gupta and Dollimore 2002), the authors compared the percent of CaO in RPCC aggregates with this reported amount of 1% of CaO to determine whether these subbases were likely to produce tufa.

In the study of Gupta and Dollimore (2002), RPCC samples were prepared from 150 mm (6 in.) diameter cores of the entire thickness of portland cement concrete (PCC) pavement. Coarse and fine aggregates, which were obtained from crushing PCC cores, were considered as RPCC aggregates. Ethylene glycol tests (also known as "sugar" tests) were used to determine the amounts of free lime in RPCC samples. Test results showed that the amount of free lime in each of 46 RPCC samples was less than 1% or negligible. On the basis of the study of Narita et al. (1980), Gupta and Dollimore (2002) determined that these samples were not likely to produce tufa because of the amount of free lime in each sample was less than 1%.

Drever (1988) determined precipitate potential of a solution based on the concentration of calcium ions in the solution. The author used the ratio of magnesium ions to calcium ions (Mg/Ca) to determine saturated conditions of the solution with respect to calcium ions. If the Mg/Ca ratio was 0.6, the solution was considered to be saturated. When the ratio was higher than 0.6, the solution was considered to be supersaturated of calcium ions and ready to produce calcium carbonate or tufa.

In another study, Gupta and Dollimore (2002) reported that the concentration of calcium ions was found to reach maximum at around 24 hours. After 24 hours, the concentration of magnesium ions increased while the concentration of calcium ions decreased. Gupta and Dollimore (2002) reported that the concentration of calcium ions was initially higher than that of magnesium. Calcium ion concentration reduced compared to magnesium ion concentration after it reached equilibrium condition. The authors

recommended that the use of RPCC aggregates should be limited to coarse sizes, and that the RPCC aggregates used for base or subbase layers should have a Mg/Ca ratio lower than 0.6. However, they did not propose a minimum grain size for the RPCC aggregates.

Bruinsma et al. (1997) developed a model for calcite precipitation in RPCC drainage and derived the components that take part in the formation of tufa. The authors reported that natural rainwater in equilibrium with the atmosphere was slightly acidic with the pH level of 5.7 and was able to dissolve portlandite in the RPCC aggregates. The dissolution of portlandite at equilibrium in RPCC subbase pore water produces a pH level of 11.75. The pH level of calcite precipitation at equilibrium was found to be 8.3 (Bruinsma et al. 1997). The residence time of pore waters in RPCC subbase layers was considered to be important in controlling the formation of tufa precipitate.
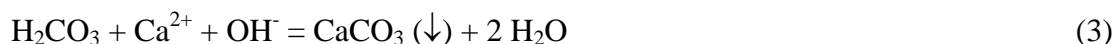
Leaching experiments were developed in the laboratory to study the effects of acidic water on the RPCC aggregates (Steffes 1999; Gupta and Dollimore 2002). Steffes (1999) conducted leaching tests by allowing distilled water to flow through a box containing RPCC material. The pH values of the water collected from the boxes were recorded on a weekly basis for one year. Results of the tests showed that pH values of the water collected from the RPCC boxes rose to the range of 12.5, and then gradually decreased and leveled at around 11.5 until the end of the tests after one year. Considerable amounts of calcium carbonate deposits were observed around the outlet holes of the boxes.
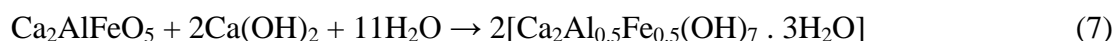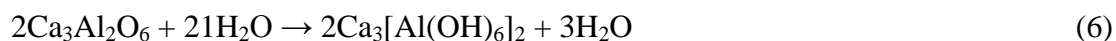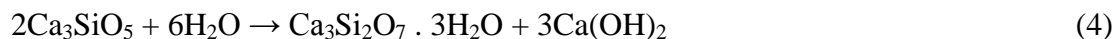
FORMATION OF TUFA PRECIPITATE

Previous studies have indicated that RPCC aggregates can produce calcite precipitates, but that natural aggregates, such as gravel and crushed limestone, do not produce calcite precipitates (Ford 1987; Muethel 1989; Tamirisa 1993; and Steffes 1999). These studies suggested that tufa deposits are the products of reactions between calcium hydroxide (CH), and other calcium-based compounds in portland cement paste, and carbon dioxide dissolved in water. According to Bruinsma et al. (1997), Ca^{2+} ion from CH in cement paste is the main source to produce tufa precipitate. For a fully hydrated cement paste, CH makes up about 20% by weight (Diamond 1976). CH from cement paste of RPCC aggregates dissolves to pore waters in RPCC subbases, resulting in high concentrations of Ca^{2+} and OH^-

ions. These pore waters have pH values varying from 10 to 12 (Muethel 1989; Tamirisa 1993; Bruinsma et al. 1997; and Steffes 1999).

Carbon dioxide plays an important role in precipitation of calcium carbonate of RPCC subbase. However, the precipitation process does not take place in the RPCC subbase where pore waters are mostly isolated from atmospheric CO_2 by the overlying pavement layer. Although a portion of rainwater containing carbonic acid infiltrates into the RPCC subbases through pavement cracks and joints, this amount of carbonic acid is not sufficient for large-scale precipitation of calcite. Therefore, pore waters within the RPCC subbase contain high levels of Ca^+ concentration. When the pore waters flow out of the subdrain outlets and are exposed to CO_2 in the atmosphere that contains, calcite precipitation is formed according to the following equations (Bruinsma et al. 1997):

$$CO_2 (g) = CO_2 (aq) \tag{1}$$

$$CO_2 (aq) + H_2O = H_2CO_3 \tag{2}$$

$$H_2CO_3 + Ca^{2+} + OH^- = CaCO_3 (\downarrow) + 2 H_2O \tag{3}$$

Hydration products from unhydrated cement in RPCC subbase aggregates are also considered to be parts tufa precipitate. In a parallel study on the microstructure of RPCC aggregates, Phan et al. (2010) reported that certain amounts of unhydrated cement grains existing in RPCC subbase aggregates. Under compaction during road construction and traffic loads when the RPCC subbase is in service, a portion of unhydrated cement from RPCC aggregates is exposed to pore waters to produce hydration products. The following equations summarize major calcium silicate hydration reactions that produce hydration products (Ghosh 1983):

$$2Ca_3SiO_5 + 6H_2O \rightarrow Ca_3Si_2O_7 . 3H_2O + 3Ca(OH)_2 \tag{4}$$

$$2Ca_2SiO_4 + 4H_2O \rightarrow Ca_3Si_2O_7 . 3H_2O + Ca(OH)_2 \tag{5}$$

$$2Ca_3Al_2O_6 + 21H_2O \rightarrow 2Ca_3[Al(OH)_6]_2 + 3H_2O \tag{6}$$

$$Ca_2AlFeO_5 + 2Ca(OH)_2 + 11H_2O \rightarrow 2[Ca_2Al_{0.5}Fe_{0.5}(OH)_7 . 3H_2O] \tag{7}$$

According to Diamond (1976), calcium silicate hydrate (C-S-H) and CH produced in equations 4 and 5 are two major products that accounts for 70% and 20% (by weight), respectively, of cement hydration. Ettringite and monosulfatealuminate products are present in relatively minor amounts that account for about 7% together. Other constituents account for about 3% by weight. Therefore, C-S-H is considered the major product that partially contributes to the formation of tufa precipitate of RPCC subbases.

TEST METHODS

This study included field investigations at 18 RPCC subbase sites to report tufa at the subdrains and flow channels. RPCC aggregate samples were collected from these RPCC sites for TGA in the laboratory. Spatial variation of pH values of the flow channel along one RPCC subbase (site 2) was conducted using in situ mapping and sampling of soil samples for pH tests in the laboratory. Soil and water samples were collected from different locations in the channel for pH testing in the laboratory. Tufa samples were collected from a subdrain outlet of this site for scanning electron microscopy (SEM) and X–ray microanalysis.

Field Investigations at RPCC Subbases

Field investigations were conducted in 2007 at 18 RPCC aggregate subbase sites that were geographically distributed throughout Iowa and that had been in service for 1–24 years. Test holes were cored in the middle of the concrete slabs in the travel lane and patched after testing to prevent future damage by traffic. Samples were collected from the RPCC subbases through core holes of the pavements, contained in buckets and labeled for laboratory experiments. Subdrain outlets and flow channels along the pavements at each site were examined by observation to determine whether or not a tufa problem existed at each site (Table 4.1).

pH Mapping of a Flow Channel Along an RPCC Subbase

A field investigation was conducted in a flow channel along interstate highway I 35 southbound, at the milepost 125.20 in Story County, Iowa on July 7, 2008. The highway at this location, which was constructed in 1999, consisted of a portland cement concrete (PCC)

pavement layer, a subbase layer using RPCC aggregates, and subgrade layers. A GPS rover with 2 cm accuracy was used to locate sampling points and to create an elevation map of the test area on the flow channel.

An area of about 68.6 m (225 ft) long and 15.2 m (50 ft) wide in the flow channel along the pavement shoulder was selected for elevation mapping and soil sampling. The test area was started at two subdrains that had extensive tufa and was developed over the flow channel. Cloth strings were used to create a mesh of test points in the area. Test points were marked along the strings to collect soil samples for pH tests in the laboratory. Coordinates and elevations of test points were measured using the GPS device. Soil samples at each test point were collected using a soil sampler and contained in a closed plastic bag, which was properly labeled, and transported to the laboratory for pH tests.

pH Tests

Soil samples collected from the field were air-dried for 24 hours in the laboratory environment. Each dry sample was mixed with distilled water using a ratio of 1:1 by weight and tested using an electronic pH meter (Accumet XL20) in the laboratory following the Standard Test Method for pH of Soils (ASTM. 2007).

TGA

In TGA, percents of weight loss of a sample are visually determined based on the TGA plot, its DTG, and the ranges of temperatures that certain reactions occurred. The mass of the initial sample, atmosphere, and heating rate were factors that determined temperature ranges of the reactions. In this study, the TGA curves showed two major changes in weight loss, indicating two reactions of the cement paste fraction of the RPCC aggregates. For each sample, the starting and ending temperatures of each reaction were identified from the DTG curve. A curve segment on the TGA plot corresponding to these temperatures represented the weight loss of the sample because of the reaction.

When the RPCC samples were heated from the temperature, chemiabsorbed water fully evaporated at about $200^{\circ}C$. The first stage reaction occurred by the evolution of hydroxyl water from $300^{\circ}C$ to about $540^{\circ}C$ (Eq. 8). The second stage of decomposition was the liberation of carbon dioxide from calcium carbonate in the RPCC aggregate. This stage

occurred at about 560°C and ended at about 780°C (Eq. 9). TGA and DTG curves of a RPCC sample (sample 4) are presented in Figure 4.3. The reactions occurred due to heating are as following:

$$Ca(OH)_2 + heat \rightarrow CaO + H_2O\uparrow \qquad (8)$$

$$CaCO_3 + heat \rightarrow CaO + CO_2\uparrow \qquad (9)$$

The percentages of $Ca(OH)_2$ and $CaCO_3$ were determined using the relationship of mole weights of the components and the percentages change of weight of the sample. The mole weights of the components are as follows:

$CO_2 = 44.079 \cong 44$ $\quad CaO = 56.079 \cong 56$ $\quad CaCO_3 = 100.088 \cong 100$

$H_2O = 17.99 \cong 18$ $\quad CaO = 56.079 \cong 56$ $\quad Ca(OH)_2 = 74.096 \cong 74$

The amount of $CaCO_3$ is calculated using the following equation:

$$Ca(OH)_2 = 2.273 * amount\ CO_2 \qquad (10)$$

The amount of $Ca(OH)_2$ is calculated using the following equation:

$$Ca(OH)_2 = 4.111 * amount\ H_2O \qquad (11)$$

The RPCC aggregates were oven-dried to 149°C for 24 hours to remove moisture and then cooled to room temperature. Each of the samples was ground with a rubber pestle and sieved through a #200 (75 µm) sieve. These fine particles were originated from cement paste of bulk RPCC aggregates that could potentially produce tufa. A small amount of fine material from each sample was then ground with a porcelain pestle into finer powder. Prepared and labeled samples were stored in plastic bags. These plastic bags were kept in de-aired desiccators to minimize exposure to moisture and carbon dioxide in the atmosphere. One sample representing ach site was used for TGA analysis. TGA analyses were conducted using approximately 50 mg samples in an Auto TGA 2950 HR V5.4A thermogravimetric analyzer in a nitrogen atmosphere running at a rate of 5°C per minute to 1000°C.

SEM and X-ray Microanalysis

The pavement subbase at this area was constructed in 1999 using RPCC aggregates.

At this site, tufa precipitate accumulated around the subdrain outlet into a body of dense and flaky parts in white and light yellow color (Figure 4.1). A specimen of tufa was collected from site 2 on the interstate highway I 35 southbound in Iowa for SEM and X-ray microanalyses. The specimen of tufa was placed in a plastic bag and properly labeled. The specimen of tufa sample was composed of a dense part in yellow color and a flaky part in white color. Two tufa samples used for SEM and X-ray microanalysis were prepared from this specimen of tufa. The first sample (sample 1) was prepared from the dense part of the tufa specimen. The second sample (sample 2) was extracted from the tufa flakes, which were from porous parts of the tufa deposit.

RESULTS AND DISCUSSION

Field Investigations

Extensive tufa precipitates were observed at the subdrain outlets and flow channels at two RPCC sites (sites 2 and 3). Site 2 was constructed in 1999 and had been in service for 4 years, and site 3 was constructed in 2003 and had been in service for 8 years. However, no extensive tufa formation was observed at the other RPCC sites, including several sites that had been in service for 8 years or less (e.g., sites 1, 7, 8, and 10).

pH Mapping of the Flow Channel

Tests of soil samples from the flow channel showed that pH values varied from 6.7 to 9.8, and pH values of water samples also from the flow channel were from 11.7 to 12.5. These pH values were incorporated with the coordinates and elevation profile at the test points to perform a spatial analysis of pH in the flow channel (Figure 4.2). High pH values of the water samples showed that pore waters following out of subdrain outlets carried high concentrations of Ca^+ and OH^- ions, as discussed in the previous parts.

High pH water from RPCC subbases increased pH values of soils in the flow channels. The pH map showed that soils in the lower areas of the flow channel had higher pH values than in the upper areas. High pH values of around 9.8 mainly concentrated around the subdrain area. However, pH values of soil samples collected in the lower area at 7 m (23 ft) or farther along the flow channel and away from the subdrain outlet, where pore waters

flowing out of the RPCC subbase occasionally covered, dropped to about 7.0 to 7.8. Soils in higher areas in the flow channel had the pH values varied from 6.5 to 7.0.

Mechanical Analysis

RPCC aggregate samples collected from 18 RPCC sites were performed mechanical analysis in the laboratory. The aggregates were classified as GP, GW, GW-GM, and GP-GM (ASTM. 2006a; ASTM. 2006b), or as A-1-a (AASHTO. 2002; ASTM. 2004) (Table 4.1).

TGA Results

Dehydroxylation of $Ca(OH)_2$ and dissociation of $CaCO_3$ were two phases observed from TGA/DTG images. Weight changes of the RPCC samples because of dehydroxylation and dissociation varied from 2.7% to 5.3% and from 9.4% to 19.1%, respectively (Table 4.2). Based on the weight change for each phase, the amounts of calcium hydroxide and calcite were determined (Eqs. 10 & 11).

Unlike the results of Gupta and Dollimore (2002) in which the amount of $Ca(OH)_2$ in old PCC pavement was around 5%, the range of portlandite in the RPCC aggregates in this study ranged from 10.9% to 21.7% (by weight) of the cement paste. This range of portlandite was similar to the range of portlandite found in newly hydrated concrete, which was from 10% to 20% (Taylor 1986). In fact, only small amounts of portlandite near or on the surface and/or cracks of old PCC pavements and/or RPCC aggregates were exposed to the environment and carbonated. The amounts $CaCO_3$ in cement paste of RPCC aggregates varied from 21.3% to 43.4%.

The results of TGA suggested that the ages of the original PCC pavements, which were recycled for RPCC aggregates, and RPCC aggregates were not the only factors that caused carbonation in concrete. The amounts of portlandite were not proportional with the ages of the RPCC sites. Low amounts of portlandite were found in several sites with low ages (site nos. 1, 3, 8, and 10), while higher amounts of portlandite were found in some other sites with high ages (i.e., site nos. 9, 14, and 16).The amounts of portlandite of site nos. 2 and 3 were 13.8% and 11.8%, respectively, and were on the lower side of the range (Table 4.2).

Several factors, such as pavement conditions, type of cement used in the original mixture, and permeability of the RPCC subbase, might affect the carbonation of the RPCC

aggregate. Pavements with little or no cracks and joints in good conditions might better prevent water from infiltrating into the RPCC subbases; thus, reducing the amount of time for the RPCC aggregates exposed to water that contained dissolved carbon dioxide. Permeability of the RPCC subbase could be a main factor for tufa precipitation. RPCC subbases usually had very low permeability that increased the residential time of water in the subbases. However, low permeability of a RPCC subbase also meant that low amounts of water could infiltrate into the subbase, limiting the amounts of high pH water flowing out through the subdrain systems to create tufa.

SEM and X-ray Results of the Tufa Samples

The analysis of the tufa precipitate samples suggested that this tufa precipitate is composed of a dense part and a flaky part that is located on the outside of the dense part. SEM images of the tufa samples showed that the samples had different morphologies (Figure 4.4). The images suggested that the dense part had different chemical components from the porous part of flakes. The texture shown in each image indicated that minerals were evenly distributed across each sample.

The elemental map and x-ray spectra of the sample 1 (Figure 4.5, Figure 4.6) showed that Ca, O, Si, and C, were the main elements of the sample. Based on the availabilities of these chemical elements and results leachate studies conducted by previous authors, calcite was identified as the major component of this sample. Si could exist in forms of a hydration product (e.g., C-S-H) or silica.

The elemental map of sample 2 (Figure 4.7) showed that Ca, O, and Si were the main chemical elements. The amount of C was not significant with a concentration of about that of the background map. X-ray spectrum of this sample showed that Ca, Si, and O were three dominant elements of the sample, suggesting that the main product of this sample was cement hydration C-S-H (Figure 4.8).

The analysis of the tufa precipitate samples suggested that this tufa precipitate is composed of a dense part and a flaky part that is located on the outside of the dense part. SEM and X-ray analyses on the dense and flaky samples showed that calcite and C-S-H were two main products of the tufa precipitate. Calcite was formed by the reaction of calcium

hydroxide from RPCC aggregates and carbon dioxide that was dissolved in the water. C-S-H gel was formed by the hydration of cement grains existing in the RPCC aggregates when the cement grains were exposed to the environment. C-S-H was considered to be the main component of the flaky part of the tufa.

CONCLUSIONS

Results of the TGA showed that the amounts of calcium hydroxide in RPCC aggregates varied from 10.9% to 21.7% (by weight) of the cement paste, while the amounts of calcite varied from 21.3% to 43.4%. The range of calcium hydroxide in the RPCC aggregates in this study was 5% higher than that reported by Gupta and Dollimore (2002). Ca^{2+} ions from calcium hydroxide in RPCC cement paste were the main donor for calcite precipitate.

At a RPCC subbase site that had extensive tufa, pH of water from the subbase was generally from 11.7 to 12.5. High pH water had increased pH values of soil within the flow channel to as high as 9.8 at the subdrain outlets. However, the area of pH effect was not extensive when soil samples at 7 m (23 ft) away or farther from the subdrain outlets and along the flow channel had pH values ranging from 6.5 to 7.0. The spatial analysis of pH values of soil samples showed that high pH soils mostly concentrated at and/or near the subdrain outlets.

Tufa sample was composed of a dense part and a flaky part that had totally different morphologies and elemental substances. The dense part was composed mostly by calcite, while the flaky part was comprised mostly by C-S-H, a cement hydration product. $CaCO_3$ was formed by the reaction of calcium hydroxide from RPCC aggregates and carbon dioxide that resolved in water. C-S-H was formed by the hydration of unhydrated cement grains. Calcium hydroxide and cement grains existing in the RPCC aggregates were two main sources to produce tufa precipitate.

ACKNOWLEDGEMENTS

REFERENCES

AASHTO. (2002). "Standard specification for reclaimed concrete aggregate for unbound soil aggregate base course." AASHTO M 319, American Association of State Highway and Transportation Officials, Washington, D.C.

ASTM. (2004). "Standard practice for classification of soils and soil-aggregates mixtures for highway construction purposes." Annual book of ASTM standards, ASTM D3282, West Conshohocken, PA.

ASTM. (2006a). "Standard practice for classification of soils for engineering purposes (unified soil classification system)." Annual book of ASTM standards, ASTM D2487, West Conshohocken, PA.

ASTM. (2006b). "Standard test method for sieve analysis of fine and coarse aggregates." Annual book of ASTM standards, ASTM C136, West Conshohocken, PA.

ASTM. (2007). "Standard test method for pH of Soils." Annual book of ASTM standards, ASTM 4972, West Conshohocken, PA.

Bruinsma, J. E., Peterson, K. R., and Snyder, M. B. (1997). "Chemical approach to formation of calcite precipitate from recycled concrete aggregate base layers." *Trans. Research Record: J. Trans. Research Board*, No. 1577, 10-17.

Diamond, S. (1976). "Cement paste microstructure – an overview at several levels." in *Hydraulic cement pastes: their structure and properties*, proceedings of a conference at Sheffield, University of Sheffield, Sheffield, England, 2-31.

Drever, J. I. (1988). "The geochemistry of natural waters." Prentice Hall, Inc., NJ.

Ford, G. R. (1987). "Geotextile/crushed concrete study – preliminary summary." Minnesota Department of Transportation.

Ghosh, S. N. (1983). "Advances in cement technology." Pergamon Press, Elmsford, NY.

Gupta, J. D. and Kneller, W. A. (1993). "Precipitate potential of highway subbase aggregates." Final Report HFWA/OH-94/004, Ohio Department of Transportation.

Gupta, J. D. and Dollimore, D. (2002). "Magnitude assessment of free lime and hydrated limes present in RPCC aggregates." Final Report FHWA/OH-2002/014, Ohio Department of Transportation.

Kneller, W. A., Gupta, J. D., Borkowski, M. L., and Dollimore, D. (1994). "Determination of original free lime content of weathered iron and steel slags by thermogravimetric analysis." *Trans. Research Record: J. Trans. Research Board*, No. 1434, 17–22.

Muethel, R. W. (1989). "Calcium carbonate precipitate from crushed concrete." Michigan Department of Transportation, Lansing, MI.

Narita, K., Onoye, T., and Takata, Z. (1978). "On the weathering mechanism of LD converter slag." Kobe Steel, Ltd. Japan.

Phan, T. H., White, D. J., Straszheim, W. E., and Taylor, P. (2010). Microstructure Characterization of Recycled Portland Cement Concrete Subbase Aggregate. In preparation for submission to the *J. Mater. Civ. Eng., ASCE*

Snyder, M. B. *Use of Crushed Concrete Product in Minnesota Pavement Foundations*. Final Report MN/RD-96/12. Minnesota Department of Transportation, 1995.

Snyder, M. B. and Bruinsma, J. E. (1996). "Review of studies concerning effects of unbound crushed concrete bases on PCC pavement drainage." *Trans. Research Record: J. Trans. Research Board*, No. 1519, 51–58.

Steffes, R. (1999). "Laboratory study of the leachate from crushed portland cement concrete base material." Final Report for MLR-96-4. Iowa Department of Transportation, Ames, IA.

Tamirisa, R. (1993). "Study of highway base/subbase aggregates that cause depositions of calcareous "tufa" in drains." Master's thesis. Department of Civil Engineering, University of Toledo, OH.

Taylor, H. F. W. (1986). "The chemistry of cements." Royal Institute of Chemistry, London, UK.

White, D. J., Ceylan, H., Jahren, C. T., Phan, T. H., Kim, S., Gopalakrisnan, K., and Suleiman, M. T. (2008). "Performance evaluation of concrete pavement granular subbase – pavement surface condition evaluation." Final Report, Iowa DOT Project TR-554, CTRE Project 06-250, Iowa Department of Transportation, Ames, IA.

Table 4.1. Summary of site information, classification, and report of tufa problems
of RPCC aggregate subbases

Site No.	Site location: highway name, mile marker	Travel direction	Construction year	Material classification		Extensive tufa formation in subdrains
				USCS (ASTM. 2006b)	AASHTO (ASTM. 2004)	
1	US 330, MM 20.05–20.10	South	2006	GW–GM	A–1–a	No
2	I 35, MM 119.95–120.05	South	1999	GP–GM	A–1–a	Yes
3	I 35, MM 140.75–140.80	North	2003	GP	A–1–a	Yes
4	I 80, MM 165.00–165.05	East	1996	GW–GM	A–1–a	No
5	I 80, MM 165.20–165.25	East	1994	GW–GM	A–1–a	No
6	I 35, MM 131.40–131.45	North	1983	SW–SM	A–1–a	No
7	I 80, MM 10.55–10.60	West	1999	GP	A–1–a	No
8	I 80, MM 10.55–10.65	East	2003	GW	A–1–a	No
9	I 80, MM 65.10–65.20	East	1988	GP–GM	A–1–a	No
10	Knapp Street, Ames, Iowa	West	2003	GW–GM	A–1–a	No
11	I 80, MM 269.00–269.10	East	1991	GW–GM	A–1–a	No
12	I 80, MM 272.30–272.40	East	1992	GP–GM	A–1–a	No
13	I 80, MM 2272.55–272.65	East	1992	GP–GM	A–1–a	No
14	I 80, MM 269.30–269.40	West	1992	GW–GM	A–1–a	No
15	I 80, MM 128.50–128.55	East	1994	GP–GM	A–1–a	No
16	I 80, MM 275.70–275.75	West	1992	GP–GM	A–1–a	No
17	I 80, MM 275.90–275.95	West	1992	GW–GM	A–1–a	No
18	I 80, MM 276.60–276.70	East	1991	GW	A–1–a	No

Table 4.2. Percentage of calcium hydroxide and calcite in the RPCC aggregates using
TGA/DTG tests

Sample number	Dehydroxylation of $Ca(OH)_2$		Dissociation of $CaCO_3$	
	Percent change of sample's weight	Percent of $Ca(OH)_2$	Percent change of sample's weight	Percent of $CaCO_3$
1	3.7	15.3	15.8	35.9
2	3.4	13.8	18.9	42.8
3	2.9	11.8	19.1	43.4
4	3.6	14.8	16.2	36.8
5	3.3	13.6	17.7	40.2
6	2.7	10.9	14.0	31.8
7	4.0	16.5	14.8	33.6
8	3.9	16.2	10.9	24.8
9	4.7	19.2	9.4	21.3
10	3.5	14.5	12.9	29.2
11	4.8	19.6	13.1	29.7
12	3.4	14.1	17.3	39.2
13	4.7	19.3	18.2	41.4
14	5.3	21.7	15.7	35.6
15	3.7	15.4	12.2	27.8
16	5.1	20.8	15.4	35.1
17	4.2	17.1	13.5	30.7
18	4.5	18.7	11.1	25.3

Figure 4.1. Yellowish tufa precipitates at the subdrain outlet
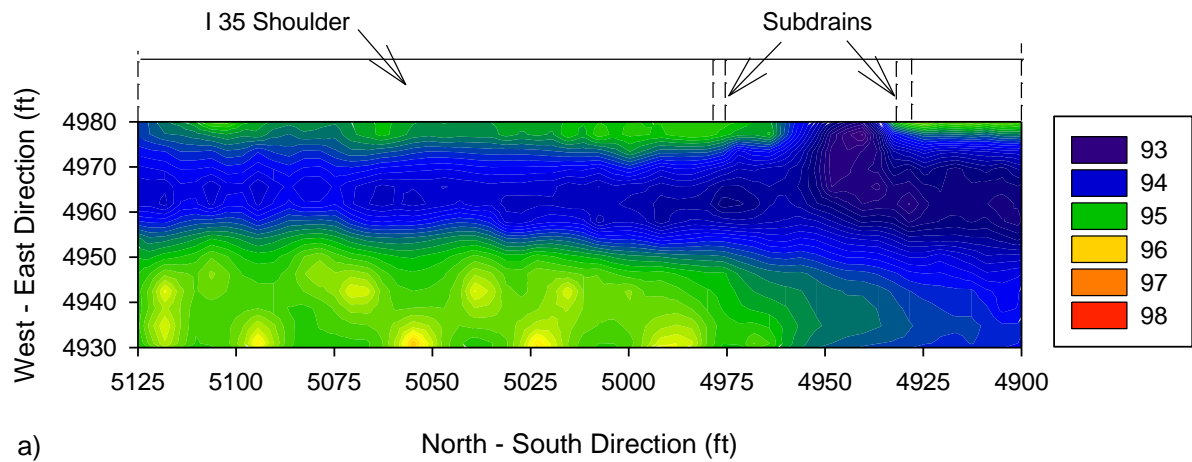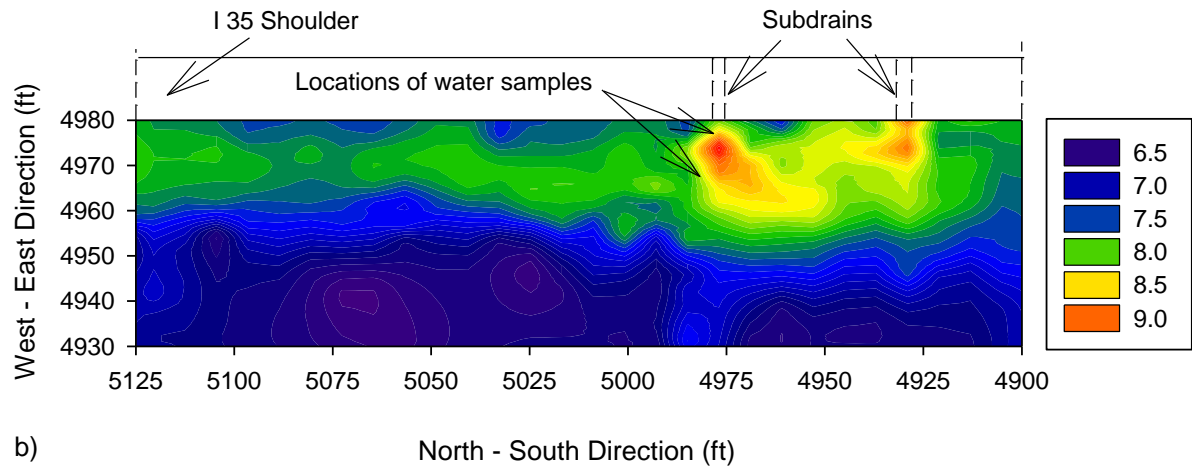
Notes: Elevation and direction measurements are in English unit (ft); 1 ft = 304.8 mm.

Figure 4.2. Spatial analysis of the flow channel: a) topography; b) soil pH map
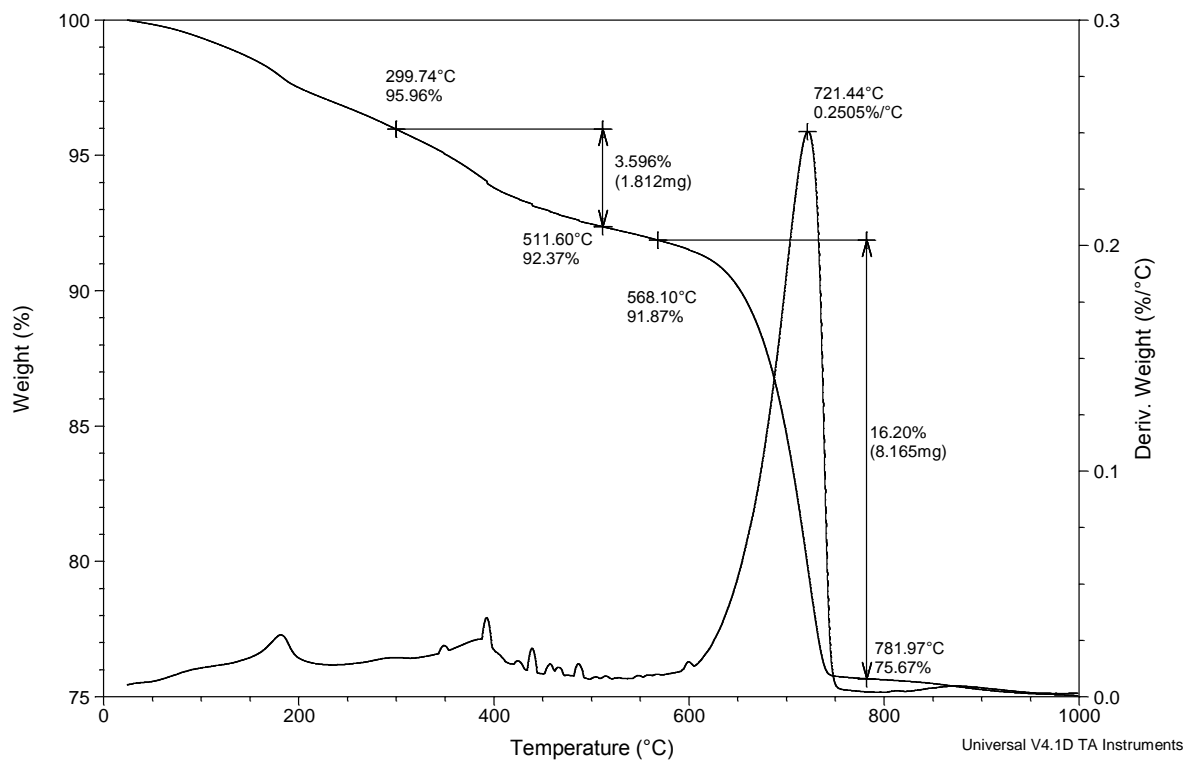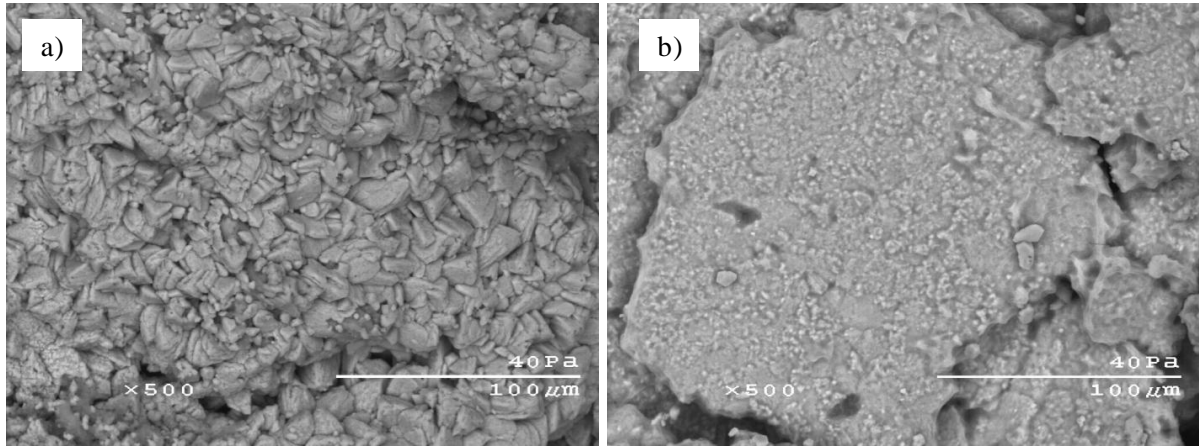
Figure 4.3. TGA plot of RPCC sample 4

Figure 4.4. SEM images of tufa samples: a) sample 1; b) sample 2 (500x magnification)

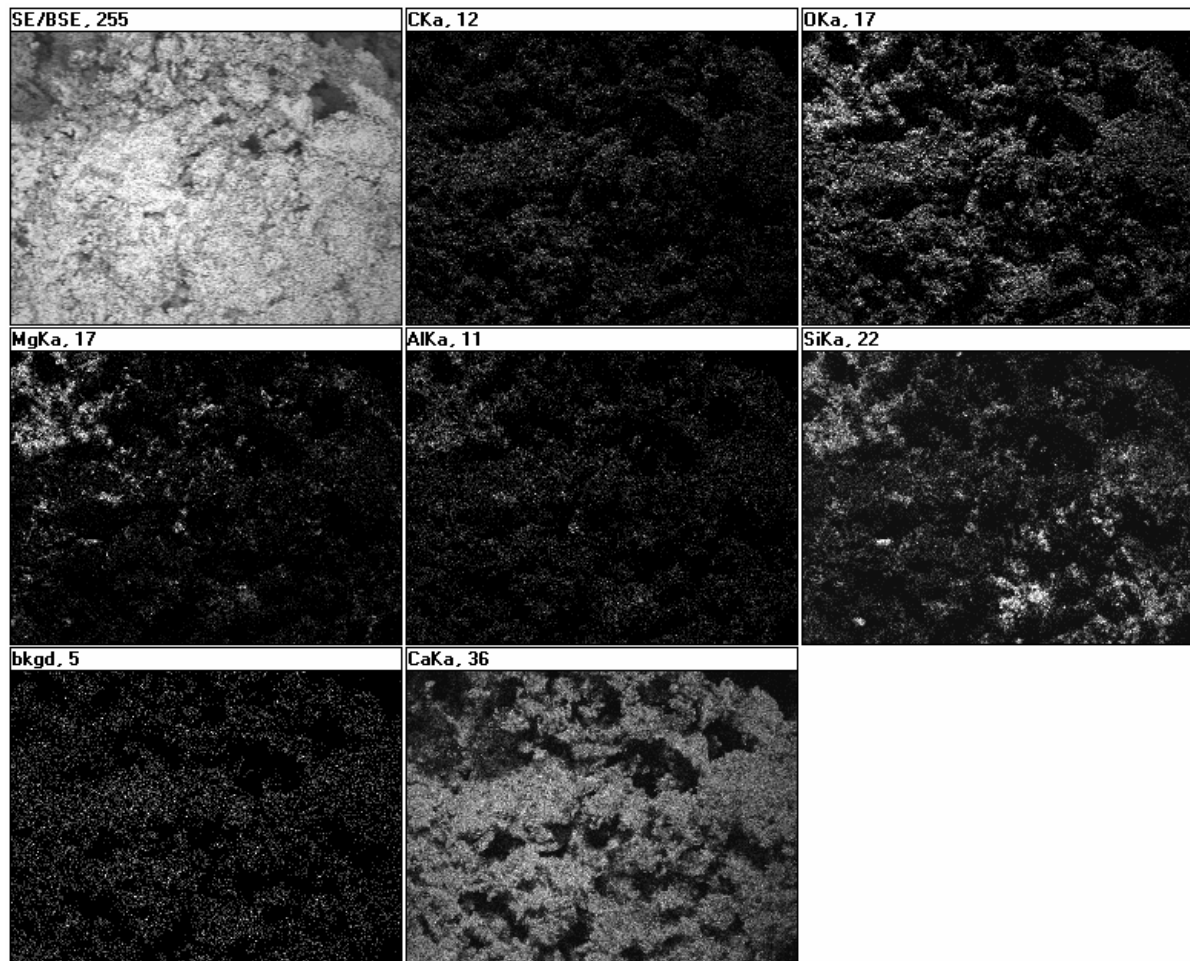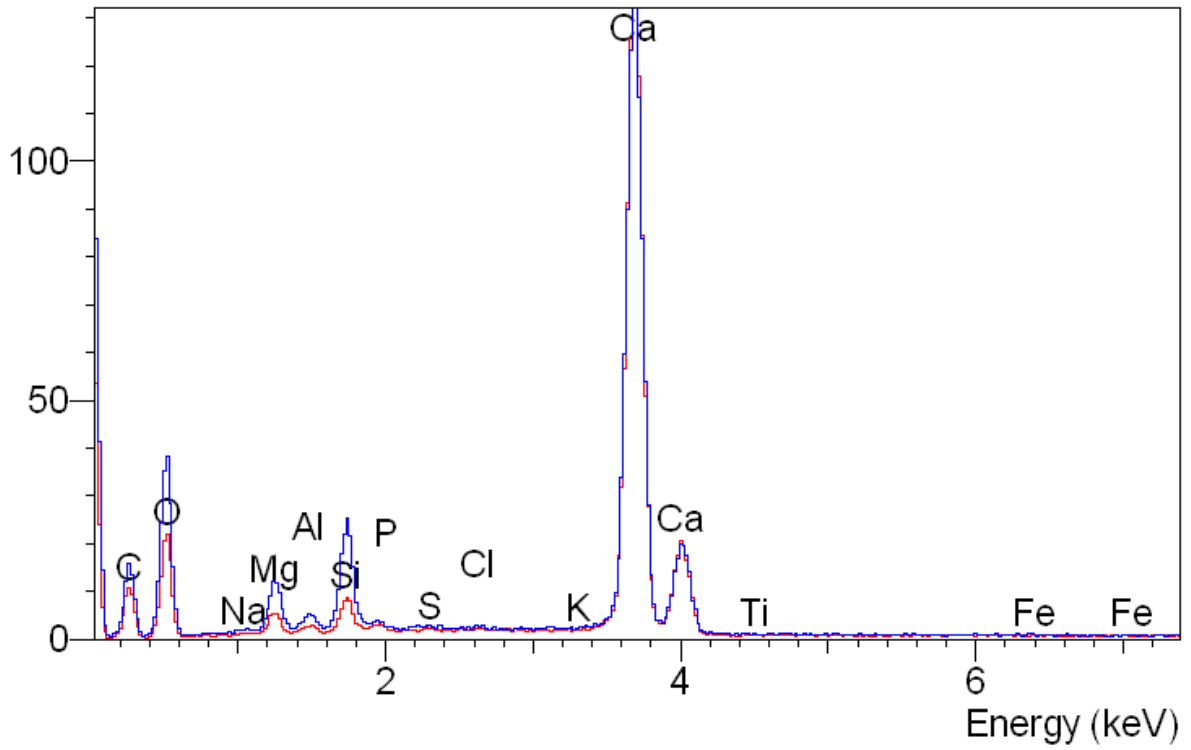Figure 4.5. Elemental map of tufa sample 1 (50x magnification)

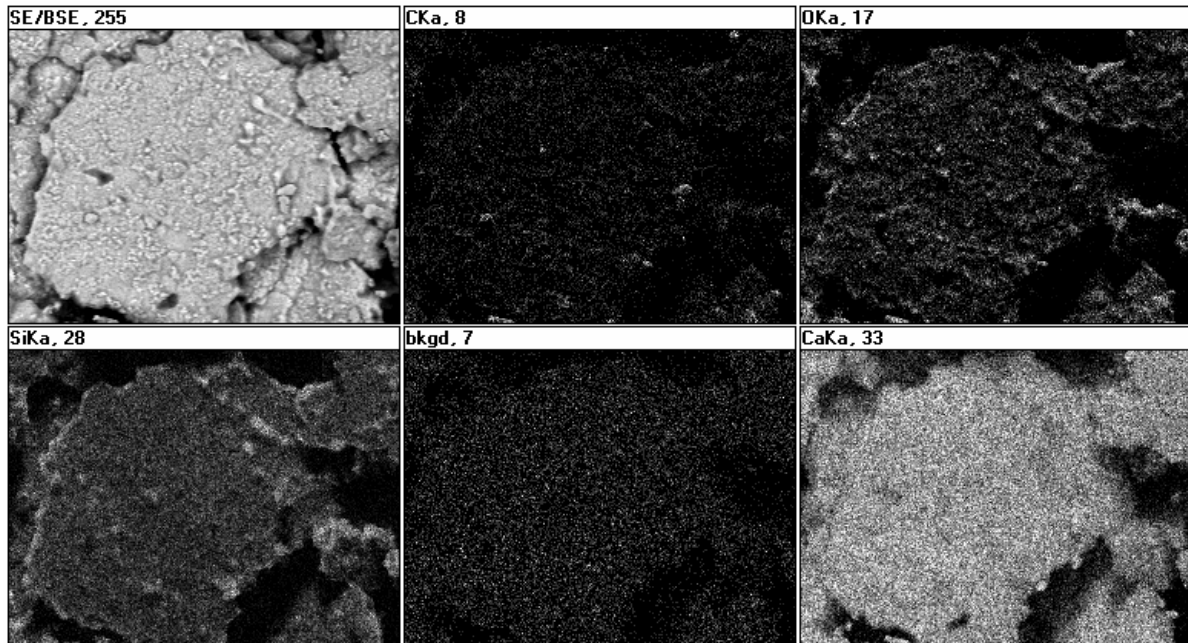Figure 4.6. X-ray spectra of tufa sample 1 (red line: 500x magnification; blue line: 50x magnification)

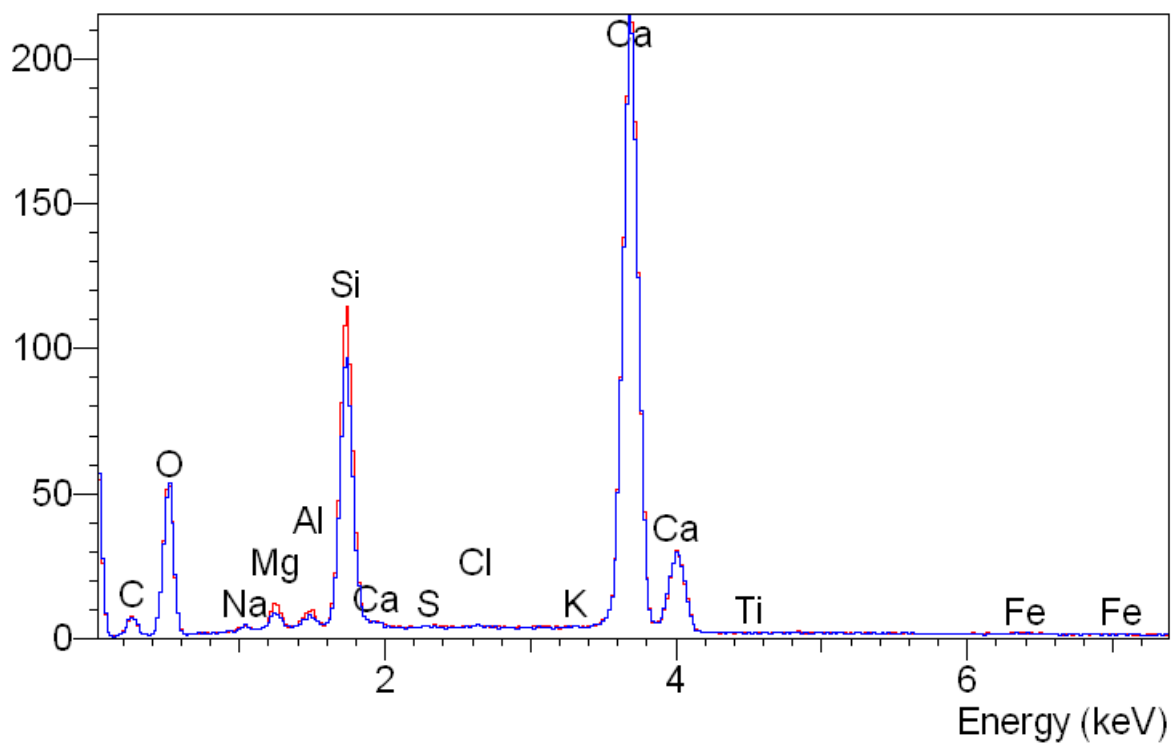Figure 4.7. Elemental map of tufa sample 2 (500x magnification)

Figure 4.8. X-ray spectra of tufa sample 2 (red line: 500x magnification; blue line: 150x magnification)

CHAPTER 5: SEASONAL VARIATION AND SPATIAL ANALYSIS OF PAVEMENT FOUNDATION LAYERS

Thang H. Phan[1], Matthew D. Cushman[2], David J. White[3], and Charles T. Jahren[4]

ABSTRACT

Seasonal variations in ground temperature and moisture content influence the load carrying capacity of pavement foundation layers. To improve pavement performance, pavement design guidelines require knowledge of environmental factors and subgrade stiffness relationships. As part of this study, in-ground instrumentation was installed in the pavement foundation layers of a newly constructed section along U.S. Highway 20 near Fort Dodge, Iowa, to monitor the seasonal variations in temperature, frost depth, groundwater levels, and moisture regime. Dynamic cone penetrometer (DCP), nuclear gauge, and Clegg hammer tests were performed at 64 test points in a 1.83 x 1.83 m grid pattern to characterize the subgrade stiffness properties (i.e., resilient modulus) prior to paving. The paper has summarized the spatial analysis of the field measurements during construction, freezing and thawing periods, and two years after construction. Results showed that moisture content linked to rain events dissipates in the subbase only after several days, field determined resilient modulus was about three times higher than the average value of resilient modulus obtained from laboratory testing, and freezing in the subgrade is affected by surface and ground temperature conditions. In the subgrade layer, freezing penetrated downward, but thawing occurred in both downward and upward directions.

[1] Graduate Research Assistant (corresponding author), Iowa State University of Science and Technology, 2711 South Loop Drive, Suite 4700, Ames, IA 50010-8664; thphan@iastate.edu
[2] Terracon Consultants, Inc., 600 Southwest 7th St., Suite M, Des Moines, IA 50309; mdcushman@terracon.com
[3] Associate Professor, Iowa State University of Science and Technology, 422 Town Engineering, Ames, IA 50011-3232; djwhite@iastate.edu
[4] Associate Professor, Iowa State University of Science and Technology, 428 Town Engineering, Ames, IA 50011-3232; cjahren@iastate.edu

INTRODUCTION

Seasonal variation in ground temperature and moisture content of the pavement subgrade and base/subbase layers influence their load carrying capacity. High moisture contents in these layers can result in decreased strength and stiffness. Loss of support conditions (i.e., a reduction in stiffness) in these layers occurs during thawing periods and/or saturated conditions and is one of the primary contributors to distresses in pavements. In addition, variation in moisture in the subgrade layer can contribute to deleterious volume change in the soil that may result in differential movement of the pavement layer. A better understanding of seasonal variation in subgrade properties would benefit pavement design and material selection.

As a part of this study, detailed field instrumentation was installed to monitor the seasonal variations in temperature, moisture content, frost depth, and groundwater levels on US 20 westbound near Fort Dodge, Iowa (near mile marker 199.90) in May 2005. The research was conducted on a newly constructed pavement, which was composed of a 28.0 cm (11 in.) Portland cement concrete (PCC) pavement, 11.4 cm (4.5 in.) limestone aggregate subbase, and a subgrade layer using glacial till material from a local borrow area. The subgrade soil materials were classified as silty clay (CL).

Further, spatial variation of the subgrade soils prior to placement of the subbase layer was analyzed using a series of field tests conducted at 64 test locations. The tests included dynamic cone penetrometer (DCP), nuclear gauge, and Clegg impact hammer. The subgrade soil was sampled for laboratory resilient modulus testing approximately two years after construction. DCP tests were also conducted at this time to observe changes in subgrade strength.

BACKGROUND

The Long Term Pavement Performance (LPTT) seasonal monitoring program (SMP) was initiated in 1992 to attain the seasonal environmental variation in pavement sub-structural layers. The SMP includes weather and pavement instrumentation. Results are being used to develop the ME pavement design guide, and specially the relationship between resilient modulus and moisture content (*1, 2, 3*). The study methodology uses LTPP test

sections to monitor continuous environmental variation and in-pavement instrumentation data. The instrumentation normally includes a thermistor probe or temperature sensors to measure the temperature profile of the pavement layers, time domain reflectometry (TDR) probes to measure moisture profile, and an electrical resistivity probe to detect freeze/thaw boundaries.

Pavement bases/subbases are used to provide uniform support of pavement surface and adequate drainage during the lifetime of the pavement. Undrained water in supporting layers is considered a major factor to distress and premature failure in pavements (*4*). Prolonged periods of undrained water, which can become trapped in the pavement's structure, may reduce strength of unbound granular materials and subgrade soils and result in cracking of PCC pavement and deterioration of shoulder under the traffic loads. Saturated subbase and subgrade layers in cold regions can lead to frost heave, which can crack the pavement and reduce the bearing capacity of the layers during the thawing period (*5*). Repetitive traffic loading on saturated subbase layer can also induce pore water pressure, resulting in loss of strength (*6*).

Most fine-grained soils moduli decrease if the water content is increased, resulting in increased deflections in the subgrade (*7*). In a study conducted by Rainwater et al. (1999), four sites in Tennessee were instrumented with comprehensive monitoring systems to collect meteorology, water content, infiltration, and temperature data. Rational methods were applied for data analysis to determine the environmental effects. The results of this study showed that subgrade volumetric water contents varied very little, except for brief periods after heavy rainfall events. These small changes in subgrade moisture content did not show significant changes in subgrade support properties.

Resilient modulus (M_r) is the ratio between repeated deviator stress (σ_d) and recoverable strain (ε_r) in the direction of the major principle stress (*8*). Resilient modulus is dependent on several factors: soil type, water content and compaction level. The authors developed relationships between the resilient modulus at varying moisture content to the resilient modulus at optimum moisture content, for constant compaction energy and dry unit weight. Given a constant dry density, resilient modulus can be three times higher than that at optimum moisture content if its moisture content is 5% lower than the optimum moisture

content (*9*). Moisture content strongly influences the stiffness of the compacted materials. The subgrade resilient modulus varies seasonally due to changes in moisture content. Resilient modulus decreases with increases in moisture content (*10*).

SEASONAL VARIABILITY – INSTRUMENTATION AND MEASUREMENTS

Instrumentation

In this study, field instrumentation was installed to monitor seasonal variation in moisture content, temperature, and freeze-thaw cycles. The instrumentation consisted of ten time domain reflectometry (TDR) probes, ten temperature sensors, one resistivity probe, two piezometers, a limited weather station and a data logger (Table 5.1). The TDR probes utilized in this study consisted of three evenly spaced stainless steel rods. The impedance along the length of the rods varies with the dielectric constant of the surrounding soils. Based on the assumption that the dielectric constant of a soil is dependent on the moisture content, the volumetric water content of the soil surrounding the TDR probe rods could be estimated from its reflected waveform. One probe was placed in the center of the aggregate subbase layer. One was placed at the subbase/subgrade interface. The remaining eight probes were placed at 0.15 m (0.5 ft) intervals below the subbase/subgrade interface. The TDR probes were installed horizontally into the sidewall of the installation trench near the outer wheel path into relatively undisturbed soil (Figure 5.1). The probes were installed using a guide tool. The guide held the TDR probe rods parallel during insertion into the subgrade soil.

Precipitation and Volumetric Moisture Content in Subbase Layer

Water can penetrate into the subbase layers from different sources, including infiltrating through cracks in the pavement and longitudinal pavement/shoulder joints, seeping from ditches and medians, and high ground water table (*4*). Figure 5.2 shows precipitation, volumetric moisture content of the subbase layer, and ground water table under the pavement surface from May 10, 2005 to June 3, 2005. During this time, the ground water table was stable at around 3 m (9.8 ft) below the top of the pavement surface, and was 2.6 m (8.5 ft) lower than the subbase/subgrade interface. Capillary water movement could be a factor that affected the moisture content in the subgrade and subbase layers. However,

fluctuations in moisture content were strongly affected by the rainfall both in amount and duration. Heavier rain resulted in higher increase of the moisture content. The volumetric moisture content of the subbase layer immediately increased at the rain events, but it took a longer period of time for the moisture to escape from the subbase after the rains ended.

Subbase and Subgrade Moisture Contents

Volumetric moisture content (VMC) in soil was collected by analyzing the waveform data from TDR probes. The TDR is based on measuring the one-way travel time of an electromagnetic wave from a source to an electrical discontinuity (*11*). Several empirical relationships between the dielectric constant and volumetric water content have been developed. A commonly used equation (and the one utilized in this study) is given as (*12*)

$$\theta_v = -5.3 * 10^{-2} + 2.92 * 10^{-2}K_a - 5.5 * 10^{-4}K_a^2 + 4.3 * 10^{-6}K_a^3 \tag{1}$$

where: θ_v = volumetric water content.

K_a = dielectric constant.

During freezing periods, the apparent dielectric constant of frozen water resulted in an artificially low moisture content. Figure 5.3a presents the moisture content of the subbase from October 2005 to February 2007. Freezing/thawing periods in the subbase layer occurred from late October 2005 to early February 2006 and from late October 2006 to early February 2007. The moisture content at the lower level (0.39 m) was higher than that at the higher level (0.34 m).

Figure 5.3b shows the fluctuation of moisture content with time at the highest, middle, and lowest levels of TDRs in the subgrade layer. The volumetric moisture content in the subgrade soils increased from late spring and peaked in the early summer. It appears that relationships exist between precipitation and moisture content of the subbase (i.e., short-term increases) and subgrade layers (i.e., a long-term annual trend). The subgrade volumetric moisture contents varied widely within a year. This finding seems to be different with what was found in the Tennessee sites that the subgrade volumetric moisture contents varied little (*13*). An increase of moisture content results in significant loss of the resilient modulus, given that the dry density is constant and the subgrade layer is compacted near w_{opt} (*8*).

The specific gravity of the subgrade materials obtained from the laboratory was 2.66. The optimum moisture content (w_{opt}) and maximum dry density obtained from the Standard Proctor compaction test were 13% and 1,866.2 kg/m^3 (116.5 pcf). Thus, the optimum volumetric moisture content was 17%. However, the maximum volumetric moisture content collected from the instrumentation in the subgrade layer at 0.53 m (1.74 ft), 1.01 m (3.31 ft), and 1.59 m (5.21 ft) were from 13% to 24% higher than the optimum volumetric moisture content.

Frost Penetration

Prior to instrumentation, it was expected that frost would develop from the top down, and that thawing would occur from the top down and bottom up. The resistivity gage readings confirmed that thawing occurs from the top down, and bottom up (Figure 5.4a). The gauge readings support observations of other researchers that as the ice lens thaws, unfrozen water is trapped in the base layer due to ice in the subgrade prohibiting infiltration.

The top of the resistivity probe was 0.40 m (1.32 ft) below the pavement surface. The resistivity probe was installed below the surface of the subgrade to limit damage during paving operations. Because of this, no frost data exists for the base layer material. To describe Figure 5.4a, moving from the left to the right, the penetration of the frost layer is first detected by the resistivity probe on Dec. 1, 2005, reaching a maximum penetration on Dec. 9, 2005 and completely thawing on Dec. 13, 2005. A couple days later, another frost lens forms and completely thaws by Dec. 30, 2005.

One explanation for thawing of the ice lens from the top and bottom is that solar radiation warms the shoulder and ditch materials. With the pavement surface the highest point in its cross-section, it is expected that thawing occurs from the pavement surface downwards, and from the shoulders inwards. The temperature at deep levels in the subgrade soils is normally about 10-15.6°C (50-60°F). Thus, the subgrade soils are warming from the bottom up. Additional instrumentation of the pavement subgrade would be required to determine the heat flow along a cross-section during thawing periods.

Frost penetration depth can also be determined by resistivity probe measurements. A significant drop of resistivity indicates that water changes from solid to liquid. The frost

front diagram in Figure 5.4a identifies freezing periods. Nine days in December 2005 were selected to highlight frost depth using the resistivity probe. Sharp changes in the measured resistivity values at the depth of 1.10 m (3.61 ft) indicated that the frost depth during this period was 1.10 m (3.61 ft) from the pavement surface (Figure 5.4b).

Pavement, Base and Subgrade Temperature Profiles

The temperature profile through the pavement, subbase, and subgrade layers on a summer day (July 4, 2005) is presented in Figure 5.5. The temperature profile shows that the PCC pavement experiences greater temperature extremes and that it changes at a higher rate than the subbase and subgrade layers. The difference in temperature between the highest and lowest temperatures over one day at 5 cm (2 in.) below the pavement surface was $10^{o}C$ ($18^{o}F$). The maximum temperatures in the subbase and subgrade layers fluctuated within $3.0^{o}C$ ($5.4^{o}F$) and $1.0^{o}C$ ($1.8^{o}F$), respectively. The subgrade materials from 0.6 m (24 in.) below the pavement surface did not experience significant temperature changes. This finding is similar with the findings of Zhou and Elkins (*14*).

EFFECTS OF SEASONAL VARIATION ON SOIL STIFFNESS

To study the effects of freeze-thaw circles on the performance of pavement foundation, a series of DCP tests were conducted in the area of testing site during freezing and thawing periods. The tests were located at the edge of the pavement.

DCP tests were conducted on the subgrade layer within the pavement area two years after construction (April 23, 2007). Shelby tube samples were taken to determine the laboratory resilient modulus using the repeated load triaxial tests and to measure moisture content of the samples. The average resilient modulus, which was converted from the DCP tests at this time, of each lift of the subgrade material (0.31m thick) was compared with the average resilient modulus obtained from the field testing during construction. The average moisture content of the Shelby tube samples was 10.6%. This value was within the range of moisture content of 10 – 11%, which was measured by nuclear gauge testing during construction.

The average values of DCP tests at different time periods were presented in Figure

5.6. The subgrade became stiff when frozen with an average DCP index of approximately
2 mm/blow. In contrast, soil was in its weakest condition during the thawing period when the
penetration index was up to about 40 mm/blow. Comparing the average DCP profile two
years after construction with the average DCP profile during construction, it was determined
that the subgrade material gained strength after construction (Figure 5.6). The increase can
also be observed in Table 5.2, in which the average resilient moduli in the subgrade layer
estimated from DCP tests after two years increased by 47% for the lower lift (0.31 – 0.62 m).
Virtually, no change occurred in the top lift (0 – 0.21 m).

The average resilient modulus value obtained from the laboratory testing is normally
used for pavement structure design (*15*). In this study, the average resilient modulus of
laboratory testing was 47 MPa (6,820 psi). The average values of resilient modulus back
calculated from DCP tests of the first and second lift were 121 MPa (17,550 psi) and
159 MPa (23,061 psi), respectively (Table 5.3). The back calculated resilient modulus values
were about three times higher than the average value of resilient modulus obtained from the
laboratory testing. This finding agreed with a report that the back calculated resilient
modulus from field testing is three time higher than the average value of resilient modulus
obtained from the laboratory testing (*15*).

SPATIAL VARIABILITY AND SUMMARY OF FIELD MEASUREMENTS

Field Measurements

Field tests by Clegg impact hammer, DCP, and nuclear moisture density gage were
used to evaluate the subgrade layer during construction. Subgrade materials at the test site
were classified as A-6(4) according to the AASHTO classification system. In the USCS
system, the soil is classified as silty clay (CL) with 97 percent passing #4 sieve (4.75 mm)
and 58 percent passing #200 sieve (0.075 mm). Liquid limit and plastic index of the subgrade
soils were 28 and 12, respectively. The maximum dry density and optimum moisture content
of the soil determined by Standard and Modified Proctor tests were 1866.2 kg/m^3 (116.5 pcf),
13% and 1970.3 kg/m^3 (123.0 pcf), 10.0%, respectively.

Clegg impact hammer and DCP were also used to measure the stability of the bases
two years after construction. Clegg impact hammer was developed by Clegg during the late

1970s (*4*). The test used a drop weight and an accelerometer to indirectly determine stiffness at the surface. Clegg impact value (*CIV*) was measured as the rebound of the fourth blow of a standard 4.5 kg hammer. The in situ Clegg impact hammer tests were conducted in accordance with ASTM D5874-02, "Standard Test Method for Determination of Impact Value (IV) of a Soil". CBR value is correlated from *CIV* by the equation (*16*):

$$CBR = (0.24\ CIV+1)^2 \tag{2}$$

The DCP consists of driving a cone tip using a 8.0 kg (17.6 pound) drop hammer, with a fall height of 57.4 cm (22.6 in.). For each hammer blow, the penetration depth is recorded. The penetration per hammer blow is the DCP penetration index (*DPI*). *DPI* was converted to *CBR* following ASTM D6951-03, "Standard Test Method for Use of Dynamic Cone Penetrometer in Shallow Pavement Applications", by the equation:

$$CBR = 292\ /\ DPI^{1.12} \tag{3}$$

Table 5.4 summarized the average values of in situ measurements during construction. The Clegg impact value was the average value measured on the surface of the subgrade layer. The *CBR* values and resilient modulus on the surface of the subgrade layer was estimated based on the average *CIV* value. The *DPI* indices with different depths were calculated by averaging the normalized DPI values for every 0.31 m (1 ft) thick lift. *DPI* values were then used to estimate DCP-*CBR* and resilient modulus, M_r. In this study, *DPI* values were widely variable in the top lift, but varied narrowly in the lower lifts. The authors found that different field measurement methods provided very different values of back calculated resilient modulus (Table 5.3).

The average moisture content of 10.2% was within the range of optimum moisture contents for Standard and Modified Proctor tests 10% - 13%. The average dry density measured by nuclear gauge was 1,866.2 kg/m^3 (116.5 pcf), which was equal to the maximum dry density obtained from the Standard Proctor tests. The subgrade layer was very well compacted. The nuclear gauge was used in accordance with ASTM D6938 – 06e1, "Standard Test Methods for In-place Density and Water Content of Soil and Soil-Aggregate by Nuclear Methods (Shallow Depth)".

Spatial Variability

One week prior to placement of the subbase layer, closely space in situ point measurements were conducted to study the spatial variability of the subgrade soils. The Clegg impact hammer, DCP and nuclear moisture density gage were used to quantify this variability. A test grid was developed which extended beyond the planned sensor installation location by about 15.24 m (50 ft) to the east and west. The test locations were spaced 1.83 m (6 ft) apart in the east-west and north-south directions. The test grid consisted of 4 rows spanning the two lanes of westbound traffic, and 16 columns for a total of 64 test locations.

The results of field tests were analyzed using a statistical technique known as Kriging. Kriging is a linear least squares estimation algorithm. This technique is used to interpolate some variable over an area where known values are recorded. In this study, the field test results along the test grid on the subgrade layer were used to develop a topographic style graph (Figure 5.7).

In a variogram model, a correlation distance, which was smaller than the test data spacing, indicated that the data points were independent of each other. Given the data set for this project, predictions could not be made using a spherical variogram model for any of the field tests. A Gaussian variogram model could not be used to predict moisture contents or *CBR* values. In addition, the Gaussian variogram model predictions of density and the Clegg impact value were limited; i.e., the correlation distances were 2.35 m (7.7 ft) and 2.74 m (9.0 ft), respectively (Table 5.4).

The exponential variogram model was used to analyze the data sets. The correlation distance for field testing ranged from 3.05 to 9.00 m (10.0 to 29.5 ft). The Kriging plot of Clegg impact hammer data showed a definite east-west correlation. This pattern followed the construction sequence typically used for highway fill. In general, a truck unloads fill materials, which were then spread in the direction of the road alignment, and then compacted in the same direction. Such a system should result in strong correlation in a direction parallel to the roadway alignment. The nuclear density data less clearly showed this trend. It was expected that the moisture content would also show strong correlation along the alignment of the roadway, but all three variogram models (i.e, spherical, Gaussian, exponential) resulted in a correlation distance less than the grid spacing.

CONCLUSIONS

The paper has summarized the in-ground instrumentation monitoring spatial analysis of in situ measurements after construction, and changes in resilient modulus up to two years after construction. These measurements were correlated with the seasonal variation to determine the effects of the seasonal changes on the subgrade stiffness. Back calculated resilient modulus from field measurements of the subgrade was compared with resilient modulus obtained from the laboratory test. Seasonal variations in temperature, moisture content, and frost depth using field instrumentation were also documented.

The spatial analysis showed the variations in moisture content, density, Clegg impact value, and DCP-*CBR* values. Clegg impact values most clearly showed transverse variation likely a result of the construction process which follows longitudinal paths. The Clegg impact values measured at different locations widely varied with a coefficient of variation of 38%. Moisture content and dry density varied in narrower ranges with coefficient of variations of 9% and 2%, respectively.

Moisture content in the subbase layer is strongly influenced by precipitation. The volumetric moisture content sharply increases with the rain events, but it took longer periods of time for the moisture to dissipate from the subbase after the rains ended. The longer time for high moisture content exists in the subbase layer the higher risk of pavement deterioration under traffic loads.

The moisture content in the subgrade layer changed significantly with the seasons. Moisture content in the subgrade soils increased during the spring thaw and peaked in the early summer. Moisture contents of the subgrade layer increased with depth and were affected by seasonal variations. The results from this study suggested that the moisture content in the subgrade layer was strongly dependent on the freeze-thaw processes and rain seasons

As expected, freezing penetrated downward, and thawing occurred in both downward and upward directions in the subgrade layer. During the thawing process, ice lenses under the pavement thawed from the top down and bottom up. The temperature in the subgrade layer decreased with depth when it was above the freezing point, but increased with depth when it was below the freezing point. The frost penetrated to the depth of 1.10 m (3.61 ft) below the

pavement surface. The PCC pavement experiences greater temperature extremes than the subbase and subgrade layers.

Stiffness of the subgrade layer slightly increased after two years. The soil becomes extremely stiff when frozen, and is weakest in a fully saturated condition. It is very well observed that different field measurement methods provided very different values of the back calculated resilient modulus. These values were about three times higher than the average value of resilient modulus obtained from the laboratory testing. This finding confirms the statement that the back calculated resilient modulus from field testing is about three times higher than the average value of resilient modulus obtained from the laboratory testing.

ACKNOWLEDGEMENTS

REFERENCES

1. Rada, G. R., Elkins, G. E., Henderson, B., Van Sambeek, R. J., and Lopez, A. *LTPP Seasonal Monitoring Program: Instrumentation Installation and Data Collection Guidelines*. Report FHWA-RD-110, FHWA, 1995.

2. Jiang, Y. J. and Tayabji, S. D. *Analysis of time domain reflectometry data from LTPP seasonal monitoring program test sections*. Final report. FHWA-RD-99-115. 1999.

3. Ovik J. M., Birgisson, B., and Newcomb, D. E. *Characterizing Seasonal Variation in Pavement Material Properties for Use in a Mechanistic-Empirical Design Procedure*. Final Report, Minnesota DOT, Report No. MN/RC – 2000-35, 2000.

4. White, J. D., Vennapusa, P., and Jahren, J. Charles. *Determination of the Optimum Base Characteristics for Pavements*. Final Report, Iowa DOT Project TR-482, 2004.

5. Yang, H. H. *Pavement Analysis and Design*, 2nd Edition, Pearson Prentice Hall, NJ, 2004.

6. Cedergren, R. H. *Drainage of Highway and Airfield Pavements*. John Wiley & Sons, Inc., New York, 1974.

7. Drumm, C. E., Reeves, S. J., Madgett, R. M., and Trolinger, D. W. Subgrade resilient modulus correction for saturation effects. *Journal of Geotechnical and Geoenvironmental Engineering*, 1997, pp. 663–670.

8. Seed, H. B., Chan, C. K., and Lee, C. E. Resilience characteristics of subgrade soils and their relation to fatigue failures in asphalt pavement. *Proc. First Int. Conf. on Struct. Design of Asphalt Pavements*, University of Michigan, Ann Arbor, 1962, pp. 611 – 636.

9. Li, D. and Selig, T. E. Resilient modulus for fine-grained subgrade soils. *Journal of Geotechnical Engineering*, 1994, pp. 939–957.

10. Heydinger, A. G. Evaluation of Seasonal Effects on Subgrade Soils. In *Transportation Research Record: Journal of the Transportation Research Board, No. 1821*, Transportation Research Board of the National Academies, Washington, D.C., 2003, pp. 47–55.

11. Diefenderfer, K. B., Al Qadi, L. I., and Loulizi, A. Laboratory calibration and in situ measurements of moisture by using time-domain reflectometry probes. In *Transportation Research Record: Journal of the Transportation Research Board, No. 1699*, Transportation Research Board of the National Academies, Washington, D.C., 2000, pp. 142–150.

12. Topp, G.C., Davis, J.L., and Annan, A.P. Electromagnetic determination of soil water content: Measurements in coaxial transmission lines, *Water Resource Research, No. 3*, 1980, pp. 574–582.

13. Rainwater, N. R., Yoder, E. R., Drumm, C. E., and Wilson, V. G. Comprehensive monitoring systems for measuring subgrade moisture conditions. *Journal of Transportation Engineering*, 1999, pp. 439–448.

14. Zhou, H. and Elkins, G.E. Pavement responses to seasonal variations. *4th International Converence, Bearing Capacity of Roads and Airfields*, Minnesota Department of Transportation, 1994, pp. 706–719.

15. American Association of State Highway and Transportation Officials (AASHTO). *Guide for the Design of Pavement Structures*, Washington D.C., 1993.

16. Clegg, B. (1986). Correlation with California Bearing Ratio. *News Letter 2*, http://www.clegg.com.au/information_list12.asp, Date Accessed: 04/30/2008.

17. ASTM. (2002). "Standard Test Method for Determination of Impact Value (IV) of a Soil." Annual book of ASTM standards, ASTM D5874, West Conshohocken, PA.

18. ASTM. (2003). "Standard Test Method for Use of Dynamic Cone Penetrometer in Shallow Pavement Applications." Annual book of ASTM standards, ASTM D6951, West Conshohocken, PA.

19. ASTM. (2006). "Standard Test Methods for In-place Density and Water Content of Soil and Soil-Aggregate by Nuclear Methods (Shallow Depth)." Annual book of ASTM standards, ASTM D6938, West Conshohocken, PA.

Table 5.1. Instrumentation elevations

Sensor I.D.	Depth below roadway surface		Location
	(m)	(ft)	
Temperature sensor 1	0.05	0.17	Pavement layer
Temperature sensor 2	0.23	0.75	
Temperature sensor 3 & TDR 1	0.34	1.10	Subbase layer
Temperature sensor 4 & TDR 2	0.39	1.28	
Temperature sensor 5 & TDR 3	0.53	1.74	
Temperature sensor 6 & TDR 4	0.67	2.21	
Temperature sensor 7 & TDR 5	0.86	2.82	
Temperature sensor 8 & TDR 6	1.01	3.31	
TDR 7	1.14	3.75	
Temperature sensor 9 & TDR 8	1.30	4.25	Subgrade layer
TDR 9	1.44	4.73	
Temperature sensor 10 & TDR 10	1.59	5.21	
VW Piezometer 1	4.22	13.86	
VW Piezometer 2	4.21	13.82	
Resistivity Probe (top)	0.40	1.32	

Table 5.2. The average M_r values from initial construction and two years after construction

Measurements	Initial construction	Two years after construction	Change (%)
M_r – estimated from Clegg *CBR* (MPa)	222	–	–
M_r – estimated from DCP *CBR* (MPa)			
0 – 0.31 m	120	121	+1
0.31 – 0.62 m	109	159	+47
0.62 – 0.93 m	128	–	–
M_r – Laboratory test (MPa)	–	47	–

Table 5.3. Summary of average in situ measurements values during construction

Measurements	Average	Coefficient of variation (%)
Clegg impact value, *CIV*	14.4	38
CBR (estimated from *CIV*)	21.5	56
M_r estimated from Clegg *CBR* (MPa)	222	56
DPI (mm/blow)		
0 – 0.31 m	18.4	190
0.31 – 0.62 m	20.3	20
0.62 – 0.93 m	18.2	28
DCP-*CBR* (estimated from *DPI*)		
0 – 0.31 m	11.6	21
0.31 – 0.62 m	10.5	21
0.62 – 0.93 m	12.4	32
M_r estimated from DCP *CBR* (MPa)		
0 – 0.31 m	120	21
0.31 – 0.62 m	108	21
0.62 – 0.93 m	128	32
Moisture content (%)	10.2	8.8
Dry density (kg/m^3)	1866.2 (or 116.5 pcf)	1.8
% Compaction (based on standard Proctor compaction energy	100.0%	–
% Compaction (based on modified Proctor compaction energy	94.7%	–

Table 5.4. Summary of Kriging correlation distances on subgrade layer

Data Set	Correlation Distance, m (ft)		
	Spherical variogram	Exponential variogram	Gaussian variogram
Clegg impact hammer	1.13 (3.7)	4.33 (14.2)	2.74 (9.0)
Nuclear density	0.70 (2.3)	4.33 (14.2)	2.35 (7.7)
Nuclear moisture content	1.01 (3.3)	–	1.52 (5.0)
Weighted DCP *CBR* (0 – 0.31 m)	1.0 (3.3)	1.98 (6.5)	1.16 (3.8)
Weighted DCP *CBR* (0.31 – 0.62 m)	0.91 (3.0)	2.59 (8.5)	1.43 (4.7)
Weighted DCP *CBR* (0.62 – 0.93 m)	0.98 (3.2)	3.90 (12.8)	1.43 (4.7)
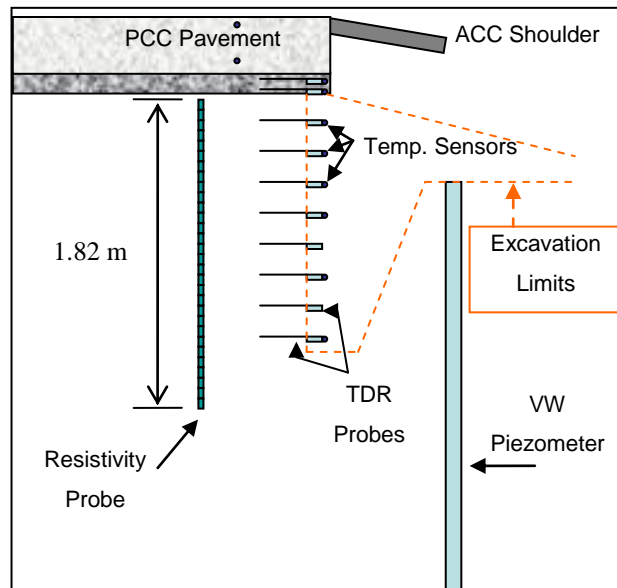
Figure 5.1. Cross section view of installation
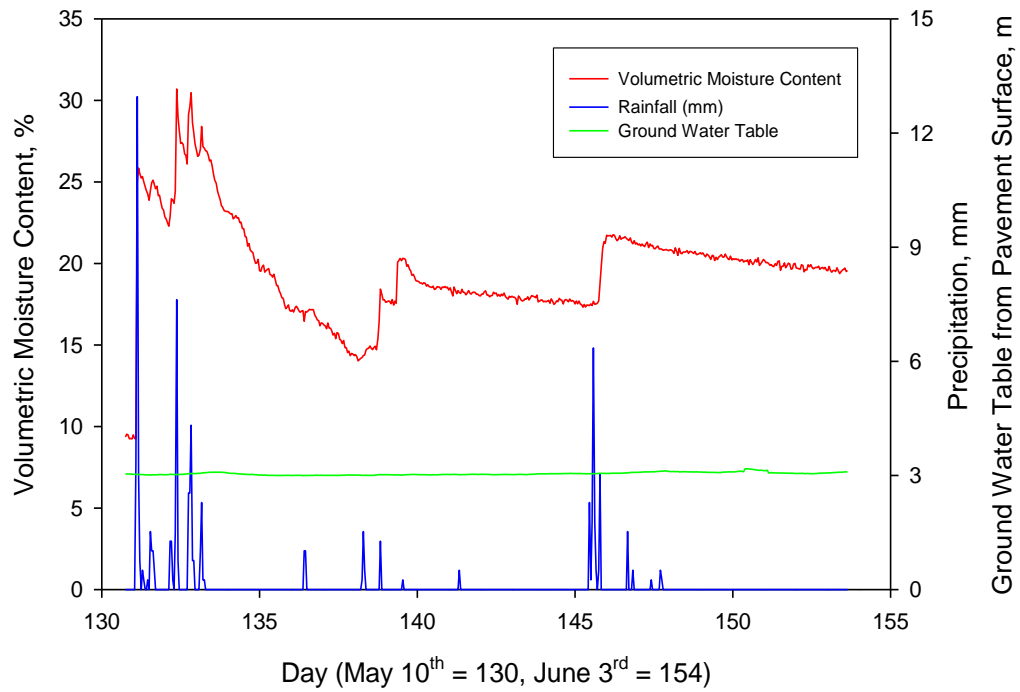
Figure 5.2. Precipitation and moisture content in subbase layer, ground water table
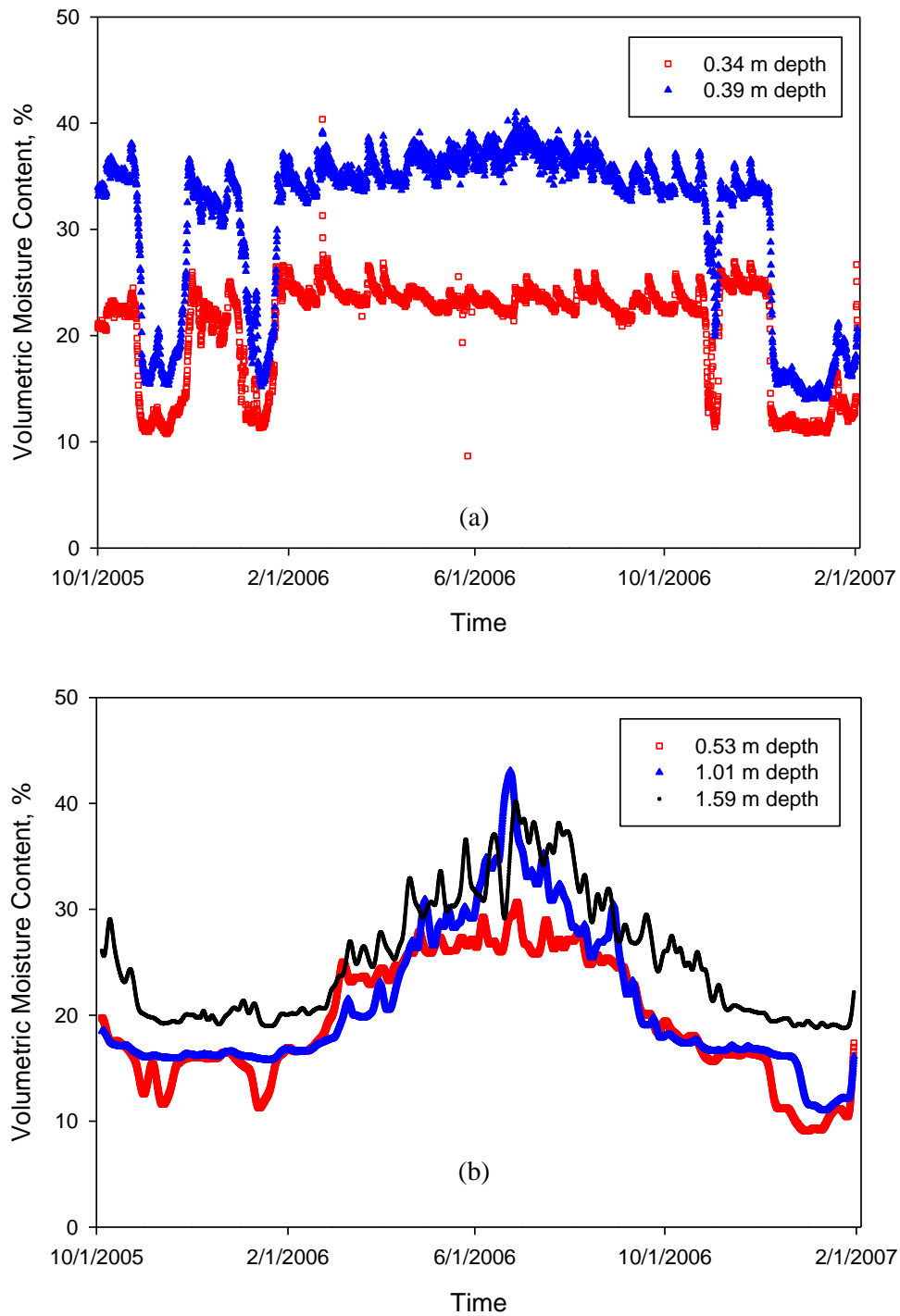
Figure 5.3. Moisture contents with depths from PCC surface: a) in subbase; b) in subgrade
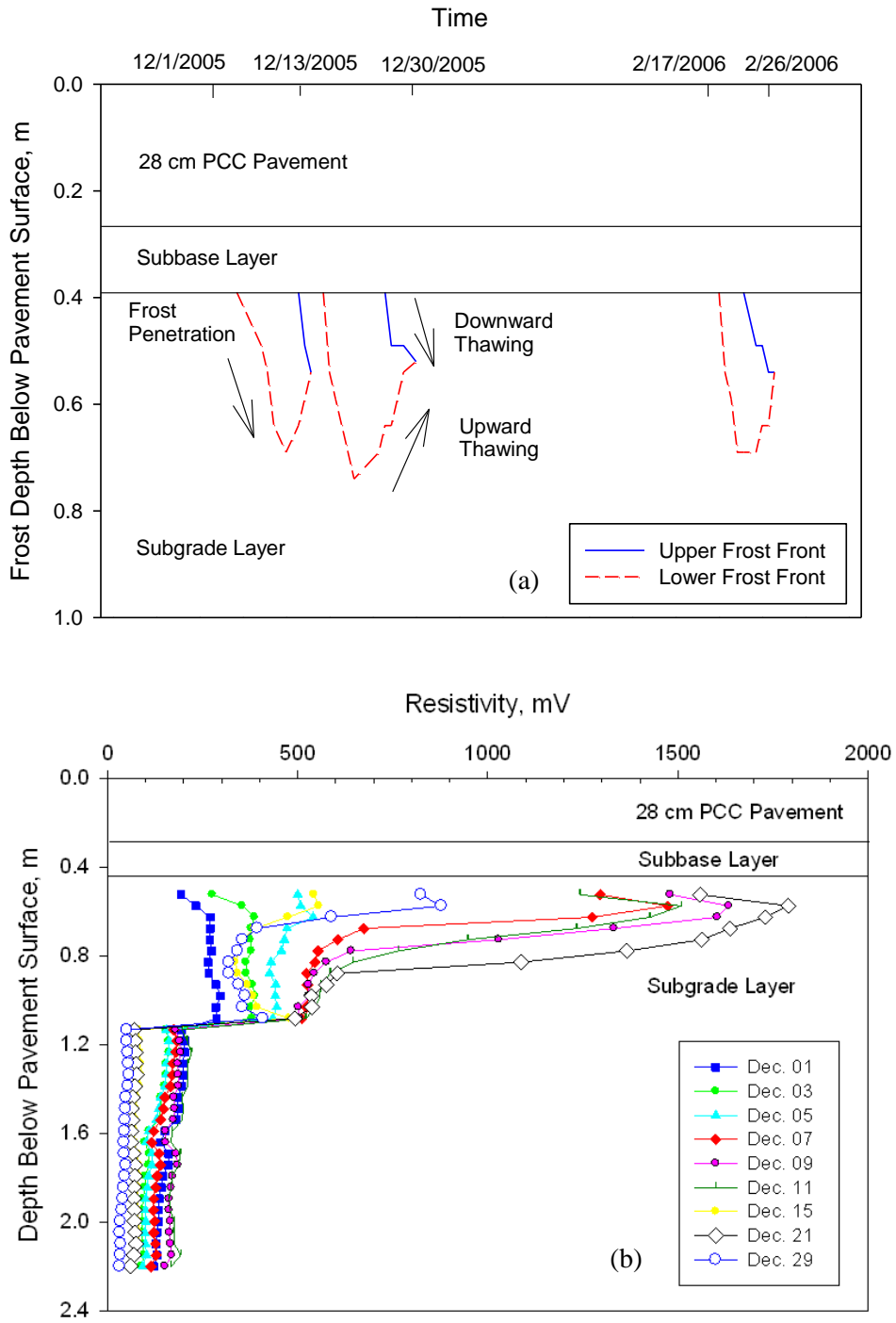
Figure 5.4. Frost penetration: a) freezing and thawing fronts; b) frost depth determination
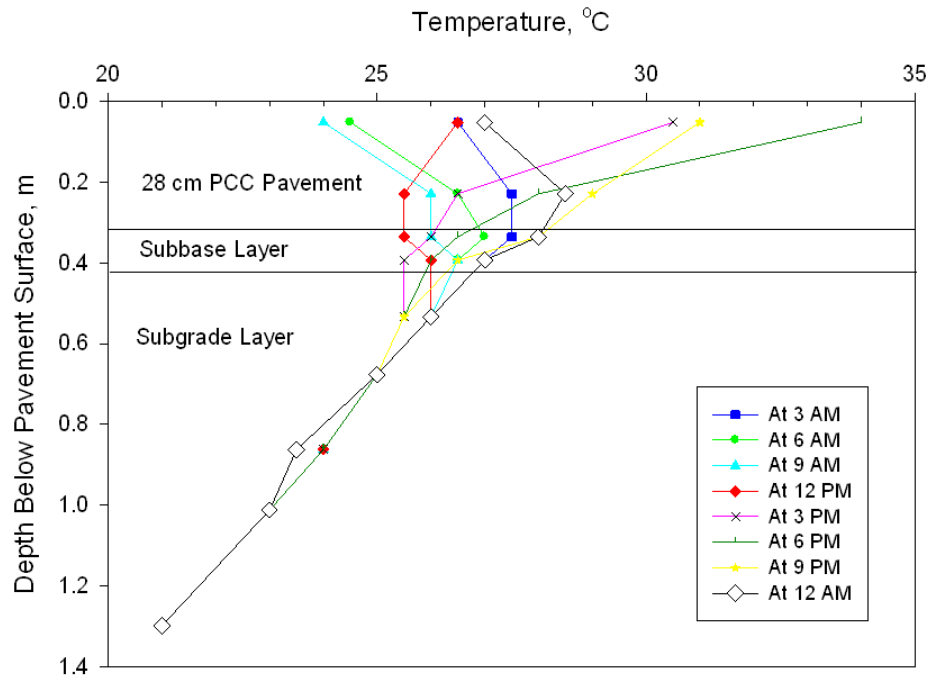
Figure 5.5. Temperature changes below pavement surface at different time in July 4, 2005
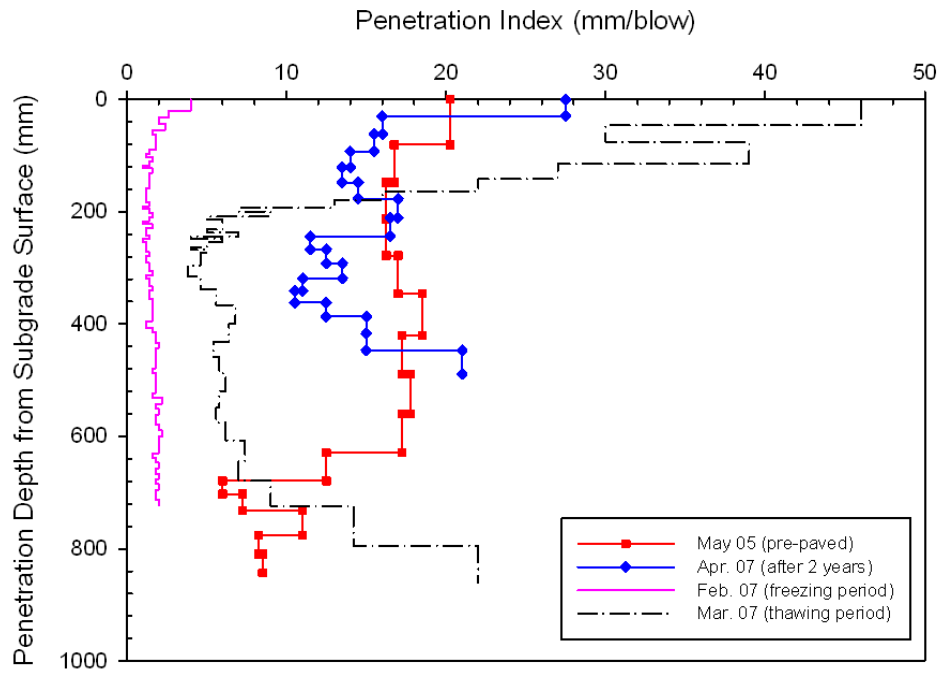
Figure 5.6. DCP tests during construction, freeze-thaw period, and two years after construction
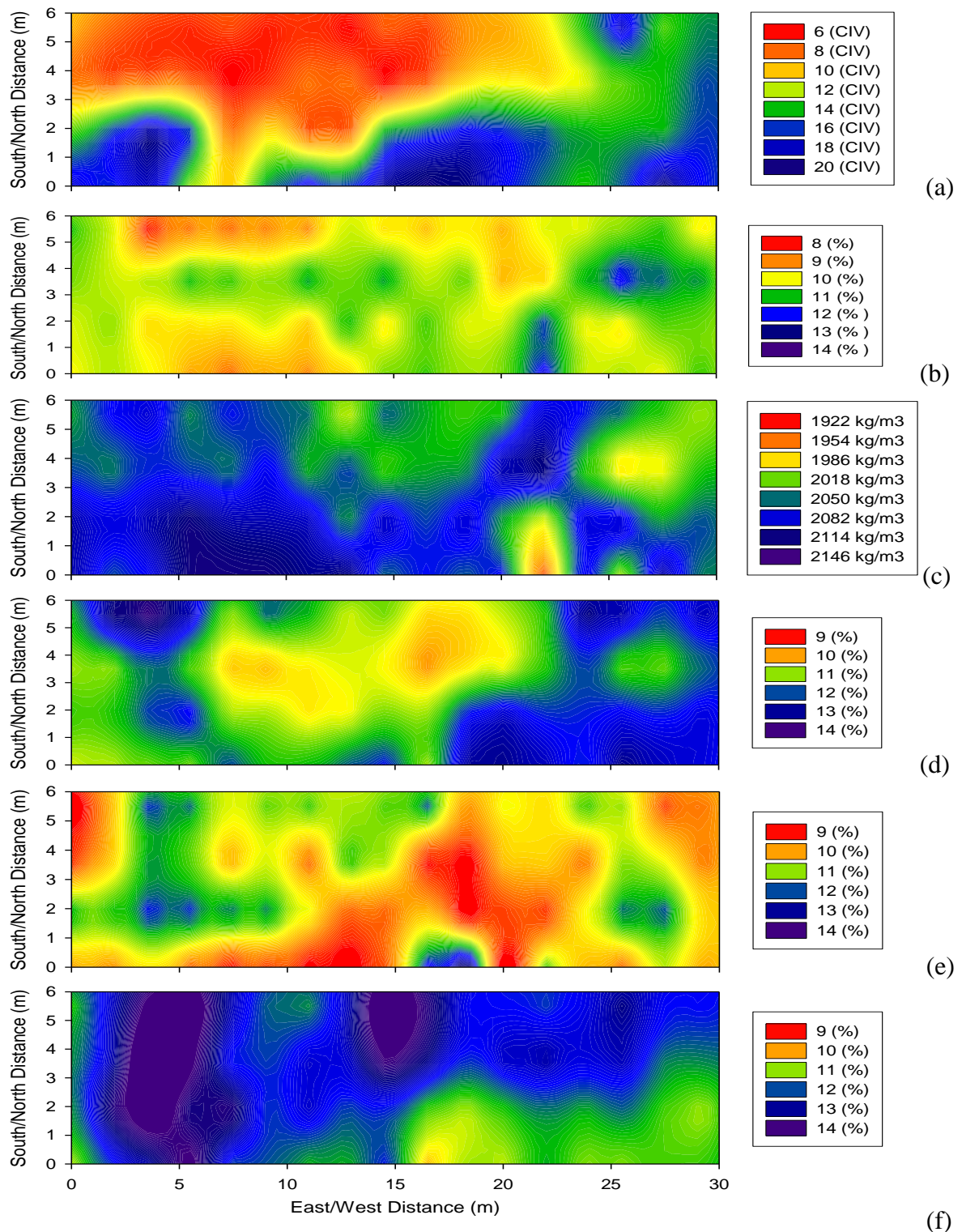
Figure 5.7. Kriging output of subgrade layers of: a) Clegg hammer; b) moisture content; c) moist density; d) DCP CBR values (0-0.31 m); e) DCP CBR values (0.31-0.62 m); and f) DCP CBR values (0.62-0.93 m)

CHAPTER 6: GENERAL CONCLUSION

The four papers that make up this dissertation were focused in two areas, recycled portland cement concrete (RPCC) subbases and seasonal variation in subgrade layers. The first three papers discuss RPCC subbases and the fourth paper reports on a study of seasonal variation of subgrade layers conducted at one site. The RPCC subbase papers report the results of field investigations that were conducted at 27 sites, including 21 sites with RPCC aggregate subbases and 6 sites with crushed limestone aggregate subbases. Aggregate samples from each of the 27 sites were collected for gradation and specific gravity analyses in the laboratory. Four RPCC aggregate samples were collected based on the ages of the RPCC aggregates from four pavement sites (constructed in 1983, 1988, 1994, and 2003). A specimen of tufa precipitate was collected from the subdrain of one RPCC subbase site. These four RPCC aggregate samples and two tufa samples prepared from the tufa specimen were analyzed using scanning electron microscopy (SEM) and X-ray microanalysis techniques. The thermogravimetric analysis (TGA) was employed for the analysis of RPCC aggregate samples collected from 18 sites.

Stiffness and drainage characteristics of the subbase layers were obtained at the 27 sites using a dynamic cone penetrometer (DCP), light weight deflectometer (LWD), Clegg impact hammer, and Minnesota Department of Transportation (Mn/DOT) field permeameter. Stiffness values including LWD modulus of elasticity (E_{LWD}), Clegg impact value (*CIV*), dynamic penetrometer index (*DPI*), California bearing ratio (*CBR*), and modulus of subgrade reaction (*k*-value) and permeability value (*k*) of RPCC subbases were compared with those of crushed limestone subbases. The comparison was aimed at the following hypothesis: "RPCC subbases are generally stiffer than crushed limestone subbases". Results of SEM analysis of four RPCC samples were used as an evidence of strength improvement resulting from cementation of RPCC subbase materials. The hydration of cement grains from RPCC aggregates in the RPCC subbases was a factor that increased the stiffness of RPCC subbases.

Subbase and subgrade layers are the structures that provide support for pavement layers. Loss of support conditions (i.e., a reduction in stiffness) in these layers occurs during thawing periods and/or saturated conditions and is one of the primary contributors to distresses in pavements. Variation in moisture in the subgrade layer can contribute to

deleterious volume changes in soils that may result in differential movement of pavement layers. A better understanding of seasonal variation in subgrade properties would benefit pavement design and material selection. Field instruments monitored the seasonal variations in temperature, moisture content, frost depth, and groundwater levels in subgrade layer of the state highway US 20 westbound near Fort Dodge, Iowa. Spatial variation of the subgrade soils prior to placement of the subbase layer was analyzed using a series of field tests (DCP, Clegg impact hammer, and nuclear gauge) conducted at 64 test locations. The subgrade soil was sampled for laboratory resilient modulus testing approximately two years after construction.

Results and analysis of these investigations were presented as stand-alone papers arranged in four chapters:

- Chapter 2: Comparison of permeability and stiffness for recycled portland cement concrete subbase;
- Chapter 3: Evidence of self-stabilizing recycled portland cement concrete subbase aggregate using field measurements and microstructure characterization;
- Chapter 4: Tufa precipitate formation from recycled portland cement concrete subbases;
- Chapter 5: Seasonal variation and spatial analysis of pavement foundation layers.

CONCLUSIONS

Although the use of RPCC aggregates for pavement subbase has been a common practice in Iowa since the 1980s, performance of RPCC subbases and engineering properties including subbase strength/stiffness, permeability, and precipitate potential of RPCC aggregates has not been fully understood. Results of experimental investigations and analysis in this dissertation provide an evaluation of field performance of pavements supported by RPCC subbases, in comparison to crushed limestone aggregate subbases.

SEM and X-ray microanalysis revealed that RPCC aggregates contained unhydrated cement. When RPCC aggregates were used for pavement subbases, some unhydrated cement grains were exposed to the surrounding environment and reacted with water. The hydration of these cement grains increased the stiffness/strength of the RPCC subbases. The

comparison of the strength/stiffness of four RPCC subbases to five crushed limestone subbases showed that RPCC aggregate subbases were stiffer than crushed limestone aggregate subbases. The average *CIV* and *DPI* values of stiffness of the RPCC subbases were between 200% and 222% of the *CIV* and *DPI* values of crushed limestone aggregate subbases.

Field results at 21 RPCC subbases and 6 crushed limestone subbases indicated that the average values of modulus of elasticity, and *CBR* values estimated from Clegg impact hammer and DCP tests of RPCC subbase layers were $1,108*10^3$ kPa (1,576 psi), 73, and 89, respectively, compared to those of the crushed limestone subbase layers of $449*10^3$ kPa (639 psi), 43, and 45, respectively. The RPCC subbases had an average permeability of RPCC subbases was 0.3 m/day (1 ft/day), which was much lower than the minimum permeability of 300 m/day (1,000 ft/day) recommended for subbase layers. Despite this low permeability, pavements using RPCC subbases performed adequately.

Extensive tufa precipitates were observed at subdrain outlets and flow channels at two out of twenty-one RPCC subbase sites. The amounts of calcium hydroxide in the cement paste of RPCC aggregates varied from 10.9% to 21.7% (by weight). Ca^{2+} ions from calcium hydroxide in RPCC cement paste were the main donor for calcite precipitate. Even though all RPCC aggregates were ready to produce tufa, tufa precipitate also depends on pavement conditions, type of cement used in the original mixture, and permeability of the RPCC subbase. At the RPCC site that had extensive tufa at the drain outlets and in the flow channel, high pH soils (9.8) mostly concentrated at the subdrain outlets. pH values of soils dropped to around 7.0 at locations of 7 m (23 ft) or farther along the flow channel from the subdrain outlets.

SEM and X-ray microanalysis on tufa samples showed that tufa precipitate from the RPCC aggregate subbases was composed of a dense part and a flaky part that had totally different morphologies and chemical components. The major component of the dense part was calcite resulting from the reaction of calcium hydroxide from RPCC aggregates and carbon dioxide that resolved in water. C-S-H was the major component of the flaky part of tufa and was formed by the hydration of unhydrated cement grains.

Spatial analysis of *CIV*s, DCP-*CBR* values, moisture content, and density showed the

influence of construction procedures on subgrade stiffness. *CIV*s from different locations showed clear transverse variations that likely resulted from construction procedures and that varied widely, with a coefficient of variation of 38%. Moisture content and dry density varied in narrower ranges, with coefficients of variation of 9% and 2%, respectively.

Seasonal variations in moisture content and freeze/thaw cycles also influenced subgrade stiffness. Subgrade stiffness decreased as moisture content increased, and moisture content in subgrade soils increased during the spring thaw and peaked in the early summer. Instrumentation results showed that freeze/thaw cycles in the subgrade also decreased the stiffness of the subgrade and that moisture content in the subbase was strongly influenced by precipitation. The volumetric moisture content increased sharply with rain events and changed significantly with the seasons.

RECOMMENDATIONS FOR FUTURE RESEARCH

Some recommendations for future study are as follows:

- Correlate the stiffness and permeability values of RPCC subbase with pavement performance to have a better comparison between rigid pavements with RPCC subbases and those with crushed limestone subbases.

- Incorporate the stiffness values, permeability, and thickness of RPCC subbases into design parameters of the pavement design.

- Correlate the properties (modulus of elasticity, CBR values, modulus of subgrade reaction k-value, and permeability) of RPCC subbases with pavement performance parameters such as the pavement condition index (*PCI*), the total number of distress (*TOD*), and the international roughness index (*IRI*). Regression models based on the material properties should be created to estimate the performance of pavement.

- Include the permeability values of RPCC subbase in rigid pavement design guides.

- Although there are economic and environmental benefits in using RPCC for subbase aggregate materials, the use of RPCC has not been widely adopted in many states, so a comparison of the economics of RPCC and crushed limestone subbases is recommended.

- Because RPCC subbases provide very good support to pavement layers, they might replace cement-treated base or subbase layers. A study is suggested to compare the strength properties (i.e., k-value, *CBR*, modulus of elasticity) of RPCC subbases with those of cement-treated base/subbases.

RECOMMENDATIONS FOR FUTURE PRACTICE

Some recommendations for future practice are as follows:

- RPCC aggregate materials should be used for newly constructed and/or rehabilitated pavement subbases.

- To increase permeability of RPCC subbase and reduce freeze/thaw cycles, RPCC aggregates could be screened to reduce or eliminate fine aggregates.

- RPCC aggregate materials could be recycled a period of time prior to subbase construction as a possible measure to mitigate tufa potential of the RPCC subbases.

GENERAL REFERENCES

AASHTO. (1993a). AASHTO guide for design of pavement structures, American Association of State Highway and Transportation Officials, Washington, D.C.

AASHTO. (1993b). Standard specification for aggregate and soil-aggregate subbase, base and surface courses M-147, Part I Specifications, 16th Edition, American Association of State Highway and Transportation Officials, Washington, D.C.

AASHTO. (2002). Standard specification for reclaimed concrete aggregate for unbound soil aggregate base course M-319, American Association of State Highway and Transportation Officials, Washington, D.C.

ASTM. (2000). "Standard practice for classification of soils for engineering purposes (unified soil classification system)." Annual book of ASTM standards, ASTM D2487, West Conshohocken, PA.

ASTM. (2001a). "Standard test method for sieve analysis of fine and coarse aggregates." Annual book of ASTM standards, ASTM C136, West Conshohocken, PA.

ASTM. (2001b). "Standard tests method for density, relative density (specific gravity), and absorption of coarse aggregate." Annual book of ASTM standards, ASTM C127, West Conshohocken, PA.

ASTM. (2002). "Standard tests method for determination of the impact value (*IV*) of a soil." Annual book of ASTM standards, ASTM D5874, West Conshohocken, PA.

ASTM. (2003a). "Standard tests method for resistance of concrete to rapid freezing and thawing." Annual book of ASTM standards, ASTM C666, West Conshohocken, PA.

ASTM. (2003b). "Standard tests method for resistance of coarse aggregate to degradation by abrasion in the micro—deval apparatus." Annual book of ASTM standards, ASTM D6928, West Conshohocken, PA.

ASTM. (2003c). "Standard test method for use of the dynamic cone penetrometer in shallow pavement applications." Annual book of ASTM standards, ASTM D6951, West Conshohocken, PA.

Al-Amoudi, S. B. O., Asi, M. I., Wahhab, A-A. I. H., and Khan, A. Z. (2002). "Clegg Hammer—California-Bearing Ratio Correlations." *Journal of Materials in Civil Engineering*, 14 (6), 512–523.

Applied Pavement Technology, Inc. (2001). *Hot Mix Asphalt Pavement Evaluation and Rehabilitation: Course No. 131063*, U.S. Department of Transportation, Federal Highway Administration, National Highway Institute, Washington, D.C.

Burke, T.T., Cohen, D. M., and Scholer, F. C. (1992). *Synthesis Study on the Use of Concrete Recycled Pavements and Building Rubble in the Indiana Highway System*. Final Report, Indiana DOT Project: C-36-50m, File: 6–19–13, Indiana Department of Transportation.

Clegg, B. (1986). Correlation with California Bearing Ratio. *News Letter 2*, http://www.clegg.com.au/information_list12.asp, Date Accessed: 04/30/2008.

Chini, A. R., Kuo, S. S., Armaghani, J. M., and Duxbury, J. P. (2001). "Test of Recycled Concrete Aggregate in Accelerated Test Track." *Journal of Transportation Engineering*, 127(6), 486–492.

Collins, R. J. and Ciesielski, S. K. (1994). Recycling and use of waste materials and by-products in highway construction, National Cooperative Highway Research Program, Synthesis of Highway Practice No. 199, National Academy Press, Washington, D.C.

Drumm, C. E., Reeves, S. J., Madgett, R. M., and Trolinger, D. W. (1997). "Subgrade resilient modulus correction for saturation effects." *Journal of Geotechnical and Geoenvironmental Engineering*, 123 (7), 663–670.

Gupta, J.D. and Kneller, W. A. (1993). *Precipitate Potential of Highway Subbase Aggregates*, Final Report HFWA/OH-94/004, Ohio Department of Transportation.

Huang H. Yang (2004). Pavement analysis and design, 2nd Ed., Pearson Prentice Hall, NJ.

Jin, M., Lee, S., Wayne, K., and Kovacs, W. D. (1994). "Seasonal Variation of Resilient Modulus of Subgrade Soils." *Journal of Transportation Engineering*, American Society of Civil Engineers, 120(4), 603–616.

Kasai, Y. (2004). "Recent trends in recycling of concrete waste and use of recycled aggregate in Japan." Proceedings, International Concrete Research and Information Portal, American Concrete Institute, ACI SP–219, 11–34.

Marks, J. V. (1984). *Recycled Portland Cement Concrete Pavement in Iowa*. Progress Report, Iowa DOT Project HR–506, Iowa Department of Transportation, Ames, IA.

NCHRP. (2004). *Guide for Mechanistic—Empirical Design of New and Rehabilitated Pavement Structures.* www.trb.org/mepdg., National Cooperative Highway Research Program, Transportation Research Board, Washington, D.C.

Seed, H. B., Chan, C. K., and Lee, C. E. (1962). "Resilience characteristics of subgrade soils and their relation to fatigue failures in asphalt pavement." Proceedings, First International Conference on Structure Design of Asphalt Pavements, University of Michigan, Ann Arbor, 611–636.

Steffes, R. (1999). *Laboratory Study of the Leachate from Crushed Portland Cement Concrete Base Material*, Final Report, Iowa DOT Project MLR-96-4, Iowa Department of Transportation, Ames, IA.

Vennapusa, P. K. R. and White, D. J. (2009). "Comparison of light weight deflectometer measurement for pavement foundation materials." *Geotechnical Testing Journal*, 32(3), 239–251.

Vukov, J. (2003). *Guidance Document for Reclaimed Portland Cement Concrete*, Final Report, PennDot State–wide Open End Contract No. 440128, Assignment 13. Pennsylvania Department of Transportation.

White, D. J., Jahren, C. T., Cackler, E. T., and Vennapusa, P. (2004). *Determination of the Optimum Base Characteristics for Pavements*, Final Report, Iowa DOT Project TR-482, CTRE Project 02–119, Iowa Department of Transportation, Ames, IA.

Yrjanson, W. A. (1989). *Recycling of Portland Cement Concrete Pavements*, NCHRP Synthesis 154. Transportation Research Board, Washington D.C.

GENERAL ACKNOWLEDGMENTS